Synthesis and Preliminary Evaluation of an F-18 Labeled Fluoropyridine Losartan Analog as a Novel PET Tracer for Imaging AT_1 Receptors

By

Natasha Arksey

uOttawa

A thesis submitted to the Faculty of Graduate and Postdoctoral Studies
in partial fulfillment of the requirements for the
Master of Science (M.Sc.)
in the Department of Cellular and Molecular Medicine
at the University of Ottawa

Supervisor: Jean N. DaSilva, PhD
Co-Supervisor: Rob S. B. Beanlands, MD, FRCPC
National Cardiac PET Centre,
University of Ottawa Heart Institute

ABSTRACT

SYNTHESIS AND PRELIMINARY EVALUATION OF AN F-18 LABELED FLUOROPYRIDINE LOSARTAN ANALOG AS A NOVEL PET TRACER FOR IMAGING AT_1 RECEPTORS

Several cardiac diseases, including hypertrophy, cardiomyopathy, and myocardial infarction, result in the upregulation of cardiac angiotensin II type-1 receptors (AT_1R). Imaging the AT_1R *in vivo* via PET provides the potential to monitor disease progression and guide therapy accordingly. The aim of this research was to develop a novel F-18 labeled losartan analog as an AT_1R PET tracer and begin evaluation in rats. Due to the longer half-life and shorter positron range of F-18, we presume that an F-18 labeled tracer will be more beneficial than current C-11 labeled tracers. Prior structure-activity relationship (SAR) studies suggested the addition of substituents to the hydroxyl group of losartan would minimally affect AT_1R binding affinity. [^{18}F]Fluoropyridine losartan ([^{18}F]FPyrLos) was synthesized in an automated module through conjugation of [^{18}F]fluoro-3-pent-4-yn-1-yloxypyridine ([^{18}F]FPyKYNE) to azide-modified losartan via the Cu(I)-catalyzed azide-alkyne 1,3-dipolar cycloaddition (CuAAC) 'click' reaction. [^{18}F]FPyrLos was produced in approximately 10% yield (decay-corrected) with > 97.5% purity and specific activities up to 4,200 mCi/µmol. MicroPET (Siemens Inveon) images of normal Sprague Dawley rats displayed high uptake in the kidneys (ratio of 8.3 compared to surrounding tissue at 10 min). Metabolite analysis in the kidneys and plasma by column-switch HPLC revealed that roughly two-thirds of the tracer was unchanged 10 min post-injection and that one labeled hydrophilic metabolite exists, accounting for roughly 6% of the total activity. Both microPET and metabolism studies displayed a dose-dependent reduction in renal uptake upon co-injection with AT_1R blocker candesartan indicating specific binding. Further work in rat disease models is required to evaluate the potential of this tracer for imaging cardiac AT_1R.

STATEMENT OF ORIGINALITY

Portions of the work discussed in this thesis were presented at the 2010-2012 Imaging Network of Ontario (ImNO) conferences, the 4th Annual Molecular Function and Imaging (MFI) symposium put forth by the MFI Program at the University of Ottawa Heart Institute (June, 2011), the Science in Nuclear Medicine (SNM) Annual Meeting (June, 2011), the 19th International Symposium on Radiopharmaceutical Sciences (ISRS) (August, 2011), and the Canadian Cardiovascular Congress (CCC) (October, 2011).

ACKNOWLEDGMENTS

I would like to begin by giving credit to post-doctoral fellow Ana Carola Valdivia for the generous contribution of her knowledge, time and patience. If it weren't for her work, my project would not have come into fruition and for this I am most humbled and appreciative. I would also like to thank Dr. Tayebeh Hadizad for her mentorship throughout my master's and for tracer production in the end stages of my project. I would like to express gratitude to my supervisors Dr. Jean N. DaSilva and Dr. Rob S. Beanlands for providing me with the opportunity to further my experience in organic chemistry and for the introduction to the fields of radiochemistry, pharmacology and PET imaging. I am forever grateful to my fellow coworkers, the radiochemistry staff and the animal care staff for which I could not have completed my project without. A special mention is owed to PhD candidates Stephanie Thorn and James Thackeray who selflessly gave up their time, and likely some of their sanity, to assist me through the PET/bio-testing portion of my project. Not only did they impart valuable skills and knowledge but their camaraderie got me through the many frustrations inherent to research.

I would also like to express my gratitude to our sources of funding, notably the Ontario Pre-clinical Imaging Consortium (OPIC), the Heart and Stroke Foundation of Canada and the University of Ottawa for funding my admission scholarship.

TABLE OF CONTENTS

LIST OF TABLES

Page

CHAPTER 1: INTRODUCTION

CHAPTER 4: RESULTS

LIST OF FIGURES

Page

CHAPTER 1: INTRODUCTION

CHAPTER 3: METHODS

CHAPTER 4: RESULTS

CHAPTER 5: DISCUSSION

LIST OF ABBREVIATIONS AND ACRONYMS

ACE	angiotensin I converting enzyme
AF	ammonium formate
AngII	angiotensin II
AT_1R; AT_2R	angiotensin II type 1 receptor; angiotensin II type 2 receptor
ARB	angiotensin II type 1 receptor blocker
BBB	blood-brain barrier
B_{max}	maximum binding capacity
BP	binding potential ($BP = B_{max}/K_d$)
cAMP	cyclic adenosine monophosphate
CT	x-ray computed tomography
CuAAC	Cu(I)-catalyzed Huisgen 1,3-dipolar cycloaddition of azides and alkynes
$CuSO_4$	copper sulphate
DBU	1,5-Diazabicyclo(5.4.0)undec-5-ene
DCM	dichloromethane
DIPEA	N,N-diisopropylethylamine
DMF	dimethylformamide
DMSO	dimethylsulfoxide
DPPA	diphenylphosphoryl azide
DV	volume of distribution
EGFR	epidermal growth factor receptors
EI-MS	electron impact mass spectrometry
EOB	end-of-beam
ESI-MS	electrospray ionisation mass spectrometry
EtOAc	ethyl acetate
EtOH	ethanol
FBA	fluorobenzoic acid
FDG	fluorodeoxy glucose

FEtTos; FPrTos	fluoroethyl tosylate; fluoropropyl tosylate
FPy5yne	2-fluoro-3-hex-5-yn-1-yloxypyridine
FPyKYNE	2-fluoro-3-pent-4-yn-1-yloxypyridine
FWHM	full-width-at-half-maximum; used to characterize PET resolution
GPCR	7 transmembrane G-protein-coupled receptor
HPLC	high performance liquid chromatography (RP: reverse phase)
IC_{50}	inhibitory concentration 50%; concentration of inhibitor required to reduce specific binding of the radioligand by 50%
K_d	equilibrium dissociation constant; ratio of the rate of dissociation to the rate of association
K_i	equilibrium dissociation constant for the inhibitor
KF	potassium fluoride
Kryptofix222 (K_{222})	an aminopolyether phase-transfer agent (4,7,13,16,21,24-hexaoxa-1,10-diazabicyclo[8.8.8]-hexacosane)
LA; LV	left atrium; left ventricle
LAH	lithium aluminum hydride
Losartan	AT_1 receptor blocker; antihypertensive under brand name *Cozaar*
LOR	line of response
logP	logarithm of the octanol-water partition coefficient (P); descriptor of lipophilicity of a neutral compound
MeCN	acetonitrile
MeOH	methanol
MeOTf	methyl trifluoromethansulfonate, methyl triflate
MRI	magnetic resonance imaging
MS	mass spectrometry
MW	molecular weight
$NaHCO_3$	sodium bicarbonate
NMR	nuclear magnetic resonance
NO_2PyKYNE	2-Nitro-3-pent-4-yn-1-yloxypyridine
PET	positron emission tomography

Pk_a	the negative base-10 logarithm of the acid dissociation constant (K_a) of a solution ($pK_a = -\log_{10}K_a$); descriptor of acid strength.
PEEK	Polyetheretherketone
PP	Polypropylene
PTFE	Polytetrafluoroethylene; Teflon
RAS	renin-angiotensin(-aldosterone) system; also RAAS
ROI	region of interest
ROS	reactive oxygen species
SA	specific activity
SAR	structure-activity relationship
SD	standard deviation
SFB	N-succinimidyl 4-fluorobenzoate
SPECT	single photon emission computed tomography
SNAr	nucleophilic aromatic substitution
S_N2	bimolecular nucleophilic substitution
SUV	standard uptake value
R_f	retention factor on TLC
TAC	time-activity curve
$t_{1/2}$	half-life
TEA	triethylamine
TFA	trifluoroacetic acid
THF	tetrahydrofuran
TLC	thin layer chromatography
TOF	time-of-flight
TPP	triphenylphosphine (Ph_3P)
Trityl	triphenylmethyl
TSTU	O-(N-succinimidyl)-1,1,3,3-tetramethyluronium tetrafluoroborate
VSMC	vascular smooth muscle cells
$^{A}_{Z}X$	X = nuclide, A = # of protons and neutrons (mass number), Z = # of protons (atomic number)

1 INTRODUCTION

1.1. The Renin-Angiotensin (-Aldosterone) System

Activation of the renin-angiotensin(-aldosterone) system (RAS) results in blood pressure elevation, water and sodium retention, stimulation of the sympathetic nervous system and cellular growth and differentiation. Angiotensin II (AngII) is the major effector and exerts its physiological actions in several target organs including the kidneys, adrenal glands, heart, blood vessels and brain (Allen et al., 2000).

1.1.1. Systemic RAS

The traditional scheme of the RAS (Figure 1-1) begins with the renal enzyme renin which cleaves hepatic-derived angiotensinogen to the decapeptide angiotensin I (AngI). Angiotensin converting enzyme (ACE), produced in the lungs, is secreted into the pulmonary circulation where it cleaves two amino acids from AngI to produce AngII (Duncia et al., 1992). This scheme has since been updated to accommodate for evidence of increased complexity, including novel signal transduction pathways, angiotensin derivatives and their possible binding sites, and alternative pathways of AngII formation (Paul et al., 2006). For example, there is evidence that Ang(1-7), produced from AngI or AngII via ACE2, binds to the AT_2R and the Mas receptor. AngIII is produced from AngII and is thought to bind to the AT_1R and AT_2R. AngIV, a derivative of AngIII, binds to the AT_4R, an insulin-regulated aminopeptidase (IRAP) (Albiston et al., 2001; Jones et al., 2008; Thomas and Mendelsohn, 2003). AngIV and Ang(1-7) possess low affinity for the AT_1R and AT_2R (De Gasparo, 2000). The regulation and function of these peptides and their corresponding receptors has yet to be firmly established.

1.1.2 Tissue RAS

Beyond the endocrine effect of AngII in the conventional systemic RAS, a local tissue RAS is also strongly suspected (Kaschina and Unger, 2003; Lindpaintner and Ganten, 1991), introducing paracrine and autocrine effect (Dzau, 1988; Dzau et al., 1993; Katz, 1988). Whereas the systemic RAS is seen as a regulator of systemic volume, electrolyte balance and blood pressure homeostasis, the local RAS is thought to be more involved in growth (Gibbons et al., 1992; Itoh et al., 1993), proliferation, protein synthesis, regional heamodynamic regulation, and organ function (De Gasparo, 2000; Paul et al., 2006). Most tissues and organs are thought to contain a tissue RAS capable of synthesizing the enzymes, hormones and receptors of the RAS based on findings of ACE, angiotensinogen and renin mRNA (Dzau et al., 1987; Jin et al., 1988; Kunapuli and Kumar, 1987), as well as ACE, renin, AngII, and AngII receptors (Allen et al., 1990; Dostal and Baker, 1993). Activation of the local RAS in the heart (Baker et al., 1992; Lee et al., 1993) is thought to induce growth of smooth muscle and myocardial cells (Baker and Aceto, 1990; Baker et al., 1990; Dostal and Baker, 1993; Geisterfer et al., 1988; Katoh Y et al., 1989; Morishita et al., 1994). In fact, inhibition has shown to prevent or reduce left ventricular hypertrophy caused by pressure overload (SOLVD investigators, 1991; Devereux et al., 1987; Kromer and Riegger, 1988; Linz W et al., 1989; Nakashima et al., 1984; Pfeffer et al., 1988; Sen, 1983). There are still many questions surrounding the tissue RAS, including the involvement of circulating RAS components for the local production of AngII, the functional significance of local AngII, and the conditions that regulate these processes. It is suspected that the systemic RAS may influence the tissue RAS (Dzau and Re, 1994). For example, AT_1R activation in the kidney (Crowley et al., 2006; Crowley et al., 2005) and brain (Veerasingham and Raizada, 2003) may indirectly affect the cardiovascular system. Most cardiac AngII is thought to be produced locally rather than from uptake of circulating AngII (Shirani et al., 2006; van Kats et al., 1998; van Kats et al., 2000). However, it is

suspected that variations in the concentrations of systemic RAS components may regulate local RAS activation, effecting pathologies such as cardiac remodelling, hypertrophy, and atherosclerosis (Dzau and Re, 1994).

1.1.3 Angiotensin II Receptors

AngII produces its physiological response through activation of two main receptors: the AT_1 receptor (AT_1R) and the AT_2 receptor (AT_2R). However, it is the AT_1R that mediates most of the physiological effects of AngII. Both receptors belong to the family of seven transmembrane G-protein-coupled receptors (GPCRs) and are distinct in their pharmacological and biochemical properties (Timmermans et al., 1993). For example, AngII-stimulated AT_1R are robustly phosphorylated, leading to rapid endocytosis and subsequent degradation or recycling to the cell surface (Thomas and Mendelsohn, 2003). The two subtypes were first discovered through the differential selectivity of AT_1R antagonist Losartan (DuP753) and AT_2R antagonists PD123319 (Chiu et al., 1989; Timmermans et al., 1993; Wong et al., 1990c) and CGP42112 (Whitebread et al., 1989). Losartan displays 10,000-fold greater selectivity for the AT_1R than the AT_2R (Timmermans et al., 1991) whereas PD123319 and CGP42112 show 3,500-fold (Timmermans et al., 1991; Timmermans et al., 1993) and 1000-fold (Whitebread et al., 1989) more selectivity for the AT_2R, respectively. Unlike AngII, which possesses a similarly high affinity for both AT_1 and AT_2 receptor subtypes (Chang and Lotti, 1991), these antagonists share a 1000-fold affinity for their respective receptor subtype . Today, there are a multitude of high-affinity selective non-peptide AT_1R antagonists, most of which belong to the sartan class of pharmaceuticals.

1.1.3.1 AT_1 Receptor

The physiological effects of AngII are mediated primarily through the AT_1R. These effects include thirst, salt appetite, vasoconstriction (De Gasparo, 2000), decreased renal blood flow, water and sodium reabsorption, growth and proliferation of vascular smooth muscle cells (VSMCs), coronary endothelial cells and cardiomyocytes, vasopressin and aldosterone secretion, increased noradrenergic output, extracellular matrix formation (Unger, 2002), and superoxide production (Saijonmaa, 2008).

Unlike in humans, cows, dogs and rabbits, the AT_1 gene in rats and mice codes for two receptor subtypes, AT_{1A} and AT_{1B}, which are 94-96% identical in their amino acid sequences(Iwai and Inagami, 1992), (Elton et al., 1992). The two subtypes are also similar in terms of their ligand binding and activation properties but differ in their tissue distribution, chromosomal localization, genomic structure, and transcriptional regulation (De Gasparo, 2000). It is the AT_{1A} receptor subtype that mediates the blood pressure response to AngII (Ito et al., 1995). In adult mice, the $AT_{1A}R$ is expressed in the adrenal gland, ovary, brain, testis, heart, and adipose tissue (Burson et al., 1994), but is most predominant in the liver, lungs, kidneys and vascular smooth muscle (Allen et al., 2000). In fact, the liver, heart, and lung contain solely $AT_{1A}R$ (Gasc et al., 1994). The $AT_{1B}R$ is located mainly in the adrenal gland, anterior pituitary (Allen et al., 2000), brain and testis (Burson et al., 1994). *In vitro* binding assays in monkeys suggest the adrenal cortex and kidney cortex could have significantly more AT_1R than the heart, potentially 300 fold compared to the adrenal cortex or 40 fold compared to the heart (Chang and Lotti, 1991). Significant homology exists between human AT_1, rat AT_{1A} and rat AT_{1B} receptors, showing 92-97% protein homology and 95-98% transmembrane domain homology, compared to 32-34% amino acid homology between the human AT_2R and rat $AT_{1A}R$ (Allen et al., 2000). It is important to note that the amino acid homology between rat AT_1R isoforms and the human AT_1R translates

to their binding affinity and selectivity for a multitude of AT_1R ligands (Chiu et al., 1993; Hunyady et al., 1996).

1.1.3.2 AT_2 Receptor

During fetal development, AT_2R are highly and ubiquitously expressed. However, their levels rapidly decline following birth. Thus, it is proposed that the AT_2R plays a role in early growth and development (Wang et al., 1998). In adults, the AT_2R appears localized to sites of cellular stress, such as inflammation, tissue damage or ischemia. Current evidence suggests that the AT_2R mediates protective actions counterbalancing the effects of the AT_1R by promoting natriuresis, vasodilation (Hein et al., 1995; Ichiki et al., 1995), apoptosis (Yamada et al., 1996), neuronal regeneration, and inhibiting cell growth and proliferation (De Gasparo, 2000; Haywood et al., 1997; Nakajima et al., 1995; Saijonmaa, 2008; Stoll et al., 1995; Tuccinardi et al., 2006). It has been proposed that the therapeutic effect of AT_1R blockers, or ARBs, arises not only from reduced AT_1R stimulation but by increased AT_2R stimulation (Wiemer et al., 1993).

1.1.4 AT_1 and AT_2 Receptor Expression and Distribution

In addition to the brain, aorta, kidneys and vasculature, high concentrations of AT_1R can be found in the adrenal gland (Chang and Lotti, 1991), liver (Kim and Iwao, 2000), lung, and adipose tissue (De Gasparo, 2000) of most species. AT_2R are found mostly in the adrenal medulla, ovary, uterus (Thomas and Mendelsohn, 2003), and certain brain nuclei (Kim and Iwao, 2000), but has also been localized to the kidney, pancreas, retina, skin, and both endothelial and smooth muscle of the vasculature (Jones et al., 2008) (Table 1-1). AngII receptor levels in the heart are low (Chang and Lotti, 1991; Crabos et al., 1994; Kijima et al., 1996; Sechi et al., 1992; Suzuki et al., 1993).

1.1.4.1 Adrenal Gland

In the mammalian adrenal gland, AT_1R and AT_2R are differentially expressed in the cortex and medulla (Allen et al., 2000). In the adrenal cortex of rodents, rabbits, monkeys, and humans (Chang and Lotti, 1990; Chiu et al., 1989; Whitebread et al., 1989), the AT_2R comprises 10-40% of the AngII binding sites with the AT_1R comprising the remaining 60-90%. The adrenal medulla of most species, however, consists of predominantly AT_2R (Allen et al., 2000; Thomas and Mendelsohn, 2003; Timmermans et al., 1993). The location of the receptors is consistent with known actions of AngII in the biosynthesis and release of aldosterone and catecholamines (Allen et al., 2000). From Scatchard analysis of [^{125}I]AngII binding in the rat adrenal, densities of 18 ± 0.7 and 17 ± 1.0 pmol/g were obtained for AT_1R and AT_2R, respectively (Chang and Lotti, 1990).

1.1.4.2 Kidney

In the kidney, the distribution of AT_1R is conserved among all adult mammals, including rats and humans (Allen et al., 2000; Sechi et al., 1992), indicating the importance of the AT_1R in the regulation of glomerular filtration, renal microcirculation, fluid and electrolyte balance, and renal cell proliferation (Allen et al., 2000). The highest density of AT_1R is found in the glomerular mesangial cells and the inter-glomerular area of the cortex with the greatest amount found throughout the inner stripe of the outer medulla. Only a few AT_1R are located in the outer stripe of the outer medulla and in the inner medulla toward the papilla (Allen et al., 2000). Specifically, the AT_1R appears to be distributed between the medulla and the cortex in a 4:3 ratio (Huang et al., 2009; Tan et al., 2004), with AT_1R representing more than 90% of the AngII receptors in the cortex (Chang and Lotti, 1991). Regarding rats, the $AT_{1A}R$ is the predominant subtype in all nephron segments except the glomeruli, where the $AT_{1A}R$ and $AT_{1B}R$ were found in similar proportions (De Gasparo, 2000) translating to nearly 95% of the renal AT_1R (Kakinuma et al.,

1993). According to quantitative autoradiography in mice, the density of AT_1R in the kidney are as follows: 72 ± 19 fmol/mg in the glomeruli, 9 ± 4 fmol/mg in the rest of the cortex, 8 ± 1 fmol/mg in the outer stripe of the outer medulla, and 29 ± 6 fmol/mg in the outer stripe of the outer medulla (Saavedra et al., 2001). These values correlate with the B_{max} of 3.0 fmol/mg protein stated by Lopez (Lopez et al., 1994). In rats, much higher values were reported: 1,186 ± 73 fmol/mg in the medulla and 872 ± 35 in the cortex (Huang et al., 2009).

1.1.4.3 Heart

The myocardium is composed primarily of cardiac myocytes, interstitial cells, vascular endothelial cells, vascular smooth muscle cells, fibroblasts, and macrophages (Zhu et al., 1997). Myocytes form the major functional and structural portion of the heart. However, very low expression has been detected in the myocardium or interstitial regions (Brink et al., 1996; Tsutsumi et al., 1998; Wharton et al., 1998). The AT_1R appears to be predominantly expressed in cardiovascular cells such as vascular smooth muscle cells (VSMCs) (Higuchi et al., 2007; Unger, 2002). In humans, the greatest density of AT_1R occurs in association with the conduction system and vasal ganglia (Brink et al., 1996; Tsutsumi et al., 1998; Wharton et al., 1998), consistent with known ionotropic and chronotropic effects (Kawano et al., 2000; Zhu et al., 1997). Despite the amount of research, the proportion of AT_1R to AT_2R in the heart of both rats and humans remains mixed (Table 1-2). In the human heart, the density of AngII receptors is roughly 2-3 times greater in the atria than the ventricles with the AT_1R constituting > 70% of AngII receptors (Wharton et al., 1998) which translates to roughly 10 times more AT_1R in the atria than in the ventricles (Baker et al., 1984; Rogg et al., 1996; Urata et al., 1989). In the rat heart, the results are conflicting. One source suggests 30% of AngII receptors in the atria (Rogg et al., 1996) and whole heart (Regitz-Zagrosek et al., 1995) are of the AT_1 subtype, whereas another states the

ventricles contain approximately 69% AT_1R (Lopez et al., 1994). The proportion of AT_1R in the heart ranges from around 91% (Della Bruna et al., 1995), to equal (Rogg et al., 1996; Sechi et al., 1992; Suzuki et al., 1993) to only 10% (Chang and Lotti, 1991). One study found an AngII receptor density of 16 ± 0.7 fmol/mg protein in ventricular membranes with equal proportions of AT_1R to AT_2R (Suzuki et al., 1993). Seemingly agreed upon, however, is that rat cardiac fibroblasts mainly express AT_1R, ranging from 65% (Matsubara et al., 1994) to 100% (Villarreal et al., 1993) with a maximum binding capacity of 31.4 ± 11.4 x 10^3 sites/cell (Crabos et al., 1994). In fact, fibroblasts may contain nearly 8 times as many AT_1R as myocytes (Matsubara et al., 1994). Neonatal rat cardiomyocytes are estimated to contain 188 ± 21 fmol/mg AngII receptors, of which roughly 60% are AT_1R (Kijima et al., 1996).

1.1.5 AngiotensinII and the AT_1 Receptor in Disease

The onset of heart failure and cardiovascular disease begins with the presence of risk factors, such as hypertension, dyslipidemia, and diabetes which predisposes one to atherosclerosis, left ventricular hypertrophy and coronary artery disease (CAD). Atherosclerotic plaque poses the risk of dislodgment and constriction of blood flow to the heart resulting in myocardial infarction (MI). Consequent remodelling, fibrosis, ventricular dilatation, and loss of cardiac muscle can progress to heart failure and, ultimately, end-stage heart disease (Figure 1-2) (Unger, 2002). Accumulated evidence from animal model experiments suggests that over-stimulation of AT_1R by AngII is implicated in the pathophysiology of various cardiovascular diseases (Cohn and Tognoni, 2001; Griendling et al., 1996; Pitt et al., 2000) such as hypertension, atherosclerosis, congestive heart failure, fibrosis, thrombosis, coronary ischemia, left ventricular and vascular hypertrophy, and inflammation (Dimitrijevic et al., 2009; Dzau and Re, 1994; Higuchi et al., 2007; Ibrahim, 2006). Elevated levels of AngII and subsequent over-stimulation of

the AT_1R may also contribute to the pathophysiology of impaired glucose tolerance and hyperglycemia, glomerulosclerosis (Kim and Iwao, 2000) and renal failure (Dzau and Re, 1994).

The effects of the RAS as it pertains to the cardiovascular system are mediated not only by direct action on the vasculature (Higuchi et al., 2007), but through AT_1R on other organs, such as the kidney (Crowley et al., 2006; Crowley et al., 2005) and brain (Veerasingham and Raizada, 2003). However, there are questions surrounding a direct role of cardiac AngII in cardiac hypertrophy and fibrosis (Reudelhuber et al., 2007; van Kats et al., 2001). It seems as though elevated AngII levels may only become damaging in combination with other stimuli (Danser), such as elevated blood pressure (Xu et al., 2010).

1.1.5.1 Cardiac Hypertrophy and Remodeling

Cardiac hypertrophy is a detrimental state reached as an attempt to compensate for a hemodymanic (Kim and Iwao, 2000) or pressure overload and is associated with an increased risk of cardiovascular morbidity and mortality, regardless of blood pressure (Kjeldsen et al., 2006). However, hypertrophy and dilatation are largely associated with hypertension (Kjeldsen et al., 2006). In fact, left ventricular hypertrophy is the second strongest predictor, after age, of cardiovascular disease. The classic definition of hypertrophy describes an enlargement of the myocytes and the ventricular wall, in particular, resulting in reduced contractility (Kim and Iwao, 2000; Harada et al., 1996). The current definition includes activation of several protein kinases including extracellular-signal-regulated kinases (ERKs) (Komuro and Yazaki, 1993) and fetal gene reprogramming (Kim and Iwao, 2000), which results in changes of myosin isoforms, membrane receptors, transporters, ion channels and aspects of intracellular signalling (Zhu et al., 2003). Cardiac remodeling, or cardiac fibrosis, is the architectural change associated with hypertrophy involving increased production of extracellular matrix (ECM) proteins, such as collagen and

fibronectin, in the interstitium and around blood vessels by VSMC and fibroblasts (Mehta and Griendling, 2007) resulting in increased stiffness.

It is well-documented that overactivity of the RAS, and of AngII in particular, contributes to the development of cardiac hypertrophy (Baker et al., 1992; Lee et al., 1993). AngII induces hypertrophy via its growth factor properties on cardiomyocytes (Baker and Aceto, 1990; Kjeldsen et al., 2006; Kojima et al., 1994; Thomas et al., 2002) and to cardiac fibrosis via induction of fibroblast proliferation and collagen deposition (Berk et al., 2007; Kaschina and Unger, 2003; Nicoletti A et al., 1995; Sadoshima and Izumo, 1993). It is important to note however that hypertrophy occurs regardless of an increase in blood pressure (Baker et al., 1992; Hein et al., 1997; Morishita et al., 1994; Paradis et al., 2000; Zhu et al., 2003).

Evidence increasingly implicates AngII-induced activation of the AT_1R in the development of the aforementioned cardiovascular pathologies (Allen et al., 2000; Kawano H et al., 2000; Zhu et al., 1997). For example, both overexpression and constitutive activation of AT_1R have induced cardiac hypertrophy and fibrosis independent of blood pressure effect (Billet et al., 2008; Hein et al., 1997; Paradis et al., 2000; van Kats et al., 1998). On the other hand, ARB treatment appears to reverse cardiac fibrosis (Kawano H et al., 2000), reduce cardiac hypertrophy, and prevent progression of heart failure (Griendling et al., 1996; Hein et al., 1997; Kojima et al., 1994; Paradis et al., 2000). Furthermore, AT_1R knockout mice have shown improved survival rates following an MI (Harada et al., 1999). Interestingly, AngII-induced cardiac hypertrophy can be observed in rats expressing the $AT_{1A}R$ only in the kidney (Crowley et al., 2006).

It has been suggested that AngII-induced activation of AT_1R may contribute to the remodelling following compensated hypertrophy by inducing cardiomyocyte apoptosis (Cigola et al., 1997; Diep et al., 2002; Diez et al., 1998; Goussev A et al., 1998; Kajstura et al., 1997; Leri et al., 1998). Several studies revealed that treatment with losartan attenuated the

observed increase in AT_1R and increased AT_2R expression alongside a decrease in apoptosis. However, there are conflicting results regarding the anti-apoptotic effect of AT_2R (Dubey RK et al., 1997; Sugino H et al., 2001; Yamada et al., 1996) which may be due to differences between neonatal and adult hearts (Goldenberg et al., 2001).

Beyond organ development, exercise, age, hypertension, cardiomyopathy and MI (Zhu et al., 2003), mechanical stretch resulting from hemodynamic overload has recently gained acceptance as a significant stimulus for cardiac hypertrophy (Chien, 1998; Yasuda et al., 2008; Zou et al., 2004). It has been suggested that AngII is secreted by cardiomyocytes in response to stretch, resulting in AT_1R activation by an autocrine effect (Zhu et al., 2003). However, studies suggest that mechanical stress can induce cardiomyocyte hypertrophy without the involvement of AngII (Miyata S et al., 1993; Sadoshima et al., 1993; Zou et al., 2004). For example, mechanical stretching of cardiomyocytes has shown to induce a hypertrophic response and this response was significantly attenuated by ARB candesartan (Sadoshima et al., 1993; Yamazaki et al., 1995). Further, when the AT_1R binding site contained a mutation preventing AngII binding, mechanical stretch still activated the receptors and this activation was still inhibited by candesartan (Yamano et al., 1992). There is also speculation that reactive oxygen species (ROS) produced in the AT_1R signalling cascade may evoke hypertrophic responses in cardiomyocytes, enhance cellular proliferation, and stimulate production of ECM proteins by cardiac fibroblasts (Hunyady and Catt, 2006; Kim and Iwao, 2000).

AngII receptors are differentially expressed in cardiac hypertrophy (1991; Lopez et al., 1994; Poole et al., 1994). However, as hypertrophy often results from a disease involving several intertwining factors, models are used for simplification. For example, mechanical stretching of cardiomyocytes and aortic banding are used to model hemodynamic overload. An increase in both AT_1R and AT_2R (Kijima et al., 1996; Suzuki et al., 1993) resulted from the former, whereas

the latter showed a general increase in AT_1R and decrease in AT_2R (Harada et al., 1998a; Harada et al., 1998b; Lee et al., 1996).

1.1.5.2 Hypertension

Hypertension is a complicated disease involving several intertwining factors. Genetic manipulation in rats and mice has enabled models of overexpression ($AT_{1A}R$ (Le et al., 2003)' (Ramchandran et al., 2006), renin, and angiotensinogen (Ohkubo et al., 1990)), mutation ($AT_{1A}MUT$ (Billet et al., 2008)), and knock-out ($AT_{1A}KO/AT_{1B}KO$ (Audoly et al., 2000) or AT_2KO (Ichiki et al., 1995)) which have implicated the AT_1R (Billet et al., 2008), and specifically the kidney $AT_{1A}R$ (Tuccinardi et al., 2006; Crowley et al., 2006), in AngII-mediated hypertension and associated effects such as hypertrophy (Nozawa et al., 1996; Ozono et al., 2000; Wang et al., 1998) and fibrosis. Hypertension models include renal artery occlusion, spontaneously hypertensive rats (SHR), Dahl salt-sensitive rats, and rats treated with mineralocorticoid (DOCA-salt). Salt-sensitive rats fed a high-salt diet show evidence of hypertension as well as hypertrophy and fibrosis of the heart and kidney (Liang and Leenen, 2008). In these rats, the circulatory RAS decreased, but tissue RAS in the brain, heart, and kidney showed a significant increase (Bayorh et al., 2005). High doses of ARBs attenuated the rise in blood pressure and reduced the cardiac and kidney fibrosis but only minimally prevented hypertrophy. Aortic AT_1R (Nickenig et al., 1998; Tamura et al., 1999) and AT_2R densities also increased in a similar model and were both reduced by treatment with ARBs (Liang and Leenen, 2008). However, in the cortex and medulla of the kidney, both AT_1R and AT_2R levels decreased. In the heart, receptor densities were low and not affected by a high-salt diet or ARBs. However, rat models of renal artery occlusion and SHR did show a change in AngII receptor levels in the heart. In cardiomyocytes, VSMC and perivascular tissue, AT_1R expression seemed to increase whereas

AT_2R expression seemed to decrease (Ozono et al., 2000), validating previous rat (Wang et al., 1998) and human (Nozawa et al., 1996) studies. However, one study found no change in the proportion of the receptors (Suzuki et al., 1993).

1.1.5.3 Myocardial Infarction

MI is the most common cause of heart failure (Kim and Iwao, 2000). It is suspected that activation of the local and circulating RAS after MI may initiate and promote cardiac remodelling responsible for the eventual heart failure (Staufenberger et al., 2001). The process of LV remodeling after acute MI involves alterations in both infarcted and non-infarcted regions, and in both myocytes and fibroblasts (Nio et al., 1995). The infarcted region experiences dilatation and thinning (Weisman et al., 1985), while remote myocardium is subjected to increased pressure and volume overload causing myocyte hypertrophy (Anversa et al., 2000). In rat and mouse models, it has been shown that AT_1R are upregulated post-infarction (Meggs et al., 1993; Suzuki et al., 1993; Verjans et al., 2008) and has been localized to the fibroblasts (Staufenberger et al., 2001; Verjans et al., 2008). In one study, AT_1R in the non-infarcted myocardium increased 3 days after coronary artery ligation followed by a decrease at 2 weeks. In the infarcted myocardium, AT_1R and AT_2R increased by 3.2- and 2.3-fold, respectively (Nio et al., 1995). A transient AT_1R upregulation was also detected in the infarct area of an occlusion-reperfusion rat model, peaking at 1-3 weeks post-MI (Higuchi et al., 2007). In a mouse model with permanent coronary artery ligation (Verjans et al., 2008), AT_1R expression was maximally upregulated in the infarct region, nearly 2.4-fold compared to controls, at 3 weeks post-ligation. It has been proposed that the changes in AT_1R and AT_2R expression levels run in parallel with the extent of cardiac hypertrophy and mechanical load imposed on the viable myocardium (Zhu et al., 2003).

The AT_1R has both cardiac and systemic effects post-MI, including mediating vasoconstriction, cellular hypertrophy, and catecholamine release (Matsubara, 2001). The AT_2R is thought to oppose these actions (Johren et al., 2004; Voros et al., 2006; Widdop et al., 2003; Xu et al., 2002). Animal models have shown that AT_1R blockade is equivalent to AT_2R overexpression in attenuating post-MI remodeling (Voros et al., 2006). Further, it appears that a lack of AT_2R worsens outcomes post-MI and even attenuates the protective effect of AT_1R blockade (Adachi et al., 2003; Ichihara et al., 2002; Oishi et al., 2003; Wu et al., 2002). Other models of cardiovascular disease have corroborated this interplay between the AT_2R and the AT_1R (Jones et al., 2004; Varagic et al., 2001). ACE inhibitors and ARBs are currently used clinically post-MI for their protective effects (Pfeffer et al., 1988; Pfeffer et al., 2003).

1.1.5.4 Heart Failure

Several studies on human heart failure state that cardiac AT_1R density is significantly decreased compared to healthy hearts (Asano et al., 1997; Brink et al., 1996; Lee et al., 1996; Ohkubo et al., 1997; Tsutsumi et al., 1998; Wolf et al., 1996). However, as AT_2R levels either decrease (Asano et al., 1997; Wolf et al., 1996) or remained unchanged (Regitz-Zagrosek et al., 1995), the proportion of AT_1R to AT_2R remains similar at roughly 1:2 (Regitz-Zagrosek et al., 1995). In patients undergoing coronary bypass and/or valvular surgery, the proportion of AT_1R in RA tissue decreased with the degree of cardiac impairment (Lopez et al., 1994). The majority of receptors were found on nonmyocyte cells, with only 10-20% expressed on myocytes (Serneri et al., 2001). In addition, it is interesting to note that myocardial dysfunction frequently occurs in patients with diabetes mellitus and that cardiac AT_1R density (Kim and Iwao, 2000) has been shown to increase in hyperglycemia.

1.1.6 Intracellular AT_1R Signalling in Disease

It is well established that AngII, through AT_1R activation, induces a multitude of detrimental effects ultimately causing cardiac dysfunction. However, the regulatory mechanism determining AT_1R receptor expression is not well understood (Sechi et al., 1992).

The AT_1R and AT_2R belong to the class of seven transmembrane G-protein-coupled receptors (GPCRs). AT_1R coupling to heterotrimeric G-proteins, such as $G_{q/11,}$ $G_{12/13}$, and G_i, activates a signalling cascade resulting in physiological effects central to cardiovascular hypertrophy and remodeling, such as inflammation, vasoconstriction, proliferation, growth, matrix production (Figure 1-3). G_q stimulation results in activation of several complex pathways, including the Rho/ROCK pathway which is known to induce smooth muscle contraction, inflammation, and hypertrophy (Seasholtz and Brown, 2004), and the MAP/JAK/STAT pathway which promotes cellular proliferation, growth, and matrix production (Dinh et al., 2001) via increased expression of early response genes, such as *c-fos*, *c-jun* and *c-myc* (Higuchi et al., 2007). Further, G_q coupling increases Ca^{2+} levels thereby promoting aldosterone secretion and vasoconstriction. G_i coupling decreases cAMP levels which in turn causes an influx of Ca^{2+} and vasoconstriction. There is evidence that the AT_1R can activate signalling pathways independent of G-proteins (Zhai et al., 2006), including trans-activation of the EGFR (epidermal growth factor receptors) pathway. The EGFR pathway promotes transcription, protein synthesis and translation initiation making it central to vascular and cardiac hypertrophy (Asakura et al., 2002; Higuchi et al., 2007; Thomas et al., 2002). Further, it is suspected that the ROS produced as a result of AT_1R activation may promote the endothelial dysfunction found in atherosclerosis, diabetes, obesity and hypertension, and that these ROS may stimulate other growth-factor pathways resulting in cardiac hypertrophy and fibrosis (Ferreira-Machado et al.; Higuchi et al., 2007).

1.1.7 RAS Inhibitors

Clinically, the detrimental effects of AngII in diseases such as hypertension, heart failure, and end organ damage (Regitz-Zagrosek et al., 1995; Tuccinardi et al., 2006) are suppressed by two main therapeutics, 1) ACE inhibitors and 2) ARBs, such as losartan and candesartan. Recently, ARBs have become an attractive alternative to ACE inhibitors due to a coughing side effect resulting from an excess in bradykinin. Secondly, ACE inhibitors are competitive inhibitors and as such can be overcome by increased levels of AngI resulting from removal of the negative feedback effect of AngII on renin release. Although AT_1R inhibition results in increased AngII production, it is suspected that the resulting increases in AT_2R stimulation may be beneficial, accounting for some of the cardioprotective effects (Zhu et al., 2003) not seen with ACE inhibition. Several clinical studies have demonstrated the ability of losartan, and ARBs in general, to reduce the risk of cardiovascular mortality, stroke, MI and nephropathy (Berl, 2004) (see review in Naik, 2010). However, there is no evidence indicating superior efficacy of one treatment over the other.

ARBs are classified as either surmountable or insurmountable according to their capacity to inhibit or depress the effect of AngII (Naik et al., 2010; Fierens et al, 1999). Losartan is a surmountable antagonist whereas candesartan and EXP3174, the active metabolite of losartan, are insurmountable antagonists. Surmountable antagonists, also known as competitive antagonists, interfere with receptor activation by physically blocking the active site. Insurmountable antagonists, typically non-competitive antagonists, bind to an allosteric site of the receptor stabilizing it in an inactive conformation. However, it is also possible that an insurmountable antagonist may act competitively but bind so tightly and dissociate so slowly as to appear non-competitive. That is, the equilibrium dissociation constant (K_d), a ratio of the rate of dissociation (k_{off}) over the rate of association (k_{on}), is very small. Unlike with surmountable

antagonists, addition of more agonist will not reinstate the receptor's maximal response to agonist stimulation (Vanderheyden et al., 1999).

1.1.7.1 SAR of Losartan

Through the process of developing the first non-peptide, or small molecule, AT_1R antagonist DuP753, later named losartan, a structure-activity relationship (SAR) was identified (Carini et al., 1991) (Table 1-3). Compounds achieved greater AT_1R antagonism if they contained a biphenyl moiety with an acidic or hydrogen-bond acceptor group, such as a tetrazole, at the ortho position, and a heterocyclic ring, to act as a hydrogen-bond acceptor, with a short alkyl chain at the 2-position for hydrophobic interactions (Timmermans et al., 1993) (Figure 1-4). The resultant hypothesized binding pocket (Duncia et al., 1992) contained 3 lipophilic pockets, a positive charge to interact with the tetrazole, and a possible second positive charge to interact with the imidazole 5-substituent (Santella et al., 1994). In the tetrazole series (Carini et al., 1991), it was found that binding affinity was sensitive to substitution at the imidazole 5-position. The bulkier the side chain, the lower the binding affinity; anything larger than a CH_2OH group resulted in decreased binding affinity. It was thought that a large group at this position prevents the biphenylyltetrazole from achieving the optimal conformation needed for good binding affinity. Other studies (Kiya et al., 2010), have indicated that a hydrogen donor in place of the alkyl chain will provide higher binding affinity. This SAR has led to the development of multiple ARBs with this core biphenyl structure attached to an acidic moiety (Naik et al., 2010).

1.1.7.2 Losartan Metabolism

A foreign substance can undergo numerous structural changes before it is finally eliminated from the body. A major excretion pathway is the urine for which the compound must be made

sufficiently polar to dissolve in water. Polarity or hydrophilicity is increased by either: 1) insertion of polar functional groups such as hydroxyl (OH), carboxyl (COOH), or amine (NH_2) through oxidation reactions, or 2) conjugation with small polar groups such as glucuronic acid, sulfate, or glycine. The metabolism of losartan differs between rats, monkeys and humans (Stearns et al., 1992). In rats, the primary route of metabolism is oxidation by the liver, resulting in either the hydroxyl or carboxyl derivative. In monkeys, glucuronidation of the tetrazole is the predominant metabolic route. Humans metabolize losartan almost equally by both routes. EXP3174 is the major metabolite of losartan. In humans, approximately 14% of Losartan is converted to EXP3174 (Lo et al., 1995; Stearns et al., 1995). It is produced from a two-step oxidation process by cytochrome P450 in the liver: losartan is slowly converted to the aldehyde EXP3179 which is then relatively quickly converted to the 5-carboxy derivative EXP3174 (Sica et al., 2005; Stearns et al., 1995). *In vitro* studies with fresh human liver slices showed that, in addition to EXP3174, five other minor metabolites are also produced (Stearns et al., 1992). However, only EXP3174 had noteworthy activity. In fact, it is 10-40 times more potent than losartan (Chiu et al., 1990; Wong et al., 1990a; b; c). EXP3174 also has a greater affinity for the AT_1R than losartan (IC_{50} = 3.7 nM vs IC_{50} = 19 nM in rat adrenal cortex) (Chiu et al., 1990; Wong et al., 1990c) but has less selectivity for the AT_1R over the AT_2R (3,000-fold vs 30,000-fold) (Wong et al., 1990c). In rats, the oral bioavailability of losartan and EXP3174 is 33% and 12%, respectively (Lo et al., 1995). It is suspected that poor absorption and first-pass metabolism attributed to this low bioavailability. Losartan has a short biological half-life of around 1.8-2.1 h and is minimally cleared by the kidneys (12%), whereas EXP3174 has a half-life of roughly 6.3 h and undergoes significant renal clearance (55%) (Lo et al., 1995). In the plasma, protein binding was high for both losartan and EXP3174 around 99.6-99.8% (Christ, 1995) which may explain why losartan does not readily cross the blood brain barrier (Bui et al., 1992).

1.2 Nuclear Imaging

Nuclear imaging is based on the application and detection of decaying radioisotopes. In most cases, the radioisotope is combined with a biologically active compound to form a radiolabeled probe capable of imaging a specific biochemical pathway or event *in vivo*. The detection of the radiation emitted upon radionuclide decay is performed by either positron emission tomography (PET) or single photon emission computed tomography (SPECT). PET and SPECT have been used extensively for non-invasive imaging of metabolic pathways connected with the pathophysiology of a disease, enabling early detection and diagnosis (Hutchins et al., 2008). More recently, nuclear medicine has been increasingly applied to the drug discovery and development process, the study of small animal models, and in characterizing gene expression and phenotypes in genetically modified animals (Green et al., 2001). PET and SPECT are highly sensitive imaging modalities, but suffer from low resolution in comparison to X-ray, CT, ultrasound, and MRI which are used to image morphology (Table 1-4) (Price, 2001). Resolution affects the level of detail that can be visualized in an image and limits the size of structures for which accurate quantification of radionuclide concentrations can be achieved (Hoffman et al., 1979). It is mostly limited by the number of detected events (sensitivity), statistical noise, detector element size, positron range, and non-collinear annihilation (Cherry, 2001).

1.2.1 SPECT Imaging

Both SPECT and PET provide quantitative functional and metabolic information, such as perfusion, protein concentrations and ligand binding (Hutchins et al., 2008). The radioisotopes used in SPECT are produced by either a nuclear reactor or particle accelerator and typically have longer half-lives than PET isotopes (Table 1-5); Tc-99m and I-123 have half-lives of 6.02 h and

13.3 h, respectively (Gomes et al., 2011). The two image modalities also differ in the way the radionuclide decays. SPECT isotopes decay through emission of single gamma ray which is detected by gamma cameras rotating around the subject. The gamma camera converts the gamma ray to light photons via scintillation detectors. A collimator, a lead block containing many narrow parallel holes, is situated in front of the detector to gather positional information, albeit at a cost to sensitivity (Lodge et al., 2005). One advantage of SPECT over PET is the ability to image multiple tracers simultaneously; one can discriminate between two different nuclides by the unique energy range of their emitted gamma rays (Rahmim and Zaidi, 2008).

1.2.2 PET Imaging

PET tracers contain short-lived positron-emitting isotopes, such as ^{15}O, ^{13}N, ^{11}C, or ^{18}F. F-18 labeled PET tracers have the advantage of a longer 109.7 min half-life (Gad, 2008) enabling multiple patient scans from a single production as well as the ability to ship tracer to remote imaging facilities that do not have a cyclotron and radiochemistry capabilities, often required to generate PET isotopes. In a cyclotron, particles such as protons and deuterons (nucleus of ^{2}H; a neutron and proton) are produced and accelerated to a high energy after which they are directed at a target material. The particle is absorbed by the target nucleus resulting in a nuclear transformation, creating an unstable proton-rich nucleus alongside ejection of other particles. For example, when O-18 enriched water is bombarded with 11 MeV protons, F-18 is produced alongside a neutron. This nuclear reaction can be written as $^{18}O(p, n)^{18}F$ (Ferrieri, 2003).

$$^{18}_{8}O + ^{1}_{1}H \longrightarrow ^{18}_{9}F + ^{1}_{0}n$$

Proton-rich radionuclides achieve a more stable conformation through positron emission (β^+) or electron capture (Ɛ) (Hutchins et al., 2008). A positron is a positively charged particle with the same mass as an electron. In the process, a proton is converted to a neutron alongside

expulsion of a positron ($^{0}_{1}\beta$) and neutrino (ν). That is, the atomic number (Z) decreases by 1 whereas the mass number (A) remains the same. For example, decay of $^{18}_{9}$F (9 protons, 9 neutrons) produces $^{18}_{8}$O (8 protons, 10 neutrons) (Saha, 2008).

$$^{18}_{9}\text{F} \longrightarrow {}^{18}_{8}\text{O} + {}^{0}_{1}\beta + \nu + {}^{0}_{1}e$$

According to the law of conservation of energy, the increase in atomic mass of the decay product requires that the binding energy of the daughter nucleus be greater than that of the mother nucleus. The difference between these energies goes into the reaction of converting a proton into a neutron, a positron and, a neutrino and into the kinetic energy of these particles. In the case of F-18 to O-18, the difference in mass provides an equivalent of 0.630 MeV of kinetic energy according to the relationship $E = mc^2$ (Hendee et al., 2005). Alternatively, the nucleus can increase its number of neutrons by undergoing electron capture, a process whereby an electron from an inner orbital is combined with a proton to transform it into a neutron. F-18 undergoes positron emission 96.7% of the time and electron capture the rest of the time (Hutchins et al., 2008).

$$^{1}_{1}p + {}^{0}_{1}e \longrightarrow {}^{0}_{1}n + \nu$$

In the body, a positron travels only a short distance before losing kinetic energy and annihilating with a nearby electron. Abiding by the law of conservation of energy, the annihilation converts their rest masses to two 511 keV photons emitted in opposite directions (conservation of momentum) (Figure 1-5). However, the energy released during beta decay is shared by the neutrino and the positron and thus there is a spectrum of energies available to the positron and a resultant range of distances. However, only small minority of positrons reach the maximum distance. This variable distribution causes image blurring (Budinger et al., 1984).

$$^{0}_{1}\beta + {}^{0}_{1}e \rightarrow \gamma$$

PET scanners have a circular ring of paired gamma ray detectors positioned along the length of the subject which are configured to register only photon pairs that strike opposing detectors within a specific time, or coincidence window. The most common detector type is a block detector, which consists of scintillation elements, or crystals, coupled to a photomultiplier tube to collect scintillation light for crystal identification (Hutchins et al., 2008). The detection of coincidence events identifies a line of response (LOR) in which the decay occurred. By incorporating the difference in detection times of two annihilation photons, time-of-flight (TOF) PET provides the probability the event occurred at a specific voxel (volumetric pixel) along the LOR (Rahmim and Zaidi, 2008). In 2D PET, detectable annihilation events are restricted by collimation to a plane of a limited number of detector rings. However, in 3D PET, these collimators are reduced or removed enabling detection of photons spanning several detector rings. Although this method increases detection sensitivity and reduces scan time, background noise increases and more complicated reconstruction algorithms are required (Defrise, 2001).

In order to produce a more accurate image, phenomena such as partial volume effect and attenuation must be corrected. If a region of interest (ROI) is smaller than the sensitive region of the detector pairs used to detect the annihilation, partial volume effect occurs. Due to this phenomenon, activity in the ROI is either diluted by a surrounding region of lower intensity (ie. background) or over-estimated by a region of high intensity (ie. liver) (Hutchins et al., 2008). Attenuation is the loss of detection of true coincidence events because of their absorption in the body or scattering out of the detector field of view creating image noise and distortion. An attenuation correction is performed by either CT or a transmission scan with an external radioactive source, such as ^{137}Cs or ^{68}Ge. A CT scan creates a density map of the body that can be used to correct for the differential absorption of photons as attenuation is greater in the center of the body and in regions surrounded by dense tissue. For transmission scans, a blank scan is

performed and compared with a scan where the subject was exposed to the external radiation source and correction factors are applied for each LOR (Saha, 2008).

1.2.2.1 Small Animal PET Imaging

Small animal imaging holds great promise as a translation tool for the understanding of human disease. However, an important difference between preclinical and clinical PET is the size of the subject. Humans typically weigh 2,500-3750 times more than a mouse and 250-375 times more than a rat (Hutchins et al., 2008), translating to about a 10 times larger volume (Green et al., 2001). Therefore, if image resolution of small animals is to be equivalent to human images, the spatial resolution of the small animal PET scanner would need to improve by a factor of 10. Spatial resolution in PET imaging systems is typically characterized as the full-width-at-half-maximum (FWHM) of a profile that runs through the center of a point or perpendicular to a line source image. If an object is smaller than approximately 2.5 times the FWHM spatial resolution of the PET scanner, a distortion called partial volume effect occurs (Hutchins et al., 2008). Currently, clinical PET scanners have a spatial resolution around 6-8 mm, whereas microPET scanners have around 2-3 mm FWHM resolution (Cherry, 2001). Consequently, the ratio of the volumetric spatial resolution to animal mass is approximately 30 times lower for mice and 3 times lower for rats than in human PET imaging (Hutchins et al., 2008).

1.2.2.2 PET Radiotracer Design

Whereas PET tracers used to measure global or regional targets, such as glucose utilization, blood flow and oxygen metabolism, advances in our understanding of biochemistry have led to more specific target, such as specific receptors, 2nd messenger systems, and neuronal networks. Once a target has been identified for imaging, either a new compound can be synthesized or

modifications can be made to a pre-existing compound, such as a commercial pharmaceutical with a known pharmacological profile. True radiotracers are chemically identical to the natural substance and can thus 'trace' a homeostatic system without disturbing it when administered at tracer doses. Generally, the target compound is labeled with F-18 by substitution of a hydrogen (H) or a hydroxyl group (OH) (Mach and Schwarz, 2010). Regardless of the radionuclide, it is important that the labeled compound maintain the biological and chemical properties of the parent compound.

The ideal tracer should meet several important criteria: high target-to-background ratio, rapid clearance from plasma, low non-specific binding, no metabolites in the target tissue, high binding affinity, high specificity, simple kinetic modeling, and entail minimal radiation exposure (Mach and Schwarz, 2010; Vallabhajosula, 2009). With regards to the radiochemist, the reaction should be fast, easy, reproducible, high-yielding and amendable to automation. An automated synthesis module is essential for routine production in order to reduce radiation exposure to personnel, and achieve reliability and efficiency. It was not until the early 1990s that the first commercially available automated FDG system became available. The lipophilicity of the compound plays an important role in its absorption, distribution, metabolism and elimination (ADME). There is a specific window of lipophilicity that is ideal - high enough to diffuse across biological membranes, but not so great that it binds preferentially to lipid-rich tissue thus reducing its bioavailability and increasing non-specific binding. Lipophilicity is measured by the log*P* value, the logarithm of the partition between octanol and water; log *D* values are used if the compound is ionizable. The binding affinity of a tracer is important when the density of the target is low or when there is a competing endogenous ligand. Specific activity (SA), the amount of labeled to unlabeled compound, becomes an important factor when the receptor or target protein is saturable and/or present in low density. The lower the target density, the higher the

SA needed to ensure that the unlabeled compound does not compete for the binding sites, especially is the half-life is short. It is estimated that with current microPET systems, injectable activity is limited to 5.4 MBq in rats. When studying saturable receptors with an intermediate-affinity compound, this translates to a required SA of around of 100 MBq/nmol in order to maintain < 1% receptor occupancy (Hume and Myers, 2002); (Kilbourn and Shao, 2009). For ^{11}C- and ^{18}F-labeled radiotracers, 1-10 μg of unlabeled compound are usually synthesized because of the presence of dilution with the stable isotopes (Cunningham, 2005) during production, purification and/or preparation of the tracer. Achieving high specific activity is especially challenging for C-11 labeled tracers due to the ubiquity of C-12 in the environment and the short half-life of C-11.

1.2.2.3 Radiolabeling with F-18

The most commonly used methods of producing F-18 are: 1) proton irradiation of O-18 enriched water ([^{18}O]H_2O), by the $^{18}O(p,n)^{18}F$ nuclear reaction, to produce no-carrier-added nucleophilic fluoride, and 2) deuteron bombardment of neon to produce carrier-added electrophilic fluorine as [^{18}F]F_2 from the $^{20}Ne(d,\alpha)^{18}F$ nuclear reaction (Ferrieri, 2003; Kilbourn and Shao, 2009). Synthesis with [^{18}F]F_2 will clearly result in products with lower SA. The theoretical maximum SA for F-18 labeled compounds is 1710 Ci/μmol, but in practice is much lower, commonly between 0.5-10 Ci/μmol, due to dilution with F-19 (Kilbourn and Shao, 2009; Berridge et al., 2009).

There are various methods in which to label a compound with F-18 fluoride. The main synthetic strategies involve either i) direct fluorination through nucleophilic substitution, or ii) indirect fluorination via addition of a small F-18 labeled compound called a prosthetic group (Figure 1-6). In terms of optimizing specific activity, the logical sequence would be the former.

Nucleophilic substitution by anionic fluorine involves displacement of a good leaving group, such as a sulfonate ester or halide. When labeling a sensitive biomolecule, which can denature or decompose under the harsh conditions required for nucleophilic substitution (ie. high temperature and strongly basic), it has become common to use the latter method: first label a prosthetic group with F-18 and then conjugate the prosthetic group with the biomolecule under milder conditions (Li and Conti, 2010).

It is important to note that nucleophilic substitution reactions are typically performed in aprotic solvents under near anhydrous conditions; solvated F-18 is a poor nucleophile. The F-18 enriched water is typically passed through an anion-exchange cartridge to trap the F-18 anions which are then eluted by a solution containing organic solvent, such as MeCN, and a source of counterion, such as potassium carbonate, dissolved in as little water as possible. A phase transfer agent, such as Kryptofix2.2.2 (K_{222}), is added prior to removing the water in order to complex with the potassium cation, leaving the fluoride anion exposed and highly reactive (Li and Conti, 2010). Water is then removed by azeotropic evaporation with MeCN.

One method that has become popular for radiolabeling PET and SPECT tracers (Nwe and Brechbiel, 2009) is 'click' chemistry and was first described by Kolb, Finn and Sharpless (Kolb et al., 2001). These reactions abide by specific criteria: they must be feasible in mild reaction conditions (ie. neutral pH, atmospheric pressure, ambient temperature), stereospecific, wide in scope, amenable to both small and large scale, irreversible (Nwe and Brechbiel, 2009), reactants should be readily available, products should be easily purified and in good yields (Kolb et al., 2001). Further, the click reactions should be bio-orthogonal, meaning the reactants will only react with each other. The mainstay of click chemistry is the Cu(I)-catalyzed [3+2] azide-alkyne cycloaddition (CuAAC) (Kolb and Sharpless, 2003). The CuAAC reaction has been implemented in a variety of applications, including high-throughput screening of a drug library, bioconjugate

labeling of cells, proteins, sugars, or nucleic acids, and recently radiolabeling azide-functionalized nanoparticles with alkyne modified peptides as a method for targeted drug delivery (Lu et al., 2009). The relatively slow thermal reaction was first described by Huisgen in 1963 (Huisgen, 1961) and was reinvented by Sharpless (Rostovtsev et al., 2002) and Medal (Tornoe et al., 2002) in 2001 to the current kinetically driven reaction which proceeds at up to 10^7 times the rate of its thermal counterpart (Appukkuttan et al., 2004), in near-quantitative yields, under mild reactions conditions, and oftentimes in aqueous media (Kolb et al., 2001; Kolb and Sharpless, 2003; Nwe and Brechbiel, 2009; Rostovtsev et al., 2002; Tornoe et al., 2002). The CuAAC is one of only a handful of truly chemoselective and regioselective reactions; that is, the azide and alkyne preferentially react with each other and the sole product is the 1,4-disubstituted triazole. The thermal reaction, on the other hand, affords a mixture of the 1,4- and 1,5-disubstituted triazole (Figure 1-7) (Gothelf and Jorgensen, 1998). As a result of atom position and electronic properties, the triazole acts as rigid peptide bond isostere (Figure 1-8) but without the same susceptibility to hydrolysis, reduction, or oxidation under physiological conditions (Horne et al., 2004; Park et al., 2001). The triazole can interact with biomolecules through two weak hydrogen bond acceptors and one hydrogen bond donor resulting from a very strong dipole moment (Palmer et al., 1974; Purcell, 1967).

Several ^{18}F-labeled alkyne prosthetic groups (Figure 1-9) and their subsequent use in CuAAC have been described in the literature. The first was in 2006 by Marik and Sutcliffe (Marik and Sutcliffe, 2006) who investigated the use of various F-18 labeled alkynes, prepared via nucleophilic displacement of the corresponding tosylate with [^{18}F]fluoride, for the radiolabeling of azide-functionalized peptides. The volatile [^{18}F]fluoroalkynes were purified by co-distillation with MeCN. The first stable fluoroaromatic alkyne was then synthesized from the treatment of N-succinimidyl-4-[^{18}F]fluorobenzoate ([^{18}F]SFB) with propargyl amine (Ramenda et al., 2007). In

2008, Inkster et al (Inkster et al., 2008) prepared a fluoroaromatic alkyne containing a stable ether linkage, [^{18}F]FPy5yne, in > 90% radiochemical yield via nucleophilic substitution of either a nitro group or trimethylammonium triflate. An analog of this compound, [^{18}F]FPyKYNE (Dollé et al., 2008), soon followed. Conversely, the CuAAC may proceed through an F-18 labeled azide (Figure 1-9). Similar to the method instated by Marik and Sutcliffe (Marik and Sutcliffe, 2006), Glaser et al (Glaser and Arstad, 2007) synthesized 2-[^{18}F]fluoroethylazide from the corresponding tosylate precursor and purified via distillation. Soon thereafter, various ^{18}F-labeled terminal alkynes and azides containing an ether backbone, and reduced volatility, were produced (Li et al., 2007; Sirion et al., 2007). Kolb et al (Kolb, 2008) targeted the integrin receptor by functionalizing a galacto-RGD peptide (Haubner et al., 2003) with an azide for coupling with an aliphatic F-18 labeled alkyne. [^{18}F]FPyKYNE has also been used to label azide-functionalized RGD for imaging atherosclerotic plaques in our lab (Valdivia et al., 2011). It is important to note that the source of Cu(I) and the reaction conditions are oftentimes tailored to the particular application.

1.2.3 AT_1 Receptor Imaging

AT_1R were first imaged *in vitro* with [^{3}H]-labeled AngII analogs. However, due to the low energy beta particle and low specific activity of these tracers, they were replaced with iodinated analogs such as [^{125}I]AngII and [^{125}I]Sar^{1}-Ala^{8}-AngII, also known as saralasin. A slight modification on [^{125}I]saralasin provided [^{125}I]Sar^{1}Ile^{8}-AngII, a more potent antagonist. [^{125}I]AngII and [^{125}I]Sar^{1}Ile^{8}-AngII are commonly used to investigate the distribution of AngII receptors in autoradiography and binding studies (Szabo et al., 2010).

The first non-peptide AngII antagonist was DuP753, later named losartan, developed by DuPont Merck Pharmaceutical Company (Carini and Duncia, 1988). Building upon the

biphenyltetrazole structure, [^{125}I]EXP985 was developed as the first high specific activity non-peptide radioligand for imaging the AT_1R (Chiu et al., 1992). MK-996, from the non-tetrazole class of compounds, displayed the highest *in vitro* affinity for the AT_1R and was labeled with I-125 to form the [^{125}I]iodopyridyl analog (K_d = 0.52 nM) (Chen et al., 1995). Although tritium and I-125 proved useful for *in vitro* binding studies and autoradiography, it was realized that a strong gamma or positron-emitting isotope would be required if *in vivo* imaging be performed with the high sensitivity, quantitative accuracy and spatial resolution provided by SPECT or PET.

1.2.3.1 SPECT Tracers

SPECT tracers targeting the AT_1R include I-123 and I-125 analogs of [Sar^1,Ile^8]AngII and most recently, a ^{99m}Tc-labeled losartan analog (Verjans et al., 2008). The latter analog comprises a losartan backbone modified with leucine at the hydroxyl position conjugated to a tetra-amine chelate through a tetraethylene glycol diglycolic acid linker (Figure 1-10) and is actually stated to have a higher affinity for the AT_1R than losartan (K_i = 60 pmol/l vs 10 nmol/l). AT_1R upregulation was imaged in a HF mouse model with permanent artery occlusion.

1.2.3.2 PET Tracers

The first PET radiotracer targeting the AT_1R was the non-peptide antagonist [^{11}C]MK-996, developed by Johns Hopkins University (Baltimore, MD) followed by their a O-methyl *para*-substituted analog [^{11}C]L-159,884 (IC_{50} = 0.08 nM) (Hamill et al., 1996) (Figure 1-11). [^{11}C]L-159,884 showed high uptake in the kidneys, lungs, and heart. In particular, the tracer showed that the AT_1R is localized primarily to the renal cortex of the kidney. However, initial human studies showed rapid tracer metabolism (Mathews et al., 2004). The most recent advance was the development of radiotracer [^{11}C]KR31173 (IC_{50} = 3.27 nM) (Mathews et al., 2004) based on

SK1080 (Lee et al., 1999) developed by the Johns Hopkins group (Figure 1-11) in 2003. The [^{11}C]KR31173 tracer had high specific binding in the renal cortex of canine and baboon (92% and 81% respectively) as well as in baboon myocardium (96%) although total uptake was approximately 5-fold lower than in the kidneys (Zober et al., 2006). The tracer was used to detect a transient upregulation in cardiac AT_1R in the infarct area 1-3 weeks following myocardial ischemia-reperfusion injury in rats (Higuchi et al., 2010) as well as an upregulation in kidney AT_1R in a pig model of renal artery stenosis (Xia et al., 2008). Preliminary testing in humans showed increased uptake in transplanted kidneys versus controls (Szabo et al., 2010).

In 2009, the UOHI radiochemistry lab synthesized [^{11}C]methyl candesartan and its desethyl derivative [^{11}C]TH_4 (Figure 1-12) (Hadizad et al., 2009). MicroPET studies in rats showed [^{11}C]methyl candesartan had high uptake in kidneys with 75-90% specific binding and a higher selectivity for AT_1R than [^{11}C]TH_4. Both tracers showed high liver uptake and tracer wash-out from the kidneys by 30 min. MicroPET images of post-MI and 5/6 nephrectomy rat models with [^{11}C]methyl candesartan demonstrated renal AT_1R upregulation (Mackasey, 2012). In 2010, [^{11}C]methyl losartan was characterized in rats. The tracer showed good kidney uptake, high contrast to surrounding tissue, and high specific binding for renal AT_1R (Antoun, 2010). As with the candesartan analog, no cardiac uptake was observed in normal rats.

There is very little in the literature regarding F-18 labeled AT_1R tracers. Seeing the beneficial properties of F-18 over C-11, the John's Hopkins group recently developed [^{18}F]KR33943, an analog of SK-1080. However, it showed lower binding than [^{11}C]KR31173 in mice, especially in the heart (Mathews and Szabo, 2010). They suspect that a low specific activity may have saturated the low density AT_1R.

Table 1-1 Major sites of AT_1 or AT_2 receptor expression in the adult mammal.

	AT_1R	AT_2R
Kidney		
Glomeruli	+	
Proximal tubules	+	
Vasculature	+	+
Medullary interstitial cells	+	
Adrenal gland		
Cortex	+	+
Medulla	+	+
Heart		
Myocardium	+	+
Ganglia	+	
Conduction system	+	
Brain		
Circumventricular organs	+	
Thalamus	+	+
Basal ganglia	+	
Cerebellar cortex	+	+
Medulla oblongata	+	

Adapted from Allen, AM et al. *Am J Hypertens.* 2000.

Table 1-2 Proportion of AT_1 and AT_2 receptors in the human and rat heart.

	AT_1R (%)	AT_2R (%)	References
Human			
Atria	10:1 atria:ventricle		[80], [82], [83]
	70-77	23-30	[76]
	33	67	[80]
Ventricles	70-77	23-30	[76]
Whole heart	31	69	[81]
Whole heart	50	50	[101]
Rat			
Ventricle	69	31	[85]
Whole heart	50	50	[66], [80], [67]
	10	90	[46]
	91 *	9	[84]
Fibroblast	8:1 fibroblast:myocyte		[86]
	65 **	35	
	> 95	< 5	[87]

* 10:1 AT_{1A}:AT_{1B}

** $AT_{1A}R$ dominant

Table 1-3 Structure-activity relationship (SAR) for losartan derivatives modified at the imidazole 5' position

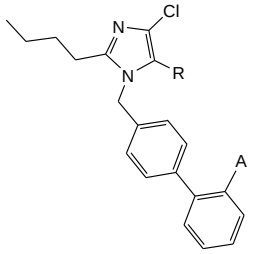

Compound	R	A	IC_{50} (μM)*
2	CH_2OH	COOH	0.23
5	CH_2OCH_3	COOH	0.099
17 *(losartan)*	CH_2OH	CN_4H	0.19
59	$CH_2NHCOOCH_3$	CN_4H	0.06
60	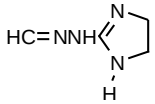	CN_4H	0.29
62	CH(OH)Ph	CN_4H	0.41

* Binding of [^{1}H]AngII (2 nM) to rat adrenal cortical microsomes. Adapted from Duncia, JV et al. *Med Res Rev*. 1992.

Table 1-4 Characteristics of some common imaging modalities.

Imaging modality	Form of energy	Spatial resolution (mm)		Sensitivity (mol/L)	Depth
		Small animal	Clinical [a]		
PET	Annihilation photons	1-2	4-6	10^{-11}-10^{-12}	no limit
SPECT	Gamma rays	1-2	8-12	10^{-10}-10^{-11}	no limit
MRI	Radio frequency waves	0.025-0.1	0.2-1	10^{-3}-10^{-5}	no limit
Ultrasound	High frequency sound waves	0.05-0.5	0.1-1	Not well characterized	mm to cm
CT	X-rays	0.05-0.2	0.5-1	Not well characterized	no limit

Adapted from Massoud and Gambhir, *Genes Dev.* 2003.
[a] Levin, C. *Proc of the IEEE*, 2008; 96 (3):439-467.

Table 1-5 Physical properties of some common positron emitting isotopes.

Isotope	Half-life (min) [b]	Common Nuclear Reaction [a]	β^+ Decay (%)[a]	Avg./max. positron energy (MeV) [c/b]	Avg./max. positron range in soft tissue (mm) [c/b]	Theoretical maximum SA (Ci/μmol) [b]	Decay Product [b]
^{15}O	2.05	^{14}N(d,n)^{15}O	99.9	0.735 / 1.70	3.28 / 8.0	90800	N-15
^{13}N	9.98	^{16}O(p,α)^{13}N	99.8	0.492 / 1.19	2.05 / 5.4	18900	C-13
^{11}C	20.4	^{14}N(p,α)^{11}C	99.7	0.386 / 0.96	1.52 / 4.1	9220	B-11
^{18}F	109.8	^{18}O(p,n)^{18}F	96.7	0.250 / 0.69	0.83 / 2.4	1710	O-18

SA; specific activity

[a] Gad, SC, ed. *Pharmaceutical manufacturing handbook: production and processes*. No.10. New Jersey: Wiley Interscience; 2008.
[b] Welch, MJ and Redvanly, CS, eds. *Handbook of radiopharmaceuticals: radiochemistry and applications*. West Sussex: Wiley and Sons; 2003.
[c] Tai, YC and Laforest, R. *Annu Rev Biomed Eng.* 2005;7:255-285.

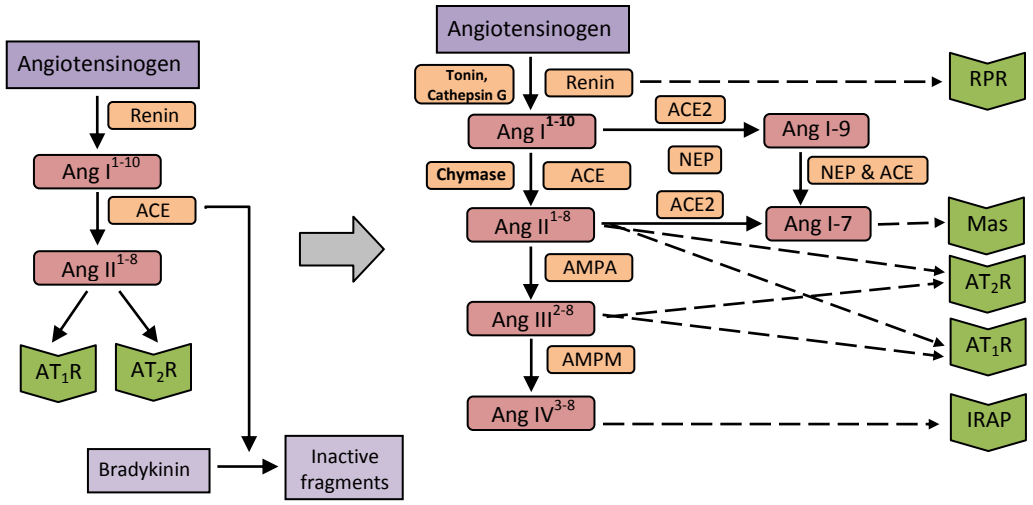

Figure 1-1 A schematic diagram of the classic and current renin-angiotensin(-aldosterone) system (RAS). The current scheme incorporates novel synthetic pathways, truncated angiotensin peptides and their respective receptors. Ang, Angiotensin; ACE, angiotensin-converting enzyme; ACE2, angiotensin-converting enzyme 2; RPR, renin / prorenin receptor; Mas, mas oncogene; AT_2R, angiotensin type 2 receptor; AT_1R, angiotensin type-1 receptor; IRAP, insulin-regulated aminopeptidase; AMPA, aminopeptidase A; AMPM, aminopeptidase M; NEP, neutral endopeptidase. Adapted from Fyhrquist & Saijonmaa. *J Intern Med*. 2008.

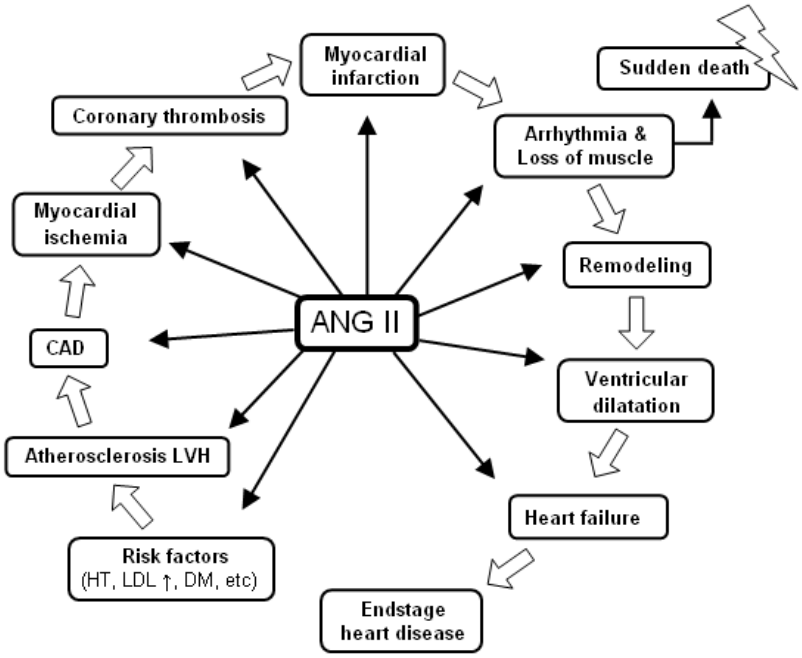

Figure 1-2 The role of Angiotensin II in the progression of cardiovascular disease. AngII: Angiotensin II; CAD: coronary artery disease; DM: diabetes mellitus; LDL: low-density lipoprotein; LVH: left ventricular hypertrophy; HT: hypertension. Adapted from Unger, T. *Am J Cardiol*. 2002.

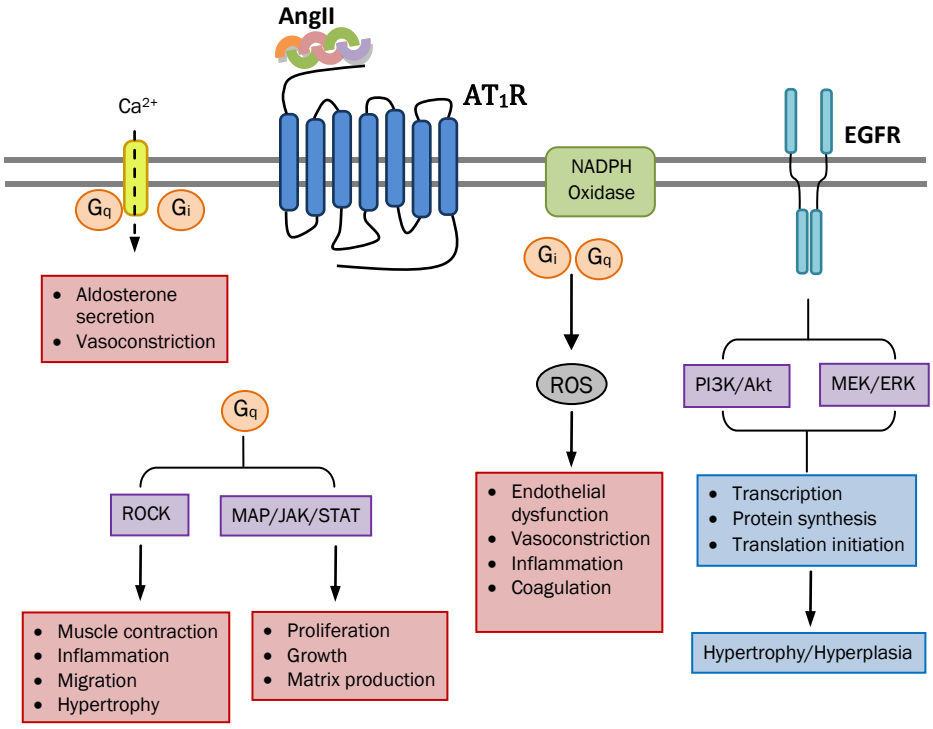

Figure 1-3 Signal transduction of AngiotensinII stimulated AT_1 receptors in VSMCs as it pertains to the pathophysiology of cardiovascular disease. AngII: Angiotensin II; AT_1R: Angiotensin II type-1 receptor; VSMCs: vascular smooth muscle cells; ROS: reactive oxygen species; EGFR: epidermal growth factor receptor. Adapted from Eguchi, S et al. *Clin Sci.* 2007.

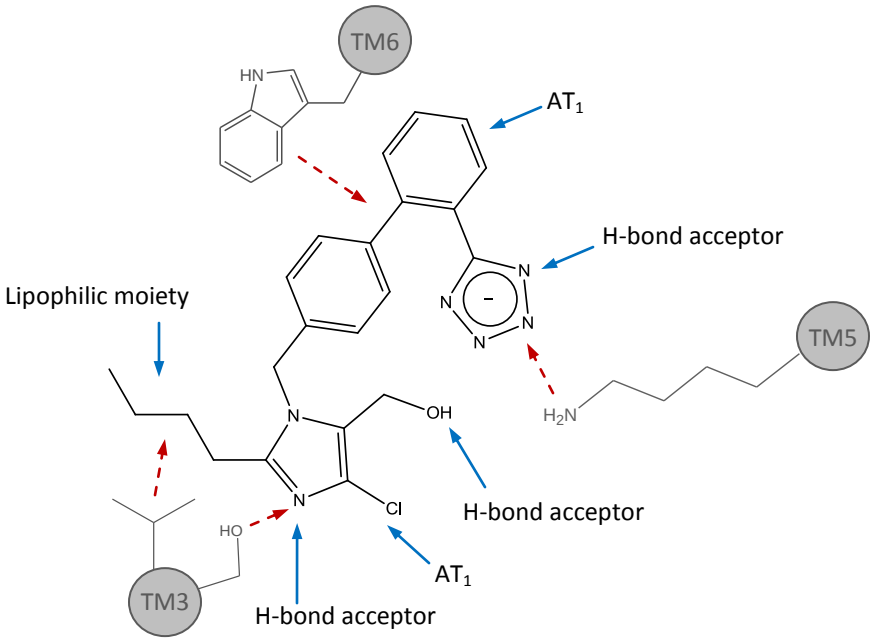

Figure 1-4 Pharmacophore required for specific binding to the AT_1R pocket (solid arrows) and proposed hydrogen bonding and electrostatic interactions (dashed arrows). AT_1: Angiotensin II type 1; TM: transmembrane domain. Adapted from Santella JB et al. *Bioorg Med Chem Let.* 1994 and Naik P, et al. *Bioorg Med Chem.* 2010.

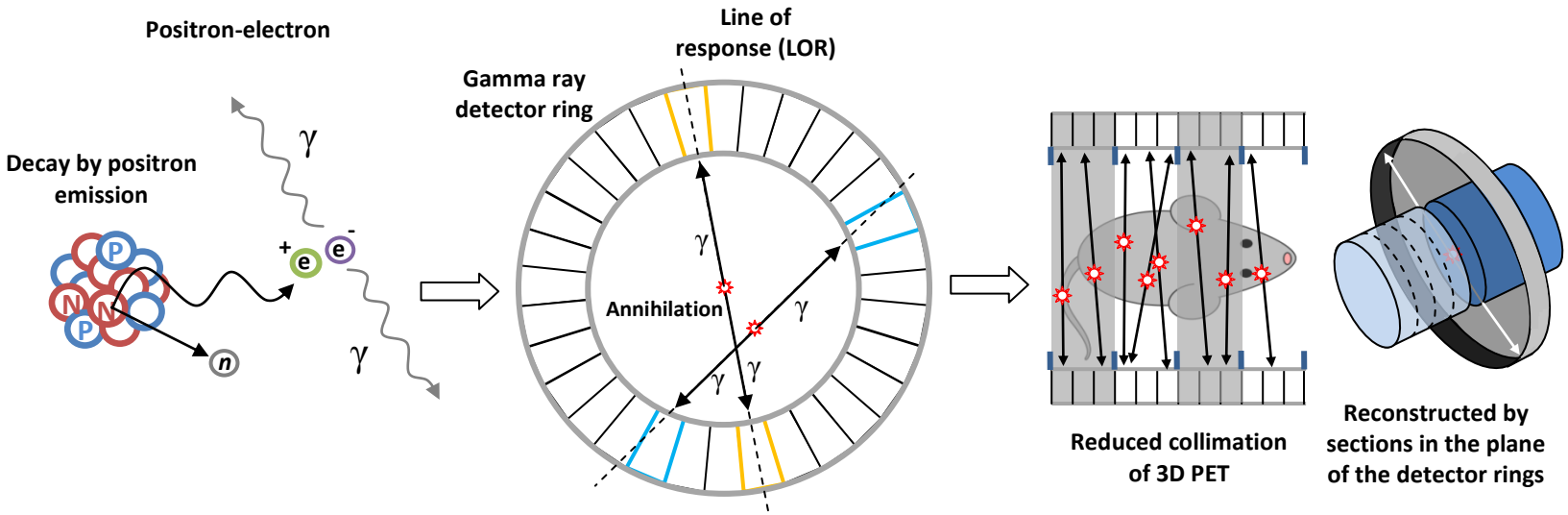

Figure 1-5 Depiction of positron emission tomography (PET). The radionuclide decays via beta decay (β^+), emitting a position which undergoes an annihilation with an electron producing two 511 keV gamma rays at 180^o to eachother. Detectors are located in a ring along the length of the subject. Gamma rays striking two opposing detectors in coincidence create what is called a line of response (LOR) which upon reconstruction by mathematical algorithms generates an image representing a cross section through the subject.

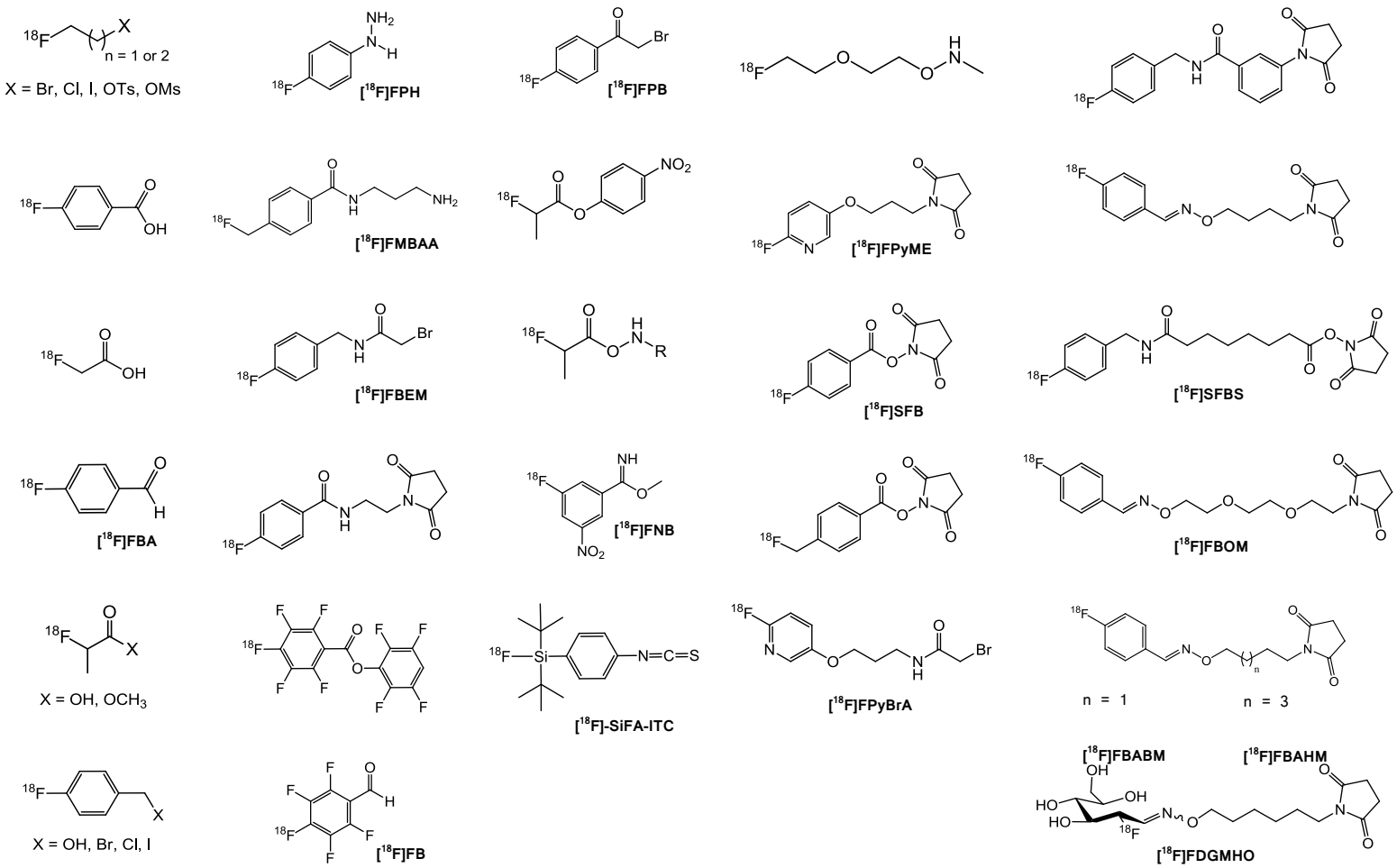

Figure 1-6 Chemical structures of some ^{18}F-labeled prosthetic groups: The majority of compounds shown are referenced in Li, Z and Conti, PS. *Adv Drug Deliv Rev*. 2010; de Bruin, B. et al. *Bioconj Chem*. 2005, 16(2), and Ferrieri R. *Handbook of Radiopharmaceuticals*. 2003. N-methylaminooxy compound, L, can be found in Olberg, DE et al. *Bioconj Chem*. 2008. Maleimide-containing thiol-reactive agent, M, is described in Toyokuni, T. et al. *Bioconj Chem*. 2003.

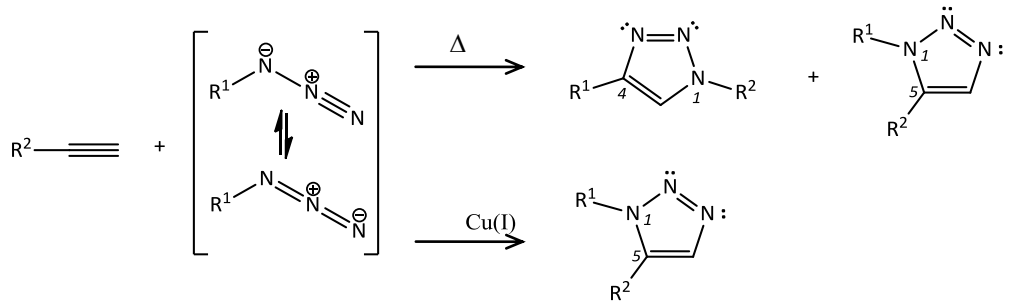

Figure 1-7 Thermal versus Cu(I)-catalysed 1,3-cycloaddition between a terminal alkyne and azide. Thermal conditions produce both the 1,4- and 1,5-regioisomers whereas Cu(I) catalysis produces solely the 1,5-regioisomer. Adapted from Bock, VD et al*. Eur. J. Org. Chem*, 2006.

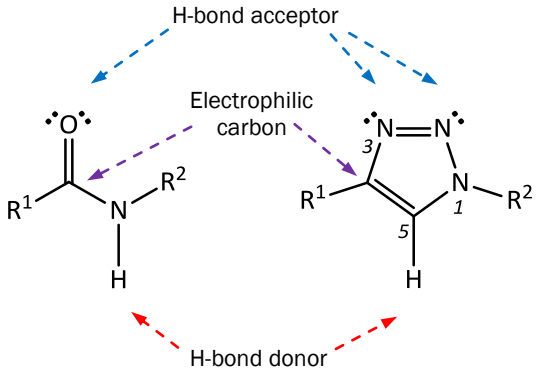

Figure 1-8 The triazole as an amide/peptide bond isotere. Triazole N(2) and N(3) may act as hydrogen bond acceptors like the carbonyl oxygen, whereas C(5) may act as a hydrogen bond donor like the amide proton. Triazole R^1 to R^2 distance is 5.0 Å, compared to 3.9 Å for the amide bond. H-bond, hydrogen bond. Adapted from Bock, VD et al*. Eur. J. Org. Chem*, 2006.

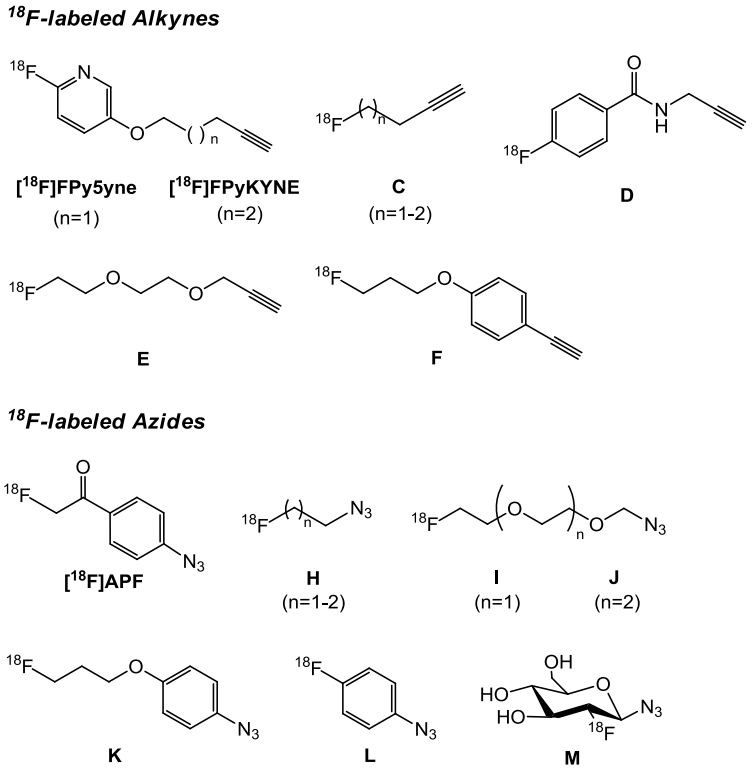

Figure 1-9 Chemical structures of some ^{18}F-labeled prosthetic groups used in the Cu(I)-catalyzed 1,3-cycloaddition 'click' reaction.

References: Compounds A and B: Kuhnast, B et al. *J. Label Compd. Radiopharm.* 2008. Compound C and H: Marik J & Sutcliffe JL, *Tetrahedron Lett*. 2006; Compound D and F: Ramenda, T et al. *Letters in Drug Design; Discovery.* 2007; Compound E: Li Z-B et al. *Bioconj Chem.* 2007. Compound G: Sirion, U et al. *Tetrahedron Lett*. 2007; Compound I and J: Li Z & Conti PS. *Adv Drug Deliv Rev.* 2010; Compound K: Mercier, F. et al. *Bioconj Chem*. 2011; Compound L: Thonon, D et al. *Bioconj Chem.* 2009; Compound M: Maschauer S & Prante O. *Carbohydrate Research.* 2009.

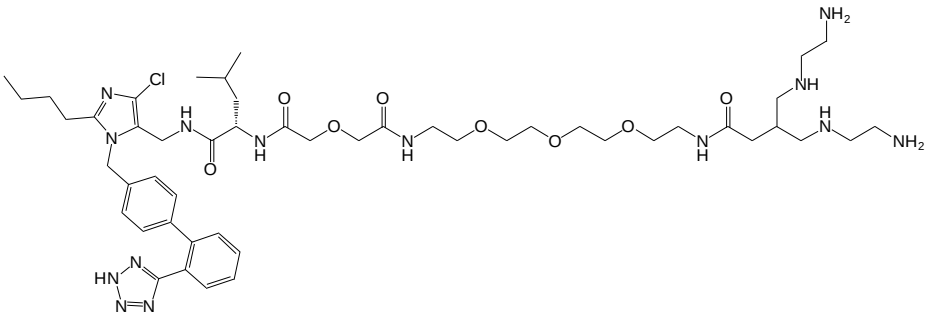

Figure 1-10 Losartan analog containing a tetra-amine chelate for SPECT imaging of the AT_1 receptor with ^{99m}Tc. Developed by Verjans, JW et al., 2008.

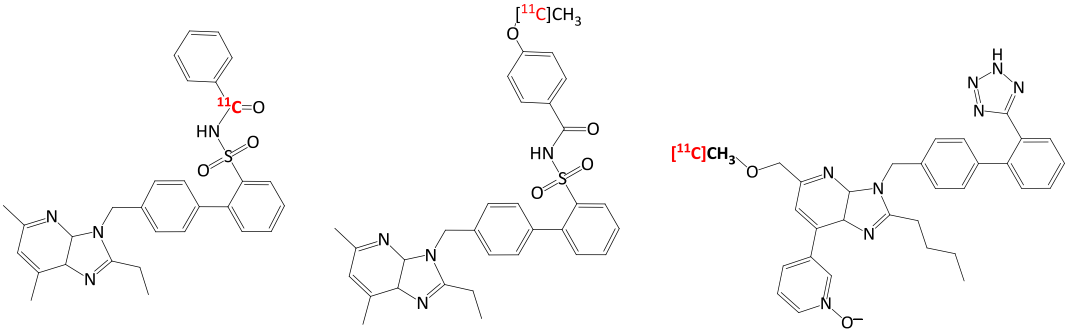

IC_{50} = 0.15 nM IC_{50} = 0.08 nM IC_{50} = 3.27 nM

Figure 1-11 First non-peptide PET tracers targeting the AT_1 receptor. Tracers developed at Johns Hopkins University (Baltimore, MD). *Left to right*: [^{11}C]MK-996, [^{11}C]L-159,884, and [^{11}C]KR31173.

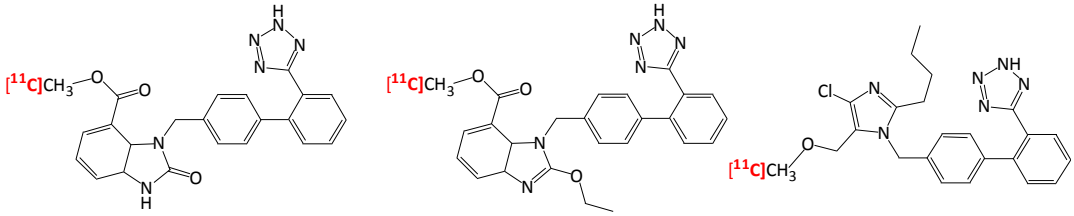

IC_{50} = 0.117 µM IC_{50} = 0.099 µM

Figure 1-12 AT_1 receptor PET tracers developed at the University of Ottawa Heart Institute, National Cardiac PET Centre (Ottawa, ON). *Left to right*: [^{11}C]methyl-candesartan, [^{11}C]TH4 , and [^{11}C]methyl losartan.

2 THESIS OVERVIEW

2.1 Objectives

The aim of this study was to label losartan with Fluorine-18 in order to image cardiac and kidney AngiotensinII type-1 receptors (AT_1R) via PET as well as to begin assessing its binding specificity for the AT_1R and *in vivo* metabolism

2.2 Hypotheses

1) The [^{18}F]FPyKYNE (2-[^{18}F]fluoro-3-pent-4-yn-1-yloxypyridine) prosthetic group will be synthesized and conjugated to losartan in > 5% radiochemical yield, in high chemical and radiochemical purity (> 95%) and with high specific activity (> 2000 mCi/μmol).

2) The higher specific activity of F-18 will allow for a lower injected mass compared to C-11 analogs, thus limiting competitive binding with cold compound and receptor saturation.

3) The strength and stability of the aromatic C-^{18}F bond and the resilience of the triazole linkage to metabolism will reduce the number of labeled metabolites.

4) The larger more lipophilic moiety will enhance the bioavailability of the radiotracer and possibly enable penetration of the blood-brain barrier (BBB).

5) The [^{18}F]fluoropyridine losartan analog will bind specifically to the AT_1R.

3 METHODS

3.1 Chemistry

3.1.1 Materials

Anhydrous (> 99%) acetonitrile (MeCN), DMSO, and pentanes (ACS grade) were purchased from Sigma-Aldrich. Ether (HPLC grade) was purchased from Fisher Scientific. All other solvents were classified as HPLC grade and purchased from EMD. Trifluoroacetic acid (TFA, 99%) was purchased from Alfa Aesar. Losartan potassium (98%) was purchased from LKT Laboratories, Inc. All other reagents were purchased from Sigma-Aldrich and classified as 98% purity or greater. No further manipulation or purification was made to purchased solvents and/or reagents.

Analytical TLC was performed on silica gel-coated aluminum sheets (Analtech). Unless specified otherwise, TLC were run with a solvent of 30:70 EtOAc/Hexanes. Preparative TLC was performed on Analtech TLC Uniplates (silica gel matrix, 1000 µM). Flash column chromatography was run on silica gel (Davisil® grade 633, 60 Å pore size, 200-425 mesh). A Phenomenex Luna C18(2) column (250 x 4.6 mm, 10 µm) was used for all analytical HPLC. A C18 sorbent is strongly non-polar, composed of octadecyl carbon chains bonded to silica. A Phenomenex Luna C18(2) column (250 x 10 mm, 10 µm) was used for semi-prep HPLC. The eluents consisted of MeCN/water (0.1 M ammonium formate) and were filtered through a 0.2 µm paper filter and degassed by sonication prior to use. PeakSimple Chromatography Data System was used in combination with a Waters 486 Tunable Absorbance Detector and Water 515 HPLC Pump.

For each procedure, a “standard workup” refers to dilution with EtOAc, washing the organic layer with water (3x) followed by brine (and sometimes back-washing the aqueous layer with organic solvent), combining the organic layers, drying over anhydrous sodium sulfate, filtering

and evaporating the organic solvent under reduced pressure with a rotary evaporator. Semi-prep HPLC purification involves the same techniques as a standard workup, except the isolated product is being extracted into EtOAc from the MeCN/water (0.1M AF) HPLC solvent.

NMR and mass spectrometry (MS) were performed by technicians in the graduate chemistry department at the University of Ottawa. ^{1}H-NMR were obtained by either a Bruker AVANCE 300 or 400 MHz or a Varian Inova 500 MHz spectrometer, in $CDCl_3$, unless otherwise indicated. ^{13}C-NMR and ^{19}F-NMR spectra were obtained on a Bruker AVANCE 300 MHz spectrometer (^{19}F frequency = 282.38 MHz, ^{13}C frequency = 75.48 MHz). Proton chemical shifts (δ) are reported in parts per million (ppm) relative to tetramethylsilane (TMS) internal standard. Coupling constants (*J*) are reported in Hertz (Hz). Multiplicity is defined by s (singlet), br (broad singlet), d (doublet), t (triplet), q (quartet), qn (quintet), sx (sextet), or m (multiplet). The mass spectra (MS) were obtained on a Q-TOF mass spectrometer (Micromass) by either electron impact (EI) or electrospray ionization (ESI).

3.1.2 Experimental

The methods described herein were performed multiple times at varying reaction conditions (ie. temperature, reagent equivalents, solution concentration, reaction time) with little change in reaction purity or product yield. A representative reaction is described for each method.

Trityl losartan

N-trityl losartan {2-Butyl-5-chloro-3-[2'-(2-trityl-2H-tetrazol-5-yl)-biphenyl-4-ylmethyl]-3H-imidazol-4-yl}-methanol

The tetrazole of losartan was *N*-protected by a trityl (triphenyl methyl) group according to previously established methodology (Hadizad et al., 2011). Losartan potassium (300 mg, 0.65 mmol), trityl chloride (199.56 mg, 0.78 mmol) and triethylamine (52 µl, 0.65 mmol) were added

sequentially to dry DMF (4 ml). The mixture was stirred at ambient temperature overnight (12-16 h) and monitored for completion by TLC (Rf 0.2); stains yellow upon reaction with *p*-anisaldehyde under heat. A standard workup was performed and the residue purified by flash column chromatography (gradient: 10:90 to 45:55 EtOAc/Hexanes).

The trityl group can subsequently be removed from any of the tritylated losartan analogs upon treatment with acid (Moises Canle L., 2001), including 1M HCl in H_2O, 12M HCl (in MeOH), or TFA (99%). The reaction was typically accelerated with heat, ranging from 50-90^{o}C for 1-10 min. Optimal conditions were found to be 70-80^{o}C for 1-2 min.

Azide-modified trityl losartan

5-[4'-(5-Azidomethyl-2-butyl-4-chloro-imidazol-1-ylmethyl)-biphenyl-2-yl]-2-trityl-2H-tetrazole

The 5'-hydroxy group of losartan was converted to an azide according to a method developed by Thompson and coworkers at Merck & Co (Thompson and Grabowski, 1995; Thompson et al., 1993). Trityl losartan (300 mg, 0.44 mmol), DPPA (105 µl, 0.49 mmol) and DBU (74 mg, 0.48 mmol) were added to 4 ml THF and stirred vigorously at room temperature overnight. The reaction was monitored by TLC for completion (Rf 0.5); stains yellow upon reaction with *p*-anisladehyde under heat. Following standard workup, the residue was purified by flash column chromatography (gradient: 5:95 to 30:70 EtOAc/Hexanes).

NO_2PyKYNE

2-Nitro-3-pent-4-yn-1-yloxypyridine

The procedure for synthesis of NO_2PyKYNE was adopted from Kuhnast and colleagues (Kuhnast et al., 2008). To a solution of 2-nitro-3-hydroxypyridine (3.00 g, 21.26 mmol) in DMF (4 ml) was added K_2CO_3 (5.88 g, 42.53 mmol), NaI (320 mg, 2.13 mmol) and 5-chloropent-1-yne (2.68 ml, 25.5 mmol). The mixture was then stirred overnight at 80^{o}C, cooled to room

temperature, diluted with water for standard workup. The product was purified by flash column chromatography (85:15 Hexane/EtOAc). TLC: Rf 0.23.

FPyKYNE

2-fluoro-3-pent-4-yn-1-yloxypyridine

NO_2PyKYNE was converted to FPyKYNE by an aromatic nucleophilic substitution (S_NAr) reaction (Kuhnast et al., 2008). Potassium fluoride (56.4 mg, 0.97 mmol) and Kryptofix2.2.2 (366 mg, 0.97 mmol) were dissolved in 3 ml DMSO and stirred at 145-165^oC for 10 min. To this solution was added NO_2PyKYNE (200 mg, 0.97 mmol) in DMSO (500 µl). After 1.5 h, the reaction mixture was cooled for standard workup. The product was then purified by flash column chromatography on silica gel (85:15 Hexanes/EtOAc). TLC: Rf 0.48.

Nitropyridine trityl losartan

3-[3-(1-{2-Butyl-5-chloro-3-[2'-(2-trityl-2H-tetrazol-5-yl)-biphenyl-4-ylmethyl]-3H-imidazol-4-ylmethyl}-1H-[1,2,3]triazol-4-yl)-propoxy]-2-nitro-pyridine

The method described herein is modified from an article using propargyl 4-[^{18}F]fluorobenzoate to label biomolecules via click chemistry (Vaidyanathan, 2009). NO_2PyKYNE (33 mg, 0.17 mmol) and trityl losartan azide (100 mg, 0.14 mmol) were dissolved in 1 ml CH_2Cl_2. $CuSO_4$ (100 µl, 4 mg in 500 µl water) and sodium ascorbate (100 µl, 6 mg in 500 µl water) were allowed to react in a separate vial for 5-10 sec (turns yellow) and added to the solution. The reaction proceeded at room temperature overnight (10-16 h) and monitored for completion by TLC (4:1 CH_2Cl_2/MeOH): Rf 0.61. The reaction can also be monitored by analytical HPLC after trityl deprotection (40:60 MeCN/H_2O (0.1M AF), 2 ml/min): azide elutes at 7.2 min, nitropyridine losartan product at 8.0 min, and NO_2PyKYNE at 11.8 min. After a standard work-up, the reaction was purified by flash column chromatography (gradient: 30:70 to 80:20 EtOAc/Hexanes).

Fluoropyridine trityl losartan

3-[3-(1-{2-Butyl-5-chloro-3-[2'-(2-trityl-2H-tetrazol-5-yl)-biphenyl-4-ylmethyl]-3H-imidazol-4-ylmethyl}-1H-[1,2,3]triazol-4-yl)-propoxy]-2-fluoro-pyridine

The synthesis of fluoropyridine trityl losartan followed a procedure similar to that used for nitropyridine trityl losartan. Trityl azide losartan (130 mg, 0.19 mmol) and FPyKYNE (41 mg, 0.21 mmol) were added to 400 µl of DMSO. Addition of 200 µl of $CuSO_4$ and 600 µl NaAsc turned the solution a milky yellow. The reaction was heated to 85^{o}C and stirred for 10 min until clear. An aliquot was deprotected with 12M HCl (drops) for 1.5 min at 85^{o}C to check for reaction completion. TLC (4:1 Hexanes/EtOAc (3x)): trityl azide: Rf 0.46, FPyKYNE: Rf 0.61, fluoropyridine trityl losartan: Rf 0.81.

Fluoropyridine losartan

3-[3-(1-{2-Butyl-5-chloro-3-[2'-(2H-tetrazol-5-yl)-biphenyl-4-ylmethyl]-3H-imidazol-4-ylmethyl}-1H-[1,2,3]triazol-4-yl)-propoxy]-2-fluoro-pyridine

Detritylation of fluoropyridine trityl losartan was performed on either purified product or on the reaction mixture. In former case, the product was simply diluted in DMSO or DMF prior to addition of the in 10-20 µl of TFA or HCl (12 M). Detritylation was effected at 80^{o}C for 2 min and completion monitored by TLC (7:2:0.5 EtOAc/Hexanes/MeOH): Rf 0.32. The reaction was then cooled and loaded onto semi-prep HPLC (35:65 MeCN/0.1M AF, 7 ml/min): azide at 12.9 min, conjugated product at 15.9 min, and FPyKYNE at 18.6 min. The product was alternatively purified by flash column chromatography (8:2:1 EtOAc/Hexanes/MeOH).

3.2 Radiochemistry

3.2.1 Materials

[^{18}F]F^- was produced in our CTI/Siemens RDS III cyclotron from proton irradiation of 97% [^{18}O]H_2O-enriched water via the $^{18}O(p, n)^{18}F$ nuclear reaction. Target water was delivered through 0.4 mm Tefzel tubing and collected in a 5 ml vial (Wheaton) in the module.

The TRACERlab® FX N Pro automated synthesis module, including UV detector, HPLC pump, and software, was purchased from GE Healthcare (Figure 3-1). Only slight modifications were made to the module: 1) the semi-prep RP-HPLC column (Phenomenex® Nucleosil C(18), 10 µM, 250 x 25 mm) was replaced with a Phenomenex® Luna C(18)2 column (250 x 10 mm, 10 µM,); 2) Sep-Pak Light Waters Accell Plus QMA cartridges were used to trap F-18 from the target water; 3) the round bottom flask and double-neck vial intended for HPLC fraction collection and product reformulation, respectively, were removed and the lines joined by proper fittings; and 4) all Teflon tubing was replaced with Tefzel tubing.

QMA cartridges were conditioned by passing through 7-8 ml of a 0.55M solution of potassium carbonate (7.60 g or 0.055 mol K_2CO_3 in 100 ml water), followed by water (7-8 ml) and drying under a stream of argon. F-18 eluent was prepared by dissolving 27.5 mg (0.20 mmol) K_2CO_3 and 150 mg (0.40 mmol) Kryptofix2.2.2 (K_{222}) in a 5 ml solution of MeCN (4.75 ml) and water (250 µl). Sep-Pak (Silica Light Accell Plus and Light C18) for SPE were purchased from Waters. Silica cartridges were used as received. The C18 cartridges were pre-conditioned by passing through 5 ml of EtOH followed by 10 ml of water.

Analytical HPLC effluent was analysed by Waters Millenium 32 or PeakSimple (v3.93) chromatography analysis software. The EtOH (99.9%), sodium bicarbonate solution (14.9%) and

saline solution (0.9%) used for reformulation were obtained from sterile capped bottles. Radioactivity was measured in a Capintec dose calibrator.

3.2.2 Experimental

The module was cleaned before every run via a pre-programmed cleaning/drying recipe which simply needs to be executed once the reservoirs are loaded with EtOH or acetone (1 ml). With regards to safety, activity in the hot cell after a run was left to decay before re-entering.

About 30 min before EOB, reservoirs 1, 2 and 3 were loaded with K_2CO_3/K_{222} solution (1.6 ml), MeCN (1.6 ml) and NO_2PyKYNE (6.0 mg in 600 µL DMSO), respectively. Reservoirs 4 and 5 were filled with a 1:1 ether/pentanes solution (2.5 ml and 5.5 ml, respectively). Copper sulphate (1.5 mg in 150 µl water), sodium ascorbate (2 mg in 200 µl water), and azide-modified trityl losartan (1.0 mg in 400 µl DCM) were loaded into reservoirs 7, 8, and 9, respectively. Reservoirs 10 and 11 were loaded with TFA (20 µl in 100 µl MeCN) and HPLC solvent (500 µl), respectively. It is important to verify that the waste is empty, the duer for the vacuum trap contains liquid nitrogen, all reaction vessels and reservoirs are closed tightly, cartridges are in place, there is eluent for HPLC and the air and nitrogen gas barometers indicate sufficient pressure.

Upon EOB, the O-18 target water was transferred to a collection vial in the module by means of a low and high pressure push from the cyclotron. It is then loaded onto a pre-conditioned QMA cartridge where $[^{18}F]F^-$ is retained while the O-18 water passes through to a separate collection vial. A solution of K_2CO_3/K_{222} from reservoir 1 is then used to elute the $[^{18}F]F^-$ from the QMA cartridge into reaction vessel 1. Azeotropic evaporation with acetonitrile at 110°C (2 x 3 min) provided active, un-solvatized F-18 in the form of $K^+/K_{222}/[^{18}F]F^-$. The NO_2PyKYNE precursor from reservoir 3 was then added and the reaction mixture heated at 145°C for 10 min to produce $[^{18}F]$FPyKYNE (Figure 3-2). The mixture was cooled to 30°C, diluted with eluent from

reservoir 4 and loaded onto a series of three silica cartridges where the nitro precursor is retained and [^{18}F]FPyKYNE is eluted into reaction vessel 2. Eluent was evaporated at 30^{o}C for 5 min, and then cooled to ambient temperature. This process was repeated with eluent from reservoir 5. Copper sulphate, sodium ascorbate, and azide-modified trityl losartan were added sequentially from reservoirs 7, 8, and 9. Conjugation was induced by heating reaction vessel 2 to 80^{o}C for 30 min. Detritylation was performed by acid hydrolysis with TFA from reservoir 10 at 80^{o}C for 2 min. The reaction mixture was then cooled to ambient temperature and diluted with HPLC solvent from reservoir 11 prior to loading onto the adjoining semi-prep HPLC column.

Following the real-time radiation spectrum, the desired product was then collected and carried, within a lead container, to another hot cell for reformulation. The HPLC fraction was diluted to half the original concentration with water (Millipore) and passed through a pre-conditioned Sep-Pak C18 cartridge followed by 20 ml water (Millipore) to wash any salts from the HPLC solvent remaining on the cartridge. Sterile ethanol (0.2-0.5 ml) elutes the product from the Sep-Pak. A sufficient amount of saline was then added to the effluent to make a solution containing a maximum of 10% EtOH. It is important to note that the volume of EtOH, and thus the volume of saline required for dilution, depends on the amount of activity produced and the concentration desired. For microPET studies, we aimed for a final concentration of at least 0.5 mCi/ml whereas for metabolism studies at least 2-3 mCi/ml was considered ideal.

3.2.3 Quality Control

Following synthesis, product identity, purity and specific activity were assessed with analytical HPLC. An aliquot of the final formulation was co-injected with standard to confirm product identity. Specific activity was determined by injecting an aliquot of the product alone and comparing the area of the UV absorbance peak (measured at 254 nm) to that of a known

amount of standard. The pH of the formulated product was tested to assure it was near physiological pH and adjusted with sodium bicarbonate solution if necessary.

3.2.3.1 Calculating specific activity

First, a specific volume of standard of known concentration (in g/ml) was injected onto the analytical HPLC and the area under the UV curve (AUC) recorded (at 254nm). Secondly, an aliquot of the product formulation containing a known amount of activity (µCi) was injected and the AUC recorded (at 254nm). The amount of cold mass in the product was determined by comparing the two AUC with respect to the amount of standard injected (Equation 2). As specific activity is typically presented in units of activity per mol, the amount of standard must be converted to mols, calculated by dividing the mass (in g) by the molecular weight (MW, in g/mol). The mass should be readily available from the concentration and volume injected (Equation 1). The specific activity can now be easily calculated (Equation 3).

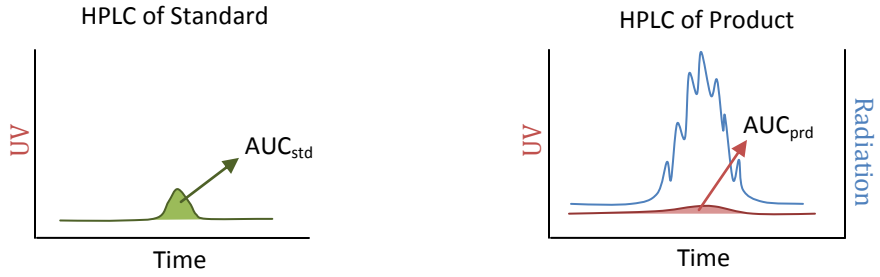

1. $mol_{std\ (mol)} = mass_{prd\ (g)} / MW_{std\ (g/mol)}$

   $= (conc_{std\ (g/ml)} * vol_{std\ (ml)}) / MW_{std\ (g/mol)}$

2. $$\frac{mol_{prd}}{AUC_{prd}} = \frac{mol_{std}}{AUC_{std}}$$

   $$mol_{prd} = (AUC_{prd} * mol_{std}) / AUC_{std,}$$

3. $specific\ activity_{(mCi/\mu mol)} = radioactivity_{prd\ (mCi)} / mol_{prd\ (\mu mol)}$

3.3 MicroPET Imaging

3.3.1 Animals

All experiments involving live animals or animal tissues were performed on normal male Sprague Dawley rats (Charles River Laboratories, Montreal, Canada) and were conducted in accordance with the guidelines of the Canadian Council on Animal Care (CCAC) and with approval from the Animal Care Committee (ACC) at the University of Ottawa. Rats were housed in pairs, kept on a 12 hour light-dark cycle, and followed a standard diet.

3.3.2 Image Acquisition

Rats (weighing 200-660 g) were anaesthetized with isoflurane (1-2%), weighed, and placed on the scanning bed of the Siemens Inveon small animal dedicated microPET scanner (Siemens, Knoxville, Tennessee)(lutetium orthosilicate (LSO) scintillation crystals, 1.4 mm spatial resolution, 12.7 cm axial FOV) (Figure 3-3) in supine position with involuntary movement restricted by light taping. Anaesthesia was maintained throughout the scanning process by a continuous flow of isoflurane (1-2%) through a nose cone. Heart rate, body temperature, blood oxygen (O_2) and carbon dioxide (CO_2) levels, and echocardiogram (ECG) rhythms were monitored throughout the study.

Dynamic PET images were reconstructed from the acquired list mode data using three-dimensional ordered subset expectation maximization (OSEM3D) in conjunction with a maximum a posteriori (MAP) algorithm with 12 x 10 sec frames (0-2 min), 3 x 1 min frames (2-5 min) and 11 x 5 min frames (5-60 min). A 10 min transmission scan with an inboard rotating Co^{57} (122 keV) point source was performed either prior to or following the dynamic F-18 emission scan for attenuation correction. Image reconstruction algorithms corrected for photon

scattering, non-collinearity, and random coincidences. The resulting images quantitatively reflect the distribution of the radionuclide in the subject.

3.3.2.1 Baseline

Baseline scans were performed to evaluate preliminary tracer pharmacokinetics. The rats were positioned in the camera as to have both heart and kidneys within the field of view (FOV). However, due to size constraints, scans containing the brain had to exclude the kidneys from the field of view. A bolus dose of 0.4-1.0 mCi of [^{18}F]FPyrLos was injected via the lateral tail vein.

3.3.2.2 Blocking Studies

In order to assess binding specificity of [^{18}F]FPyrLos for the AT_1R, the rat was injected with AT_1R blocker candesartan prior to injection of the tracer. Various doses of candesartan (2.5 mg/kg, 5 mg/kg and 10 mg/kg) were injected to identify a dose-response effect (Kirkpatrick, 2009). Candesartan was available in both the salt form and non-ionized form. As such, it was dissolved in either saline alone or required the addition of some sodium bicarbonate (10% v/v) to induce salt formation and dissolution. With complete blocking, one can assume that any binding in the region of interest (ROI) is non-specific. It should be noted that organs responsible for elimination, metabolism or excretion, such as the liver, kidneys and GI system, will contain tracer and possible labeled metabolites that may or may not be bound.

3.3.3 Image Analysis

Using Siemens' Inveon Research Workplace (IRW 4.0) image analysis software, regions of interest (ROI) were generated over various organs, including left atrium (LA), left ventricle (LV), kidneys, liver and background. A detailed method for drawing these ROI was previously

described by a colleague in his thesis (Antoun, 2010). In short, for the LA and LV, we used the frame displaying maximal uptake, usually around frame 4 (30-40 sec). A small spherical ROI was drawn over the LA or LV and a threshold placed to include only the voxels with intensities in the top 20%. As much of the right kidney was usually covered by the liver, we used the left kidney for image analyses. The best definition of the kidney cortex was typically around frame 16 (5-10 min). A spherical or cube ROI was drawn to encompass all but the top third of the kidney in order to minimize spill-over of activity from the nearby high intensity liver. A threshold was placed such that the ROI included only the voxels with intensities in the top 50%. It is important to check slices in later time frames to verify that the GI tract or liver does not enter the ROI. For the liver, multiple spherical ROIs were placed throughout the liver in various slices to provide an overall representation.

PET scanners typically provide images in terms of radioactivity concentration, that is the amount of Becquerel (Bq) or Curie (Ci) per ml, where 1 Bq = 1 disintegration per second (dps) or 2.7×10^{-11} Ci. The changing activity concentration in the ROI over time is then used to generate time-activity curves (TAC), presented as %ID (injected dose)/ml. Subsequently, standard uptake values (SUV, g/ml) or an SUV curve can be used to display the data normalized to body weight (assuming 1 ml roughly equals 1 g). SUV values allow for comparison between subjects.

$$\text{SUV} = \frac{\text{Activity concentration (MBq/ml)}}{\text{Injected dose (MBq)/Weight (g)}}$$

Provided a tracer binds to its receptor reversibly, Logan graphical analysis (Logan et al., 1990) of the PET time-activity data can be used to estimate distribution volume (DV). DV is proportional to the receptor binding potential (BP), a ratio of binding capacity or receptor density (B_{max}) to the dissociation constant (K_d). In turn, the BP is a ratio of specifically bound ligand concentration to free ligand concentration in the tissue (which at equilibrium should be

the same as in the plasma). Plotting $\int_0^T C_{PET}(t)dt/C_{PET}(T)$ (min) against $\int_0^T C_P(t)dt/C_P(T)$ (min·cm^3/ml), where $C_P(t)$ is the concentration of tracer in the plasma and $C_{PET}(T)$ is the concentration of tracer in the tissue, will transform the tissue activity to a linear plot. It is important to note that linearity is only achieved once the plasma and tissue reach equilibrium. The slope of this linear regression provides an estimate of the DV (in ml/cm^3). The effects of plasma protein binding and nonspecific binding are implicit to the DV calculation. That is, free ligand in the blood is not distinguished from plasma-bound ligand and contributions from non-specific binding in addition to free ligand and specifically bound ligand are included in the DV estimate. An ROI drawn over the left atrium was used for the blood input function. A DV of 1 indicates no contrast between the tracer in the target tissue and tracer in the blood; there is no specific binding. The DV values were determined from frames 17-26 (10-60 min). No corrections were made to account for the existence of metabolites or variation in injection doses (ie. time, volume, and rate).

To determine whether the difference in means between two groups receiving different blocking doses was statistically significant, a two-tailed independent variable *t*-test was performed, with a P value less than 0.05 deemed statistically significant.

3.4 Metabolism Studies

3.4.1 Tissue Preparation

A protocol established by fellow co-workers (Antoun, 2010; Kenk et al., 2008; Kirkpatrick, 2009; Thackeray et al., 2007) was executed without modification. Normal male Sprague Dawley rats (Charles River Laboratories, Montreal, Canada) were sacrificed by decapitation and trunk

blood collected in Heparin-coated collection tubes (followed by gentle agitation to prevent coagulation). Kidney samples were excised, collected in sterile tubes, and immediately chilled on ice. Blood was centrifuged at 3,000 rpm at 4^{o}C for 5 min after which the plasma was separated off by micropipette. Kidney samples were first homogenized in 10-15 ml of 80:20 EtOH/H_2O, and then centrifuged at 20,000 rpm for 15 min at room temperature. After evaporation of the supernatant by rotary evaporation under reduced pressure, the residue was reconstituted in 1:99 MeCN/H_2O. Urea was added to the samples (1 g per ml of plasma and 400 mg per ml of 1:99 MeCN/H_2O for the tissues) in order to disrupt protein binding (Hilton et al., 2000) and ensure maximal retention of the tracer and labeled metabolites to the capture cartridge (Hilton et al., 2000). Samples were then filtered through a syringe filter (PALL PharmAssure, 25 mm with 0.2 µM Supor membrane) prior to injection.

3.4.2 Column-switch HPLC

A general protocol set forth by prior co-workers (Antoun, 2010; Kenk et al., 2008; Kirkpatrick, 2009; Thackeray et al., 2007) was used to quantify metabolites in the kidney and plasma. This protocol is based on a modification of the column-switch HPLC method developed by Hilton (Hilton et al., 2000).

The column-switch HPLC system (Figure 3-4) comprises two pumps (Waters 510), three two-position valves (V_1 and V_2 = 6 port, V_3 = 4 port), one capture cartridge, one analytical column (Phenomenex Luna C(18)2, 250 x 4.6 mm, 10 µM), a dual bismuth germanium oxide (BGO) HPLC coincidence radiation detector (Bioscan) and a UV absorbance detector (Waters 486) connected in series. V_1 controls flow of solvent 1 through the loop (5 ml capacity), V_2 controls flow over the capture cartridge, and V_3 controls delivery to the detectors. The capture cartridge (Alltech Direct-Connect refillable guard column, 2 x 20 mm) with 2 µM filter frits (2-mm, Alltech) was

hand-packed with hydrophilic-lipophilic-balanced sorbent (HLB, Waters Oasis) and activated by sequential delivery of methanol (1 ml/min for 5 min) and deionized water (1 ml/min for 5 min). Pump 1 delivers solvent 1 (1:99 MeCN/H_2O) through the loop and over the capture column at 2 ml/min. The choice of capture column sorbent and solvent is intended to retain the hydrophobic or non-polar tracer and its labeled hydrophobic metabolites while allowing water-soluble proteins, lipids and salts to pass through. Once the UV chromatogram returns to baseline (typically 5-8 min), the direction of flow is reversed, or switched, and solvent 2 (40:60 MeCN/0.1M ammonium formate) is pumped at 1.5 ml/min by pump 2 back over the capture column and onto the analytical column. C18 packing is intended for separation of hydrophobic compounds. The capture column was re-activated between injections with 3-4 min each of MeOH and deionized water (at 2 ml/min). If the back pressure ever exceeded 2500 psi, the frits of the capture cartridge or the filter frits of the analytical guard column were replaced, depending on what was required to return the back pressure to normal (< 300 psi). Capture packing sorbent was replaced every 3-4 experiments.

Radiation and UV signals were recorded by the PeakSimple Six-Port Chromatography Data System (SRI Model 302) connected to a computer running PeakSimple chromatography acquisition and integration software (v 3.29).

3.4.2.1 Controls

Control experiments were used to determine if the metabolite extraction process itself results in any product modification or decomposition. Plasma, heart and kidneys were removed from normal, untreated rats and spiked with 50-150 µCi of tracer prior to preparation for HPLC. Tracer was also injected alone on HPLC to confirm the identity of unchanged tracer peak (based on elution time) and to assess system reproducibility.

3.4.2.2 Baseline

Rats were injected with 0.5-1.0 mCi of F-18 labeled losartan tracer via lateral tail vein injection and sacrificed by decapitation 10 min post-injection. The heart, kidneys, and blood were collected. Another rat was also sacrificed for control tissues and blood.

3.4.2.3 Blocking Studies

Rats were injected with candesartan (5 mg/kg and 10 mg/kg) via the tail vein immediately prior to injection of tracer and sacrificed after 10 min. The heart, kidneys, and blood were collected and processed. Another rat was also sacrificed for control tissues and blood, which were spiked with 50-200 μCi of tracer prior to processing.

3.4.3 Metabolite Analysis

Radiation signals were integrated and background noise determined by defining a region with no discernible peaks and calculating the average area/second to be subtracted from the identified peaks. It is important not to saturate the radiation detector in order to achieve accurate area integration. Decay-correction was applied to the peak areas to account for the time lapse between injection and elution of the last peak. The proportion of tracer not retained by the capture cartridge (Peak 1) in the control tissues was used to correct the area of the unretained peak (Peak 1) and unchanged tracer peak (Peak 3) in the experimental samples.

A two-tailed independent variable *t*-test ($P < 0.05$) was performed to assess whether the increase or decrease in peak proportion between two groups receiving different blocking doses was statistically significant.

3.4.3.1 Control-correction for metabolite peak areas

The proportion of tracer not retained by the cartridge ($\%Unret_{ctrl}$) in the control runs was corrected for in the experimental sample runs. That is, the unretained peak ($AUC_{Unret\ exp}$) was reduced and tracer peak ($AUC_{tracer\ exp}$) was increased accordingly.

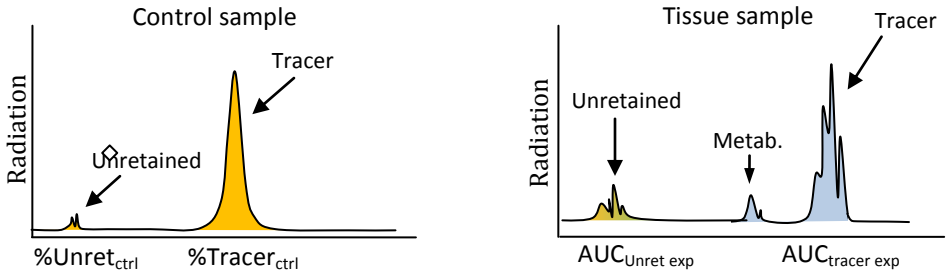

$$\frac{\%\text{Unretained in control } (\%Unret_{ctrl})}{\%\text{Tracer in control } (\%Tracer_{ctrl})} = \frac{\text{Tracer in unretained sample peak } (AUC_{Unret\ exp})}{\text{Area of tracer in sample } (AUC_{tracer\ exp})}$$

Therefore, $AUC_{Unret\ exp} = (\%Unret_{ctrl} * AUC_{tracer\ exp}) / (\%Tracer_{ctrl}$

Thus, the control-corrected areas are:

Tracer area $= AUC_{tracer\ exp} + (((\%Unret_{ctrl}/100)*AUC_{Unret\ exp}) / (\%Tracer_{ctrl}/100))$

Unretained area $= AUC_{Unret\ exp} - (((\%Unret_{ctrl}/100)*AUC_{tracer\ exp}) / (\%Tracer_{ctrl}/100))$

3.4.3.2 Decay correction for metabolite peak areas

Decay equation: $A_t = A_0 e^{-\lambda t}$

Let A_t = the AUC for a peak at some time *t* after t_o

A_0 = the AUC for the last peak to elute (ie. unchanged tracer)

$t_{1/2}$ = 109.5 min for F-18

Decay factor (λ) $= \log_e(2)/t_{1/2}$

$= \ln(2)/t_{1/2}$

$= 0.69314718056/109.5$

$= 0.00633011$

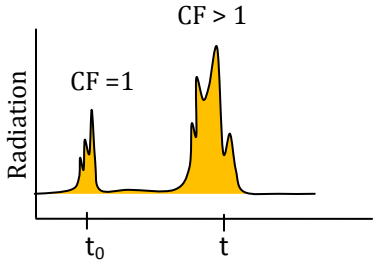

Let $A_0 = 1$

$A_t = e^{-0.00633011t}$

Correction factor (CF) $= A_t/A_0$

$= 1/e^{-0.00633011(t-t_o)}$

Therefore,

decay corrected area = CF * A_t

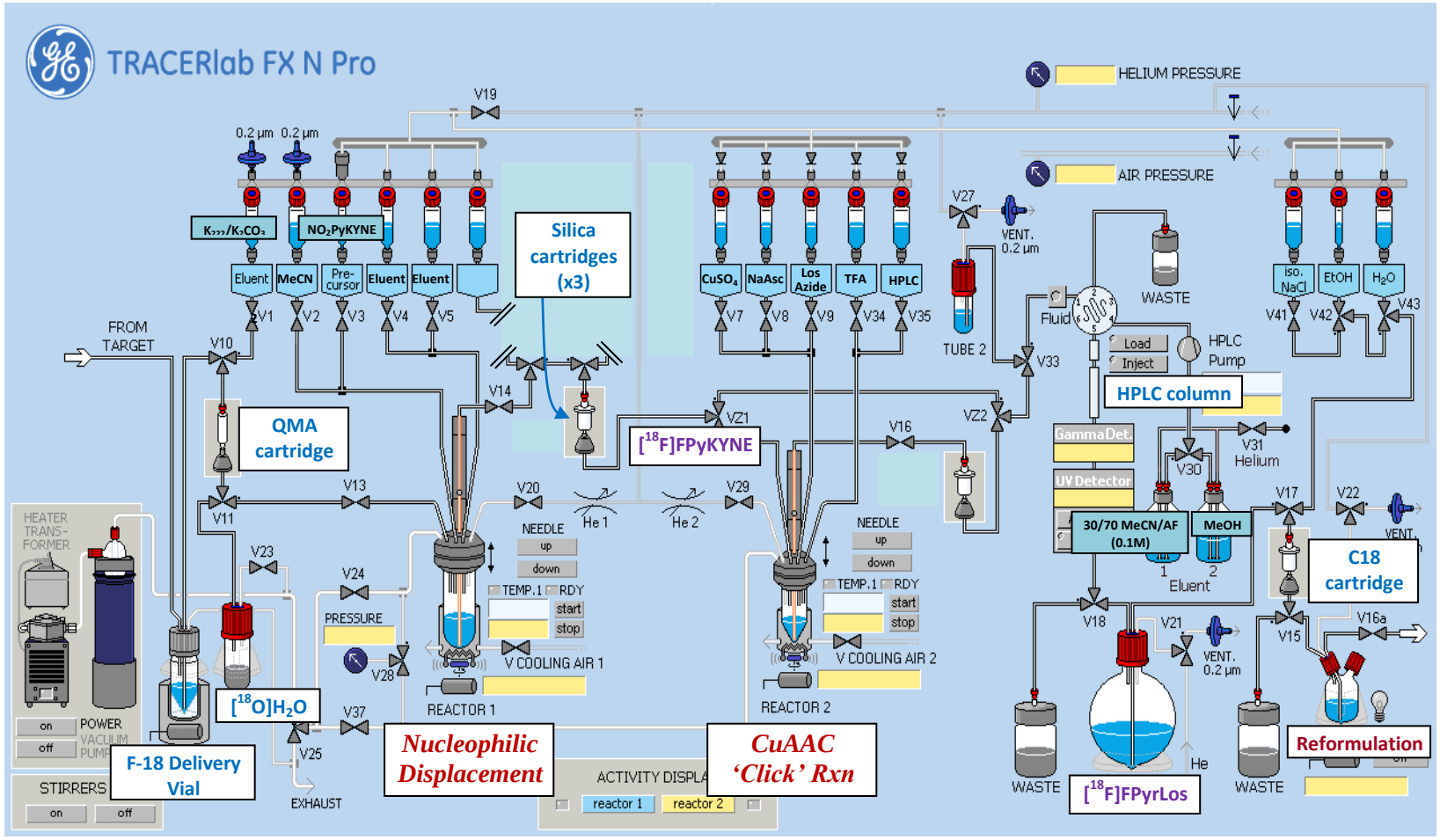

Figure 3-1 Schematic of the TRACERlab FX N Pro (by GE Healthcare) used to synthesize [^{18}F]fluoropyridine losartan. Modifications are indicated with arrows. Schematic was provided by GE Healthcare.

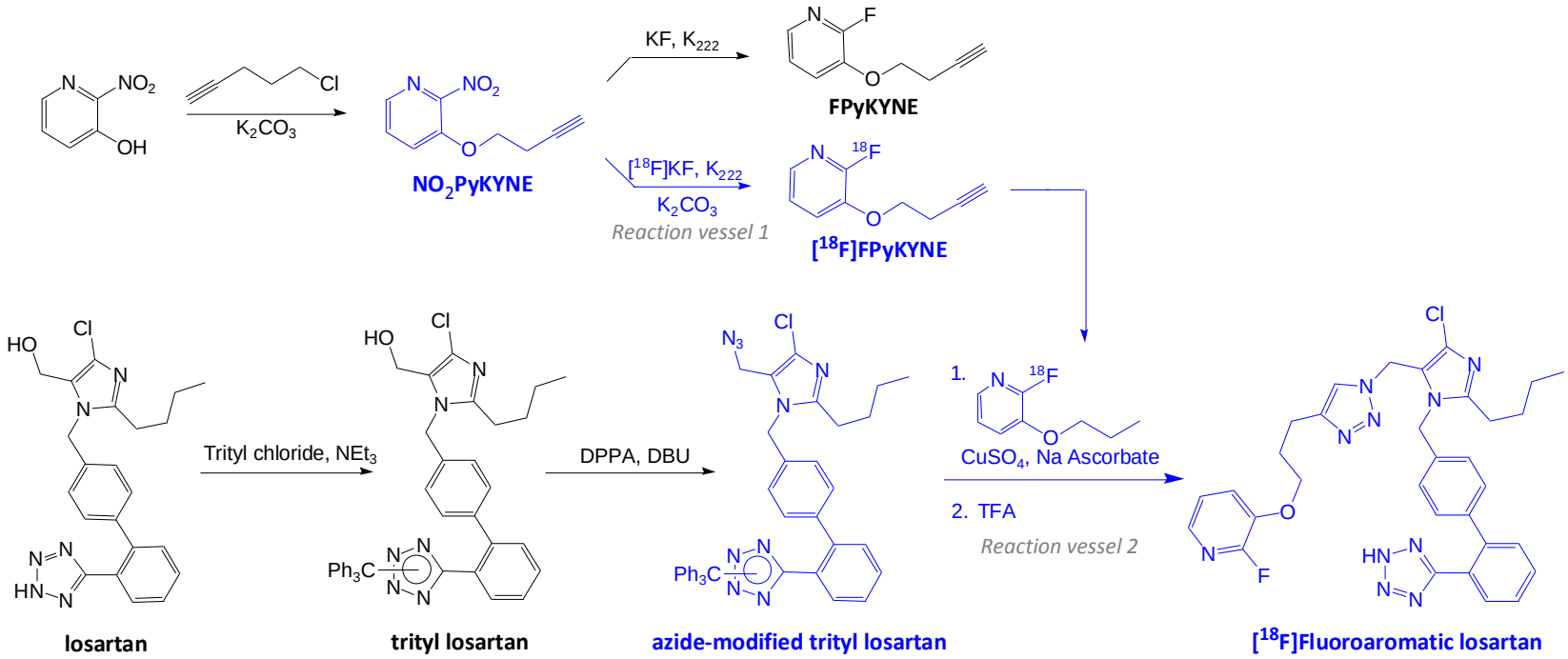

Figure 3-2 Schematic of cold (F-19) and hot (F-18) synthesis of FPyrLos via the Cu(I)-catalyzed [2+3] cycloaddition reaction between azides and alkynes (CuAAC). FPyKYNE is conjugated to azide-modified trityl losartan followed by a quick acid deprotection to afford the final product which was purified by semi-prep HPLC.

Figure 3-3 Small animal microPET scanner (Siemens Inveon). Images were reproduced from their online brochure : *www.medical.siemens.com*

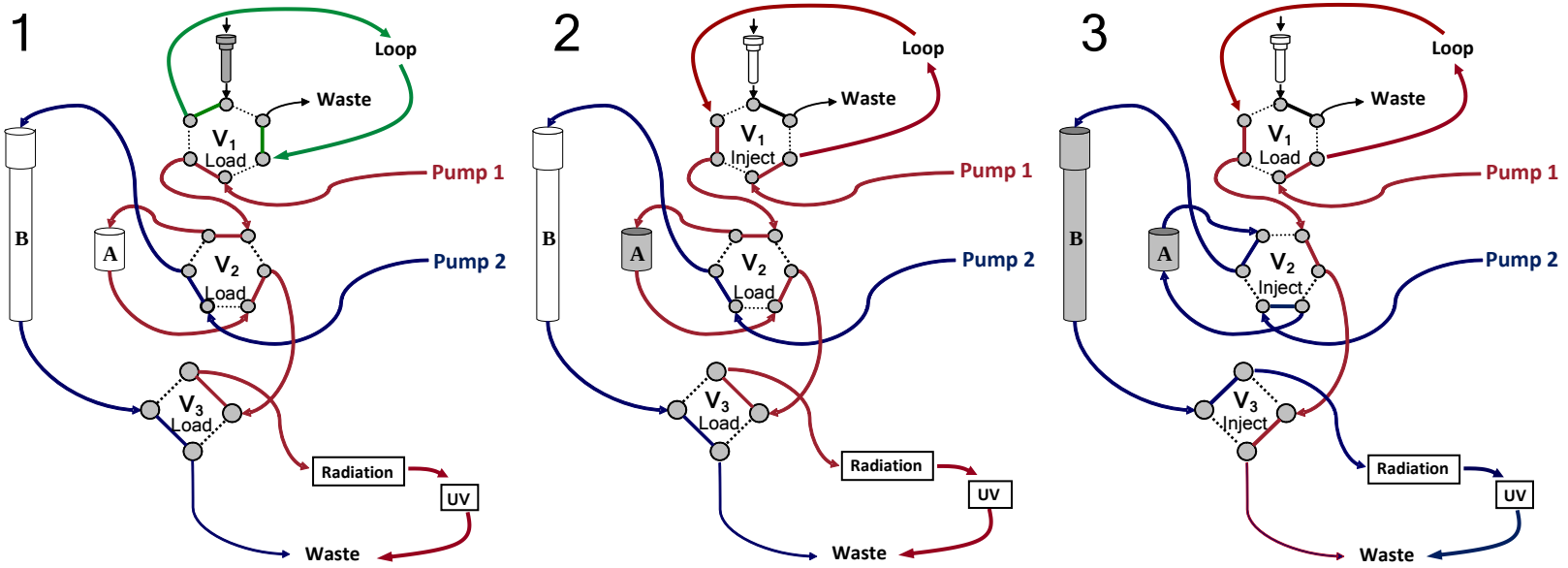

Figure 3-4 Column-switch HPLC for metabolite analysis of [^{18}F]fluoropyridine losartan in rat plasma and tissue. 1) Sample is injected into the loop. The capture cartridge and analytical column are equilibrating; 2) Sample in the loop is loaded onto the capture cartridge. Effluent from the capture cartridge passes through the UV and radiation detectors; 3) Compounds retained by the capture cartridges are eluted onto the analytical column. Effluent from the analytical column now passes through the detectors.

4 Results

4.1 Chemistry

Trityl losartan

N-trityl losartan {2-Butyl-5-chloro-3-[2'-(2-trityl-2H-tetrazol-5-yl)-biphenyl-4-ylmethyl]-3H-imidazol-4-yl}-methanol

Yield: 380 mg (86%), white powder. HPLC (35:65 MeCN/AF(0.1M), 2 ml/min): 3.6 min. ^{1}H-NMR (400 MHz, DMSO-d_6): δ 7.79 (1H, d, *J* = 6.0 Hz); 7.61 (1H, t, *J* = 6.0 Hz); 7.54 (1H, t, *J* = 6.0 Hz); 7.31-7.44 (10H, m); 7.05 (2H, d, *J* = 6.4 Hz); 6.90 (2H, d, *J* = 6.4 Hz); 6.86 (6H, d, *J* = 6.0 Hz); 5.24 (1H, t, *J* = 4.0 Hz); 5.19 (2H, s); 4.21 (2H, d, *J* = 4.0Hz); 2.37 (2H, t, *J* = 6.0 Hz); 1.41 (2H, q, *J* = 6.0 Hz); 1.15 (2H, sx, *J* = 6.0 Hz); 0.73 (3H, t, *J* = 6.0 Hz). MS: *m/z* calcd for $C_{41}H_{37}ClN_6O$: 664.2717 [MH^+], found 665.597.

Azide-modified trityl losartan

5-[4'-(5-Azidomethyl-2-butyl-4-chloro-imidazol-1-ylmethyl)-biphenyl-2-yl]-2-trityl-2H-tetrazole

Yield: 275 mg (87%), white crystalline powder. MS: *m/z* calcd for $C_{41}H_{36}ClN_9$: 689.278, found 690.489 [MH^+] (100%) and 728.507 [MK^+] (100%). ^{1}H-NMR (300 MHz, $CDCl_3$): δ 0.86 (t, *J* = 7.3 Hz, 3H); 1.29 (sx, *J* = 7.4 Hz, 2H); 1.66 (qn, *J* = 7.7 Hz, 2H); 2.51 (t, *J* = 7.8 Hz, 2H); 3.94 (s, 2H); 4.98 (s, 2H); 6.70 (d, *J* = 8.2 Hz, 2H); 6.90 (d, *J* = 7.7 Hz, 2H); 7.11 (d, *J* = 8.2 Hz, 2H); 7.30-7.36 (m, 10H); 7.41-7.51 (m, 2H); 7.96 (m, 1H).

Azide-modified losartan

Product: clear crystalline oil. MS: *m/z* calcd for $C_{22}H_{22}ClN_9$: 447.169, found 448.185 [MH^+] (100%). ^{1}H-NMR (500 MHz, $CDCl_3$): δ 0.85 (t, *J* = 7.4 Hz, 3H); 1.32 (sx, *J* = 7.4 Hz, 2H); 1.61 (qn, *J* = 7.6 Hz, 2H); 2.59 (t, *J* = 7.6 Hz, 2H); 4.40 (s, 2H); 5.27 (s, 2H); 6.94 (d, *J* = 7.8 Hz, 2H); 7.10 (d, *J* = 7.9 Hz, 2H); 7.43-7.49 (m, 2H); 7.56 (t, *J* = 7.5 Hz, 1H); 7.70 (d, *J* = 7.4 Hz, 1H).

NO_2PyKYNE

2-Nitro-3-pent-4-yn-1-yloxypyridine

Yield: 2.81 g (64%), white crystalline powder. HPLC (50:50 MeCN/H_2O (0.1M AF), 2ml/min): 4.6 min. ^{1}H-NMR ($CDCl_3$, 300 MHz): δ: 8.08 (dd, *J* = 3.2, 2.6 Hz, 1H); 7.51-7.50 (m, 2H); 4.23 (t, *J* = 6.0 Hz, 2H); 2.45 (td, *J* = 6.8, 2.6 Hz, 2H); 2.03 (qn, *J* = 6.1 Hz, 2H); 1.95 (t, *J* = 2.6 Hz, 1H). ^{13}C-NMR (75 MHz, $CDCl_3$): δ: 150 (C); 147.14 (C); 139.20 (CH); 128.53 (CH); 123.43 (CH); 82.68 (CH_2); 69.16 (CH); 69.43 (CH_2); 67.88 (CH_2); 27.58 (CH_2); 14.87 (CH_2). MS: *m/z* calcd for $C_{10}H_{10}N_2O_3$: 206.0691, found 245.030 [MK+]. The ^{1}H and ^{13}C NMR data were in agreement with the values reported in the literature (Kuhnast et al., 2008).

FPyKYNE

2-fluoro-3-pent-4-yn-1-yloxypyridine

Yield: 155 mg (89%), clear oil (crystallizes at 4°C). HPLC (50:50 MeCN/H_2O (0.1M AF), 2 ml/min): 4.6 min. ^{1}H NMR (300 MHz, $CDCl_3$): δ: 7.75 (dd, *J* = 4.8, 1.6 Hz, 1H); 7.32 (m, 1H); 7.12 (dd, *J* = 7.8, 4.9 Hz, 1H); 4.17 (t, *J* = 6.1 Hz, 2H); 2.45 (td, *J* = 6.9, 2.6 Hz, 2H); 2.05 (qn, *J* = 6.4 Hz, 2H); 2.0 (t, *J* = 2.6 Hz, 1H). ^{13}C-NMR (75 MHz, $CDCl_3$): δ: 153.85 (C, $J^1_{C\text{-}F}$ = 237.3 Hz); δ: 142.23 (C, $J^2_{C\text{-}F}$ = 25.4 Hz); 137.37 (C, $J^3_{C\text{-}F}$ = 13.2 Hz); δ: 122.81 (C, $J^3_{C\text{-}F}$ = 4.4 Hz); δ: 121.66 (C, $J^4_{C\text{-}F}$ = 4.3 Hz); 82.93 (C); 69.16 (CH); 67.50 (CH_2); 27.83 (CH_2); 14.96 (CH_2). ^{19}F-NMR: δ -84.79 (referenced with

respect to TFA). MS: *m/z* calcd for $C_{10}H_{10}FNO$: 179.0746, found 179.076 [M^+]. The ^1H and ^{13}C NMR data were in agreement with the values reported in the literature (Kuhnast et al., 2008).

Nitropyridine trityl losartan

3-[3-(1-{2-Butyl-5-chloro-3-[2'-(2-trityl-2H-tetrazol-5-yl)-biphenyl-4-ylmethyl]-3H-imidazol-4-ylmethyl}-1H-[1,2,3]triazol-4-yl)-propoxy]-2-nitro-pyridine

Product: clear oil. ^1H-NMR (300 MHz, $CDCl_3$): δ 8.06 (dd, *J* = 2.2 Hz, 1H); 7.94-7.98 (m, 1H); 7.42-7.55 (m, 4H); 7.20-7.35 (m, 11H); 7.12 (d, *J* = 8.3 Hz, 2H); 6.75 (d, *J* = 8.3 Hz, 2H); 6.89-6.94 (m, 6H); 5.13 (s, 2H); 5.03 (s, 2H); 4.17 (t, *J* = 6.1 Hz, 2H); 2.87 (t, *J* = 7.2 Hz, 2H); 2.53 (dd, *J* = 7.9 Hz, 2H); 2.21 (qn, *J* = 7.1 Hz, 2H); 1.67 (qn, *J* = 7.9 Hz, 2H); 1.28 (sx, *J* = 7.6 Hz, 2H); 0.86 (t, *J* = 7.3 Hz, 3H). MS: *m/z* calcd $C_{51}H_{46}ClN_{11}O_3$: 895.3474, found 896.60 [MH^+].

Fluoropyridine trityl losartan

3-[3-(1-{2-Butyl-5-chloro-3-[2'-(2-trityl-2H-tetrazol-5-yl)-biphenyl-4-ylmethyl]-3H-imidazol-4-ylmethyl}-1H-[1,2,3]triazol-4-yl)-propoxy]-2-fluoro-pyridine

Product: clear oil. MS: *m/z* calcd for $C_{51}H_{46}ClFN_{10}O$: 868.3529, found: 869.569 [MH^+].

Fluoropyridine losartan

3-[3-(1-{2-Butyl-5-chloro-3-[2'-(2H-tetrazol-5-yl)-biphenyl-4-ylmethyl]-3H-imidazol-4-ylmethyl}-1H-[1,2,3]triazol-4-yl)-propoxy]-2-fluoro-pyridine

Product: clear oil. TLC (7:2:0.5 EtOAc/Hexanes/MeOH): Rf 0.32. HPLC (35:65 MeCN/AF (0.1M) at 2ml/min): 10.3 min; azide losartan 9.4 min; FPyKYNE 13.7 min (Figure 4-1). ^1H-NMR (300 MHz, $CDCl_3$): δ 7.86 (dd, *J* = 7.51, 1.4 Hz, 1H); 7.65-7.68 (m, 1H); 7.52 (td, *J* = 7.47, 1.6 Hz, 1H); 7.46 (td, *J* = 7.53, 1.7 Hz, 1H); 7.24-7.36 (m, 1H); 6.98-7.07 (m, 2H); 6.81 (d, *J* = 8.4 Hz, 2H); 6.39 (d, *J* = 8.3 Hz, 2H); 5.40 (s, 2H); 5.26 (s, 1H); 5.24 (s, 2H); 3.81 (t, *J* = 6.3 Hz, 2H); 2.60 (t, *J* = 7.8 Hz, 3H); 1.86 (qn, *J* = 6.7 Hz, 2H); 1.67 (qn, *J* = 7.7 Hz, 2H); 1.34 (sx, *J* = 7.5 Hz, 2H); 0.86 (t, *J* = 7.3 Hz, 3H). ^{19}F-NMR (referenced with respect to TFA): -84.88 (d, *J* = 8.78 Hz). ^{13}C-NMR (75

MHz, $CDCl_3$): δ 153.75 (d, *J* = 237.52); 152.17 (CH); 150.15, 147.29, 142.03 (d, *J* = 25.33 Hz); 139.97, 138.30, 137.56 (d, *J* = 12.96 Hz); 135.16, 131.89, 131.55, 130.47, 130.06, 129.46, 128.49, 124.65, 123.15, 122.85 (d, *J* = 4.31 Hz); 121.93 (d, *J* = 4.28 Hz); 120.64, 120.24, 67.83, 53.62, 47.34, 42.55, 29.93, 28.33, 26.89, 22.55, 21.21, 13.85. MS: *m/z* calcd for $C_{32}H_{32}ClFN_{10}O$: 626.2433, found 627.318 [MH^+] (100%).

4.2 Radiochemistry

4.2.1 Experimental

For a standard 1 hr beam on the RD target, approximately 850-1050 mCi (31.45-38.85 GBq) is expected to be delivered to the hot cell (located roughly 24 ft away from the cyclotron). The HP target produces roughly twice the amount as the RD target. A typical synthesis of [F-18]FPyrLosartan began with a 45 min to 1 hr beam on the RD target. Following delivery of activity to the TRACERLab FX N Pro module, total synthesis took approximately 70 min, followed by a 25 min HPLC purification (Figure 4-2). The first step in the synthesis, displacement of the nitro group on NO_2PyKYNE by F-18, occurred in the first vessel and produced [^{18}F]FPyKYNE in 35 min with a 15-20% yield (decay-corrected). The second and third steps, which take place in the second reaction vessel, produce the final product in another 35 min with a 44-70% yield (decay-corrected from [^{18}F]FPyKYNE). This translates to an overall yield of 7-14% from start of synthesis. Product reformulation, including extraction from the HPLC solvent via SPE with a C-18 sep-pak, takes approximately 10-15 min. Thus, the final product can be ready for injection roughly 1 h 45 min from EOB, plus another 10 min or so for quality control by HPLC analysis.

4.2.2 Quality Control

The identity, purity and specific activity of [F-18]FPyrLos was determined by analytical HPLC (Figure 4-3). The identity of the product was confirmed by a co-injection of the formulated product with the cold standard. The chemical and radiochemical purity were consistently greater than 97%. Due to the setup of the HPLC system, the sample flows first through the UV detector followed by the radiation detector translating to a small delay between the UV peak and radiation peak elution times. Specific activity ranged from 200-4200 mCi/μmol.

4.3 MicroPET Imaging

4.3.1 Baseline

Scans of normal rats showed the greatest accumulation of activity in the liver and kidneys (Figure 4-4). During the early frames (0-60 seconds), the tracer distributes from the tail vein to the left atrium, left ventricle, aorta, lungs, liver and kidneys. An ROI drawn over the left atrium was used to represent the blood pool and served as the input function for kinetic analysis. In the first few minutes, activity rises and declines sharply to reach background level around 10 min (Figure 4-5, A). Around 10 min, activity in the liver reaches its maximum and stabilizes. Second to the liver, the kidneys also show a high uptake of activity. Following the blood input function, the kidney TAC shows a sharp increase in the first few minutes, followed by a slower wash-out to baseline around 55 minutes. The majority of the signal arises from the cortex and outer medulla (Figure 4-6). The greatest contrast between activity uptake in the kidney and surrounding tissue could be observed around 10 min and was thus chosen for the time of sacrifice for metabolite studies.

The average distribution volume of [^{18}F]FPyrLos in the left kidney of control rats, obtained from Logan the plot (Figure 4-7) generated with the Siemen's Inveon Workstation (IRW 4.0), was measured at 2.76 ± 0.68 ml/cm^3 (n=7) (Figure 4-8).

4.3.2 Blocking Studies

When the rats were co-injected with candesartan, tracer uptake in the left kidney showed a dose-dependent reduction (Figure 4-6). After co-injection with 2.5 mg/kg candesartan, activity in the left kidney again increased rapidly in the first few minutes, but was effectively cleared from the kidney by approximately 20 min. When blocked with a 5 mg/kg and 10 mg/kg candesartan, washout was achieved around 16 min and 14 min, respectively. At a dose of 2.5 mg/kg, the SUV at 10 min in the left kidneys was 1.25 ± 0.17 (n=3). At 5 mg/kg and 10 mg/kg, it dropped even further to 0.99 ± 0.38 (n=5) and 0.61 ± 0.074 (n=3), respectively (Figure 4-8).

This decreasing trend in SUV was confirmed by calculating distribution volumes in the left kidney with Logan graphical analysis. DV values decreased when the rats were co-injected with candesartan (Figure 4-8). At a dose of 2.5 mg/kg candesartan, the calculated DV dropped to 1.46 ± 0.30 ml/cm^3 (n=3). Co-administration of 5 mg/kg candesartan produced a similar DV of 1.45 ± 0.21 ml/cm^3 (n=5) whereas 10 mg/kg candesartan reduced the DV to 0.96 ± 0.06 ml/cm^3 (n=3), indicating no contrast in activity uptake between the tissue and blood. As the AT_1R should be fully blocked at the 10 mg/kg dose, any tracer retention observed should be from non-specific binding. The specific binding can thus be calculated as the difference in DV values from baseline and when blocked at the 10 mg/kg over the DV at baseline, which corresponds to a specific binding of around 65%.

4.3.3 Test-retest and Inter-operator Variability

To determine reproducibility of the DV calculation, four baseline rats were scanned a second time, less than 1 week after the first set of scans, and DV values calculated. The first group of scans produced an average DV of 2.41 ± 0.39 ml/cm^3 and the second group of scans produced an average DV of 2.40 ± 0.35 ml/cm^3. From a two-tailed paired t-test with a 95% confidence interval ($P < 0.05$) a P value of 0.97 was obtained, indicating that the difference was not statistically significant. That is, the results from the retest do no vary significantly from the original test. The variability between the first scan and second scan for each subject was also calculated by dividing the difference in DV values by the average of the two DV values for each subject. The average variability was 0.0457 or 4.57%. It is important to note that the results from the second scans were not included in the calculation for the average DV value.

Another co-worker repeated the DV calculation for the remaining baseline and blocking scans using her own ROIs to determine the inter-operator variability. The average difference between our values was found to be 0.28 ± 0.71. From a paired two-tailed *t*-test, a P value of 0.096 was found. After removing two outliers, that is, data values greater than the mean ± 2 standard deviations, the P value increased to 0.33 indicating that the difference between our results was not statistically significant.

4.4 Metabolism Studies

4.4.1 Controls

When plasma spiked with tracer was injected onto the HPLC, 86% of the activity was not retained by the capture cartridge. By disrupting the protein-binding interactions with urea, the tracer should be completely retained by the capture cartridge. The most effective concentration of urea was 1 g/ml of plasma (Figure 4-9). At 400 mg/ml, the amount of unretained activity was reduced from 86.0% to 41.7%, but with 1 g/ml, this fraction dropped even further to 12.4%. This effect was also observed with reconstituted heart and kidney samples. Without urea, the amount of activity not retained by the capture cartridge was 24% and 30%, respectively. However, with a concentration of 400 mg urea per ml of 1:99 MeCN/H_2O, the unretained fraction dropped to 11% and 1%. These observations are in agreement with previous studies on [^{11}C]methyl losartan (Antoun, 2010) and [^{11}C]methyl candesartan (Kirkpatrick, 2009). Thus, standard protocol incorporated dissolution of 1 g of urea per ml of plasma and 400 mg of urea per ml of tissue reconstituted in 1:99 MeCN/H_2O.

The control runs were used to identify the proportion of tracer not retained by the capture cartridge and use these values to correct the peaks areas of the unretained metabolites and of unchanged tracer in the experimental runs (*see §3.4.3.1 for calculations*).

4.4.2 Baseline

The plasma samples from normal rats revealed the presence of one labeled metabolite at roughly 4.7 min post-switch (peak 2) accounting for 5.94 ± 2.53% (n=6) of the total activity (Table 4-3). After control-correcting the area of peak 1 and peak 3, the amount of unchanged tracer accounted for 70.61 ± 10.15% of the total activity injected. The amount of unretained

activity, assumed to be labeled hydrophilic metabolites, represented 23.45 ± 9.18%. In the kidneys, there was a slightly smaller proportion of unchanged tracer representing 63.71 ± 24.45% (n=6) of the total activity, with the retained labeled metabolite (peak 2) accounting for 7.11 ± 3.85%.

4.4.3 Blocking Studies

When the AT_1 receptors were blocked with candesartan, both the plasma and kidneys saw a decrease in the proportion of unchanged tracer. In the plasma (Figure 4-10), a blocking dose of 10 mg/kg had the most drastic effect on the amount of unchanged tracer, dropping to 53.49 ± 15.74% (n=5, P = 0.068) from 70.61 ± 10.15% of the total activity compared to the 69.00 ± 4.72% (n=5) when blocked with 5 mg/kg. At both the 5 mg/kg and 10 mg/kg blocking doses, the proportion of metabolite (peak 2) remained similar at 2.36 ± 0.98% and 2.72 ± 0.10%, respectively (Table 4-3). The effect of blocking on the proportion of tracer in the plasma is shown in the HPLC chromatograms depicted in Figures 4-11 and 4-12.

The kidneys showed a more significant decrease in the amount of unchanged tracer with respect to the blocking dose (Figure 4-13). At 5 mg/kg candesartan, the amount of unchanged tracer dropped to 21.99 ± 19.63% (n=4) of the total activity from 63.71 ± 24.45% (P = 0.0015) and to 9.89 ± 13.73% (n=5, P = 0.0012) at a 10 mg/kg blocking dose. The proportion of activity represented by the metabolite also slightly decreased to 1.99 ± 1.96% and 2.13 ± 0.42%, respectively (Table 4-3). The reduced proportion of intact tracer due to blocking is clearly demonstrated in the HPLC chromatograms shown in Figures 4-14 and 4-15.

Table 4-1 Metabolite analysis of [F-18]fluoropyridine losartan in rats at 10 min injected with various blocking doses of candesartan: none, 5 mg/kg, and 10 mg/kg. Peak 1: activity/metabolites not retained by capture cartridge; Peak 2: activity/metabolite eluted from analytical column; Peak 3: unchanged tracer eluted off analytical column. Values indicate percentage of total activity (± SD).

	Peak #	Identity	Candesartan Dose (mg/kg)		
			None (n=6)	5 (n=5)*	10 (n=5)
Plasma	1	Unret. metabolites	23.45 ± 9.18	28.74 ± 3.63	44.24 ± 15.01
	2	Ret. metabolite	5.94 ± 2.53	2.36 ± 0.98	2.72 ± 0.10
	3	Unch. tracer	70.61 ± 10.15	69.00 ± 4.72	53.49 ± 15.74
Kidney	1	Unret. metabolites	29.18 ± 22.03	77.36 ± 20.03	89.05 ± 14.72
	2	Ret. metabolite	7.11 ± 3.85	1.99 ± 1.96	2.13 ± 0.42
	3	Unch. tracer	63.71 ± 24.45	21.99 ± 19.63	9.89 ± 13.73

* n = 4 for kidney; both kidneys were analysed for every rat (*n*)

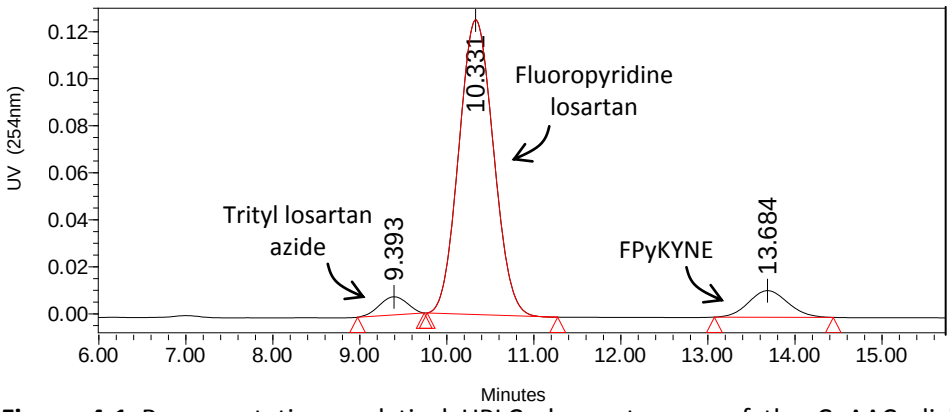

Figure 4-1 Representative analytical HPLC chromatogram of the CuAAC click reaction between azide-modifed trityl losartan and FPyKYNE. The reaction was performed with $CuSO_4$ and Na Ascorbate in DMSO/water (3:1) for 4 h at 80°C. The sample was detritylated prior to injection with TFA for 2 min at 80°C. Column: Phenomenex Luna C18(2), 10 µM, 250 x 4.6 mm; HPLC solvent: 35/65 MeCN/AF (0.1 M) at 2 ml/min; Millenium HPLC Analysis Software.

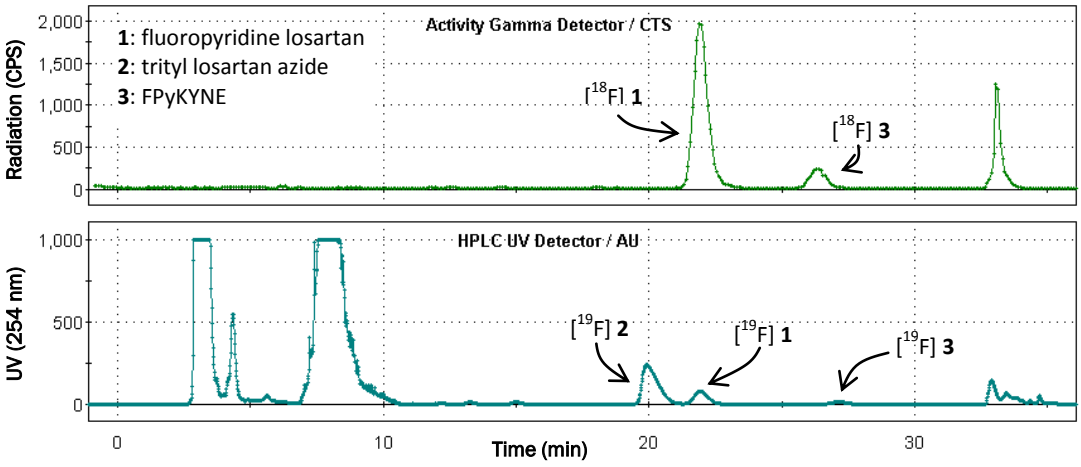

Figure 4-2 Representative semi-prep HPLC chromatogram from purification of [^{18}F]fluoropyridine losartan after synthesis on the TRACERlab FX N Pro module (by GE Healthcare). Column: Phenomenex Luna C18(2), 10 µM, 250 x 10 mm; HPLC solvent system 30:70 MeCN/water (0.1 M AF) at 10 ml/min (switch to MeOH at 30 min).

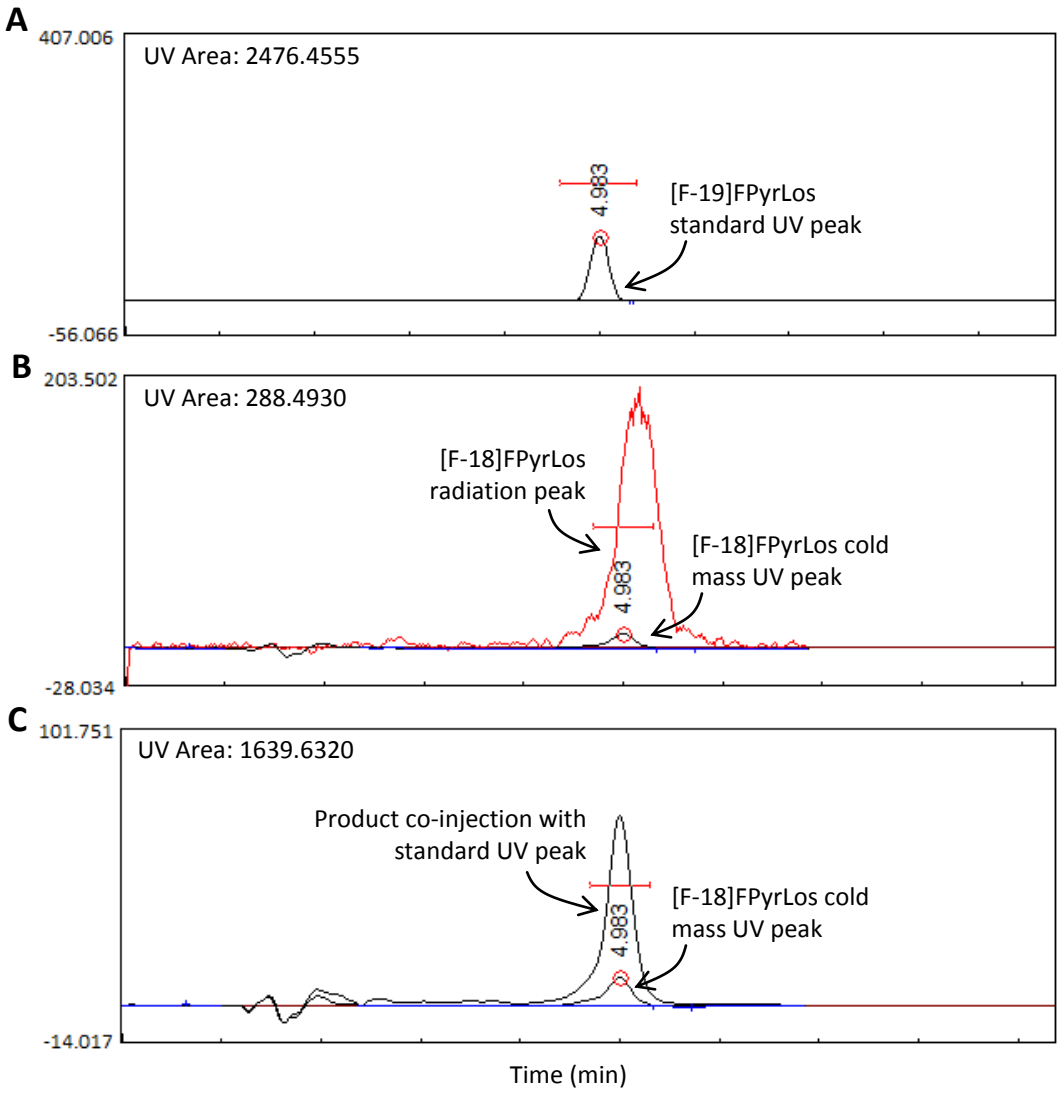

Figure 4-3 Quality control for [F-18]FPyrLosartan formulated product by analytical HPLC. A) UV chromatogram of cold product standard; B) radiation and UV chromatogram of product formulation; C) UV chromatogram from co-injection of product and standard overlaid on UV chromatogram of product from B). UV spectra were recorded at 254 nm. Column: Phenomenex Luna C18(2) (10 µM, 250 x 4.6 mm) with 40:60 MeCN/AF (0.1 M) at 2 ml/min; PeakSimple 3.93 Analysis Software.

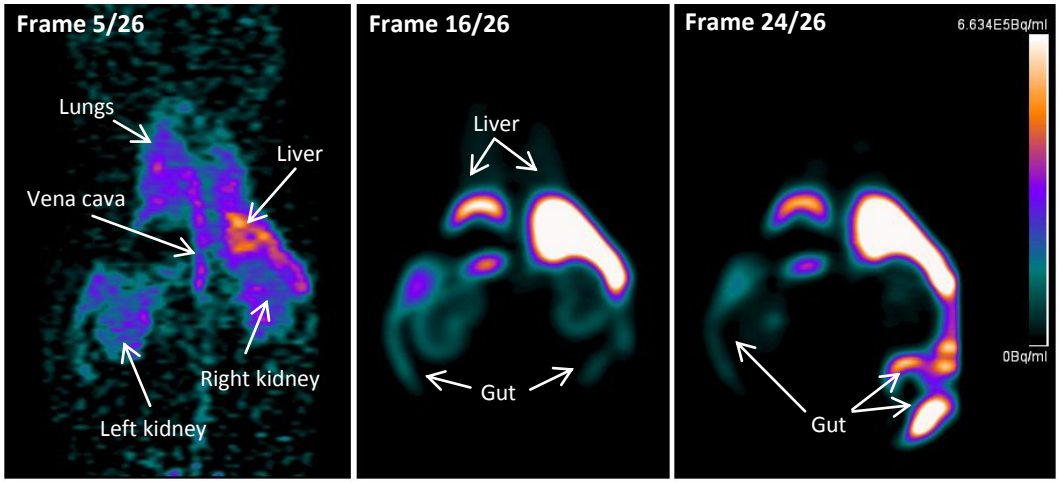

Figure 4-4 MicroPET images of [^{18}F]FPyrLosartan in a normal, untreated Sprague Dawley rat. All images are of the coronal view from slice 32/128. Frame 5/26: 40-50 seconds; Frame 16/26: 5-10 min; Frame 24/26: 45-50 min. Rats were injected with 0.45-1.1 mCi (16.6-40.7 MBq) of tracer. Images (%ID/ml) were analysed with the Siemens' IRW analysis software.

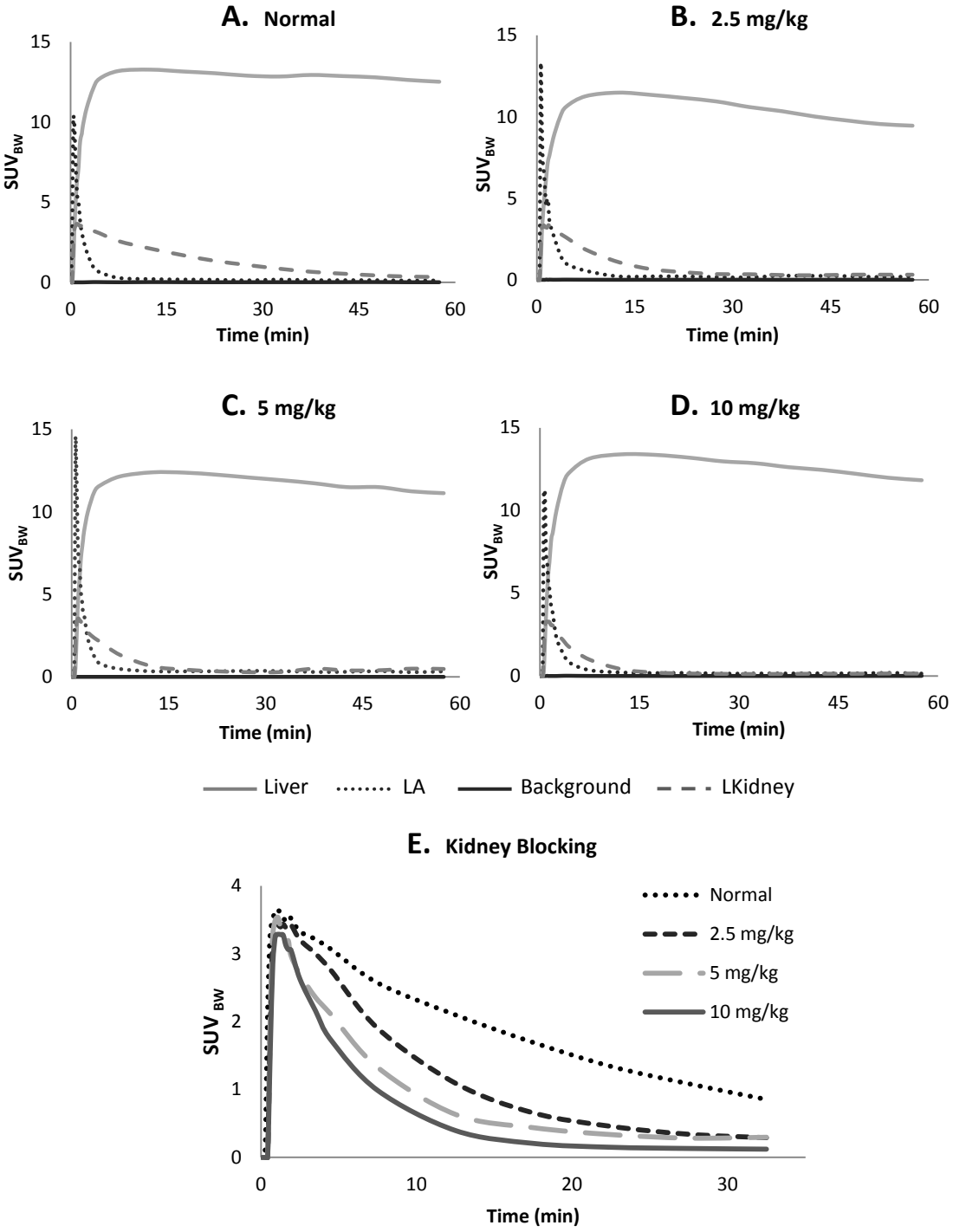

Figure 4-5 SUV curve of [^{18}F]FPyrLosartan in Sprague Dawley rats injected with various blocking doses of candesartan (A-D). E) SUVs of the kidney from the 4 blocking groups superimposed. Blocking doses were injected immediately prior to activity injection. Standard uptake values (SUV) were normalized to body weight (BW). Regions of interest (ROI) were drawn on the liver, left atrium (blood pool), background, and left kidney.

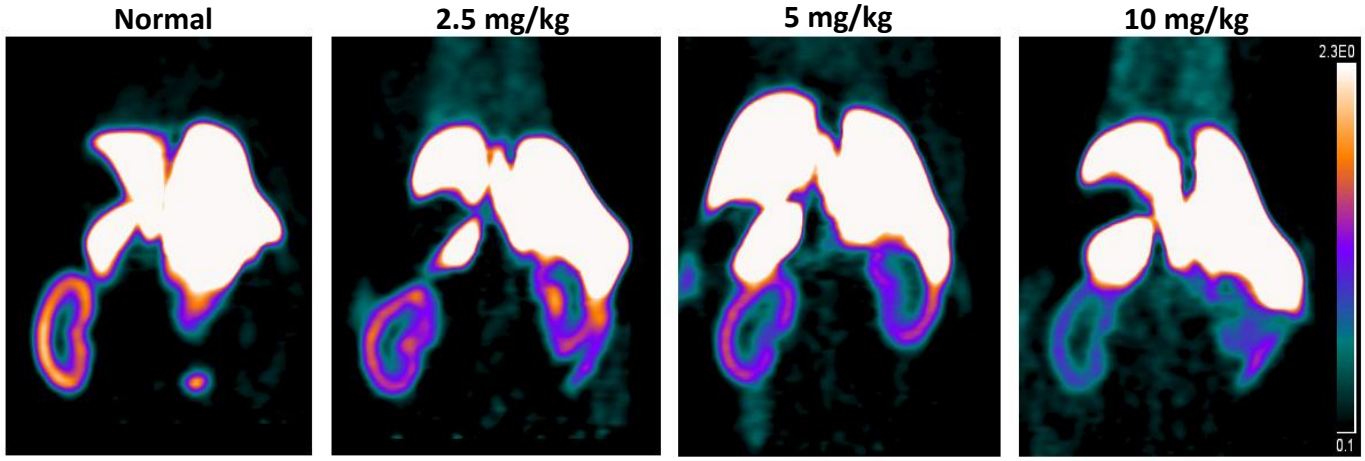

Figure 4-6 MicroPET images of [^{18}F]fluoropyridine losartan in a rats at 10 min injected with various blocking doses of candesartan: A) 2.5 mg/kg, B) 5 mg/kg, C) 10 mg/kg. All images are of the coronal view and measured in SUV. Frame 4/26: 30-40 sec; Frame 16/26: 5-10 min; Frame 24/26: 45-50 min. Injected activity: 0.50-0.54 mCi (18.5-20.0 MBq). Images were analysed with the Siemens' IRW (4.0) analysis software.

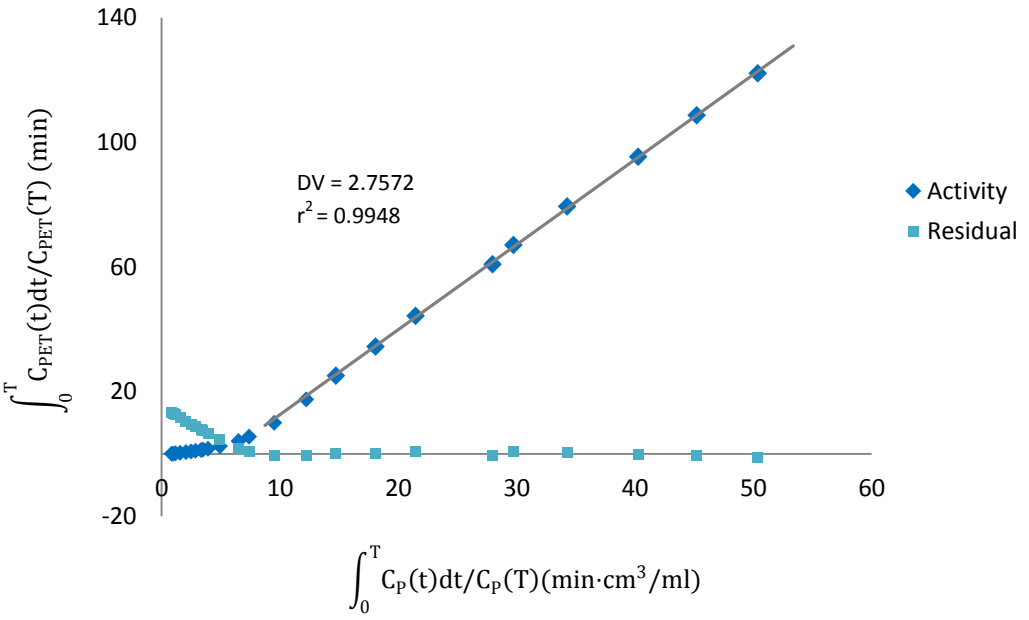

Figure 4-7 Representative Logan plot of [^{18}F]FPyrLosartan in the left kidney of a normal rat. Activity injected: 0.54 mCi (20.03 Bq). C_P; concentration of activity in the plasma, C_{PET}; concentration of activity in the tissue. Activity uptake was derived from an ROI over the left kidney (C_{PET}) and left atria (C_P). The slope of the line-of-best-fit provides a DV value of 2.76 ml/cm^3 with a correlation coefficient (r^2) of 0.9948. Graph was regenerated from IRW (4.0) data.

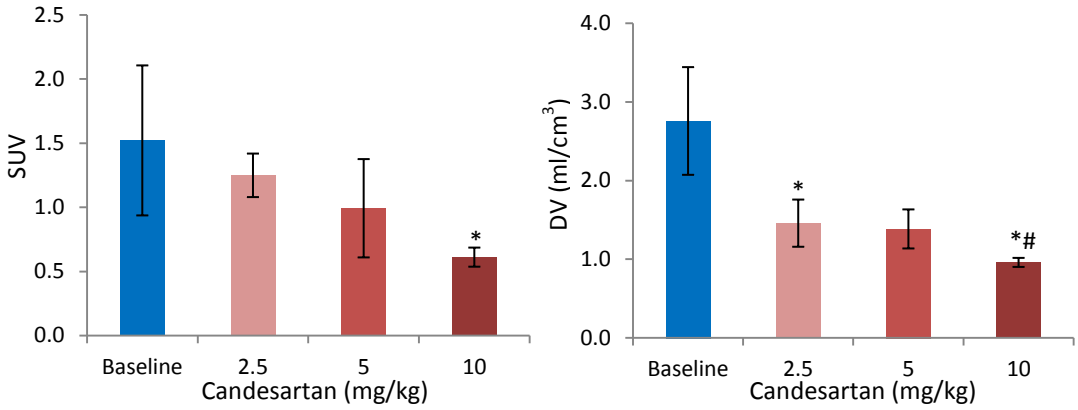

	Control	Candesartan Dose (mg/kg)		
	0.0	**2.5**	**5**	**10**
	(n=7)	(n=3)	(n=5)	(n=3)
DV (ml/cm^3)	2.76 ± 0.68	1.46 ± 0.30	1.45 ± 0.21	0.96 ± 0.06
SUV	1.52 ± 0.58	1.25 ± 0.17	0.99 ± 0.38	0.61 ± 0.074

Figure 4-8 Effect of candesartan blocking dose on distribution volume and uptake of [^{18}F]fluoropyridine losartan in the kidney of Sprague Dawley rats. Blocking doses were injected immediately prior to activity injection. Distribution volumes (DV) were determined from Logan graphical analysis of the PET images. SUV values were taken at 10 min. * $P < 0.05$ compared to baseline; # $P < 0.05$ compared to previous dose.

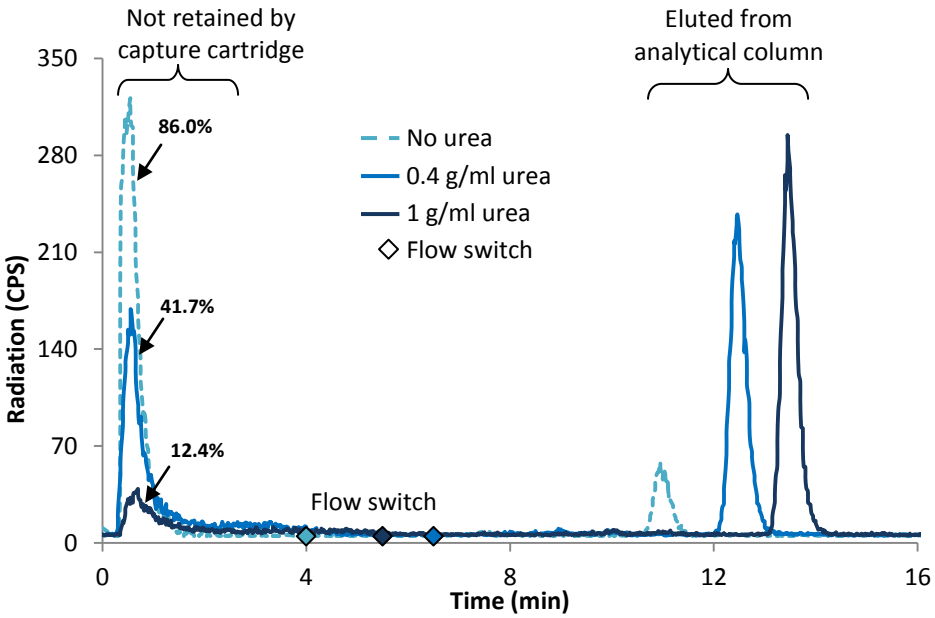

Figure 4-9 Effect of urea on tracer retention by the capture cartridge. Plasma from a normal, untreated rat was spiked with [^{18}F]fluoropyridine losartan tracer and separated into three aliquots (1 ml) to which varying amount of urea was dissolved (0g, 0.4 g, and 1 g). Flow was switched at 4 min, 6 min, and 5.5 min, respectively. Tracer elutes approximately 7 min post-switch.

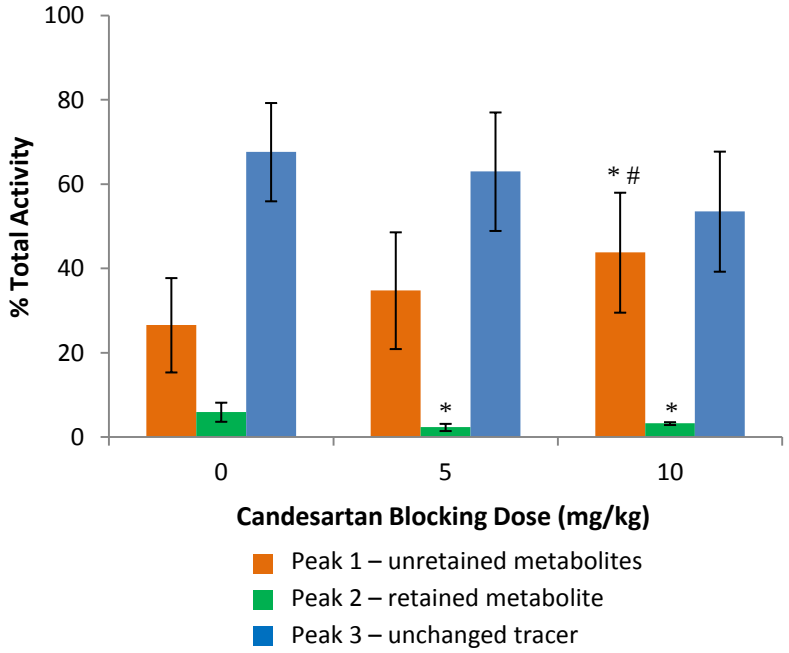

Figure 4-10 Plasma metabolite profile of [^{18}F]FPyrLosartan in rats. Blocked rats were co-injected with 5 mg/kg (n=5) or 10 mg/kg (n=4) candesartan. Baseline rats (n=6) received only tracer. Peak 1: unretained activity; Peak 2: metabolite; Peak 3: unchanged tracer. $P < 0.05$; * compared to baseline; # compared to previous dose.

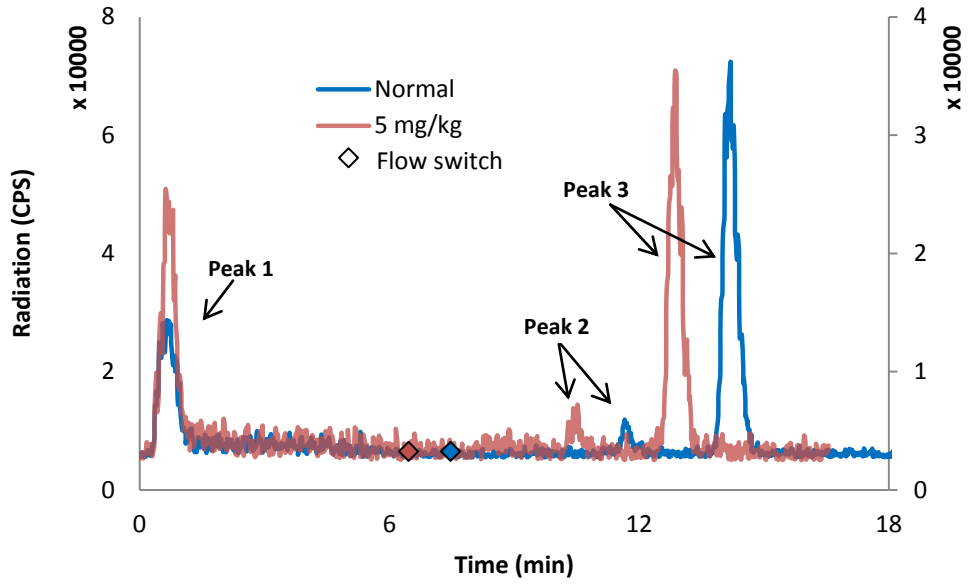

Figure 4-11 Plasma [^{18}F]FPyrLosartan metabolites in a normal and blocked rat as analysed by column-switch HPLC. Blocked rat was co-injected with 5 mg/kg candesartan. Peak 1: unretained activity; Peak 2: metabolite; Peak 3: unchanged tracer. Normal: switch at 7 min; block 5 mg/kg: switch at 6 min. Rats were sacrificed 10 min post-injection.

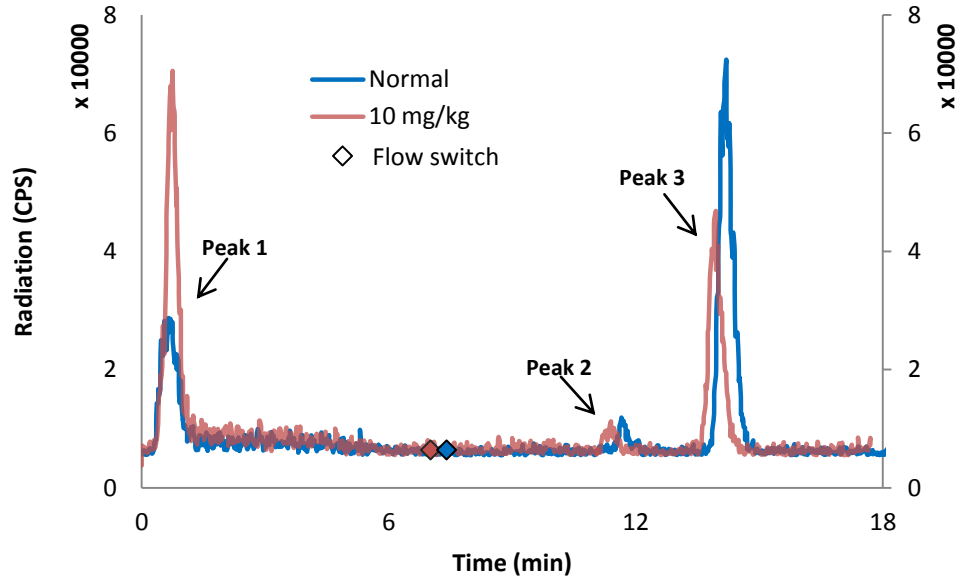

Figure 4-12 Plasma [^{18}F]FPyrLosartan metabolites in a normal and blocked rat as analysed by column-switch HPLC. Blocked rat was co-injected with 10 mg/kg candesartan. Peak 1: unretained activity; Peak 2: metabolite; Peak 3: unchanged tracer. Normal: switch at 7 min; block 10 mg/kg: switch at 6.5 min. Rats were sacrificed 10 min post-injection.

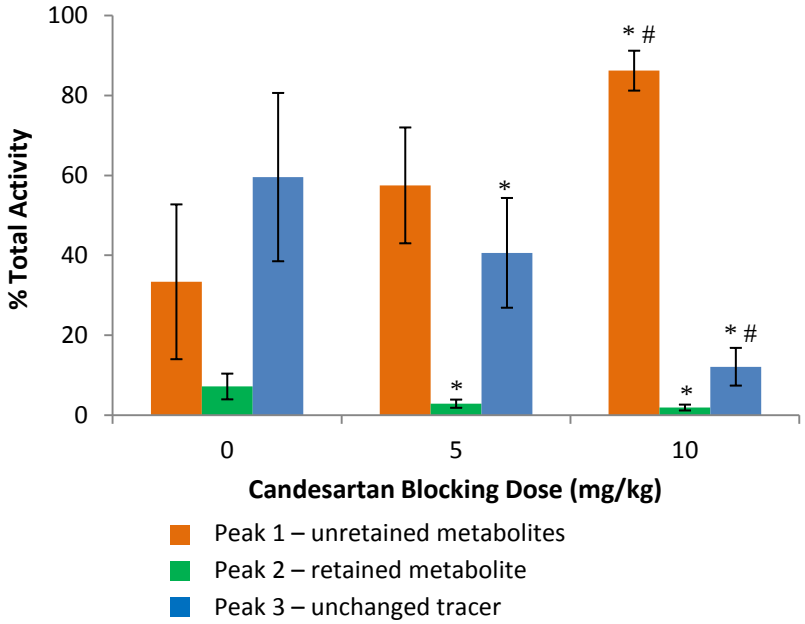

Figure 4-13 Kidney metabolite profile of [^{18}F]FPyrLosartan in rats. Blocked rats were co-injected with 5 mg/kg (n=4) or 10 mg/kg (n=5) candesartan. Baseline rats (n=6) received only tracer. Both kidneys of each rat (n) were analysed. Peak 1: unretained activity; Peak 2: metabolite; Peak 3: unchanged tracer. $P < 0.05$; * compared to baseline; # compared to previous dose.

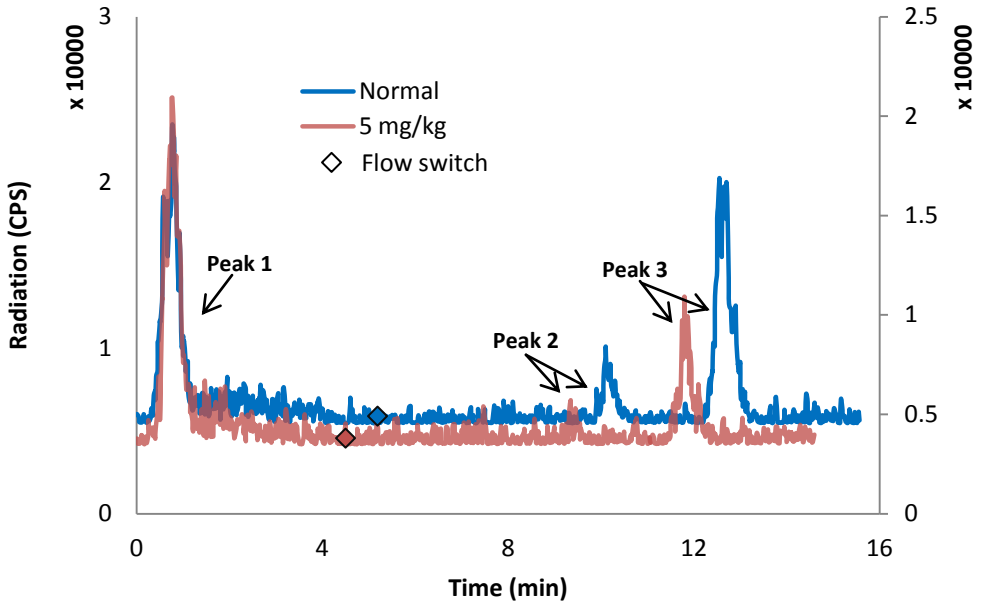

Figure 4-14 Kidney [^{18}F]FPyrLosartan metabolites in a normal and blocked rat as analysed by column-switch HPLC. Blocked rat was co-injected with 5 mg/kg candesartan. Peak 1: unretained activity; Peak 2: metabolite; Peak 3: unchanged tracer. Normal: switch at 5.4 min; block 5 mg/kg: switch at 4.6 min. Rats were sacrificed 10 min post-injection.

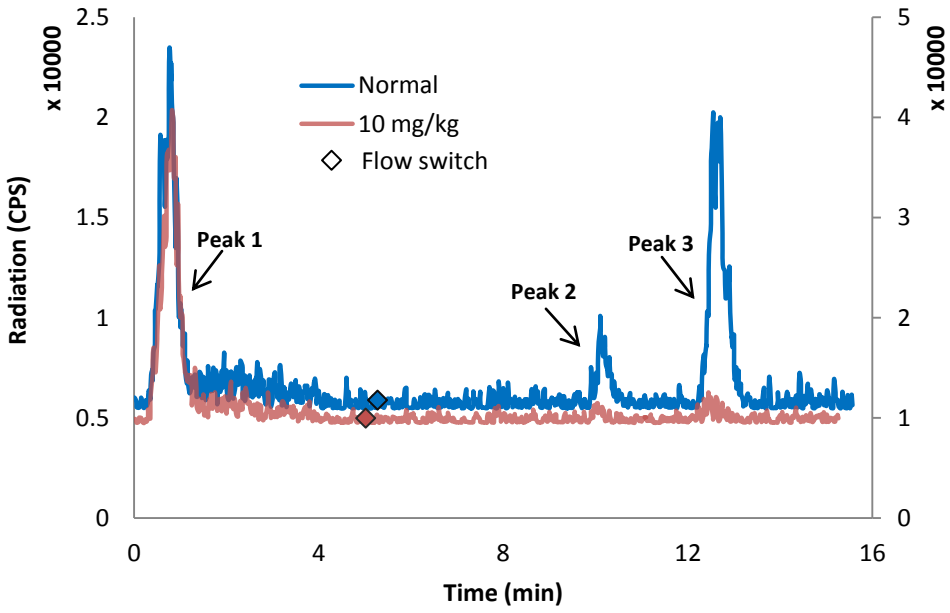

Figure 4-15 Kidney [^{18}F]FPyrLosartan metabolites in a normal and blocked rat as analysed by column-switch HPLC. Blocked rat was co-injected with 10 mg/kg candesartan. Peak 1: unretained activity; Peak 2: metabolite; Peak 3: unchanged tracer. Normal: switch at 5.4 min; block 10 mg/kg: switch at 5.3 min. Rats were sacrificed 10 min post-injection.

5 DISCUSSION

5.1 Chemistry

5.1.1 Initial Work

Before producing the F-18 labeled compound, the cold (unlabeled) compound needed to be synthesized as a standard to verify the identity of the hot (F-18 labeled) product. The initial plan was to produce F-18 labeled losartan analogs via modification of the 5' hydroxyl group through either 1) alkylation with fluorethyl tosylate ([^{18}F]FEtTos) and/or fluoropropyl tosylate ([^{18}F]FPrTos), 2) direct nucleophilic substitution with potassium fluoride ([^{18}F]KF), or 3) acylation with N-succinimidyl 4-fluorobenzoate ([^{18}F]SFB) (Figure 5-1). However, these initial synthetic methods were more difficult than anticipated.

The first alkylating agent to be synthesized was ^{18}F-CH_2-Br (Coenen et al., 1986), which is still used today. However, due to its volatility, purification often proceeds via distillation. As we had not yet acquired the new dual reactor automated module and did not know its capabilities, we did not want to proceed with a molecule that we could not purify during hot synthesis. FEtTos is much less volatile and is commonly used to label amines (Berndt et al., 2008; Hara et al., 2002; Lee et al., 2007), carboxylic acids (Erlandsson et al., 2009), and phenols (Hamacher and Coenen, 2002; Krasikova et al., 2008; Schirrmacher et al., 2002; Sharma et al., 2006; Wester et al., 1999). FPrTos has been used less extensively (Koivula et al., 2005; Yamamoto et al., 2002). At the time of my research, I could not find any literature describing the use of FEtTos or FPrTos for labeling primary alcohols. However, the synthesis of FEtTos and FPrTos was straight-forward, producing good product yields and purity. Both products were characterized by MS and ^{1}H-NMR (Appendix

II). Conjugation with losartan, on the other hand, proved much more difficult. Formation of the alkoxide at 5'-hydroxyl group was attempted by treatment with LAH, NaH, and NaOMe and the reactions were monitored by either HPLC, following deprotection of the tetrazole with acid, or by TLC. Without acid deprotection, the analogs could only be eluted with MeOH which flushes many impurities along with the product making identification impossible. The reactions were inconsistent, produced numerous biproducts, and were difficult to purify, all of which resulted in minimal yield. Further, these reactions were oftentimes performed with only a few milligrams of starting material thus compounding these issues. There are several explanations as to why these reactions were unsuccessful: 1) the alkoxide was never produced; 2) the base was too strong and decomposed the prosthetic group and/or the product; 3) acid deprotection cleaved the prosthetic group; or 4) standard work up resulted in hydrolysis of the prosthetic group. It should be noted that attempts were made to deprotect the tetrazole in milder conditions to prevent hydrolysis of the prosthetic group (ie. lower concentrations of acid or lower temperatures for a longer duration, as well as refluxing in MeOH (Kumar et al., 2005).

Direct nucleophilic substitution of F-18 into a desired molecule can be difficult, especially when labeling peptides or complex molecules due to the potential for reaction with multiple functional groups. Further, nucleophilic fluorination requires harsh reaction conditions, including high temperatures and strongly basic solutions, which can cause denature or decompose the precursor molecule. It is well known that sulfonate esters, such as the mesylate or tosylate, are very good leaving groups. Thus, we planned on first converting the hydroxyl group to a mesylate or tosylate prior to substitution. However, the lability of these groups may also explain why the MS of suspected products only showed the mass of losartan. According to one patent (Allegretti et al., 2010), only the methanol substituted product could be observed by MS. However, after

further consideration, it was decided that we proceed with the SFB analog. Previous SAR had shown that hydrogen bonding capability at the 5'-hydroxyl group is necessary for high binding affinity and selectivity for the AT_1R and thus substitution of the hydroxyl group would likely have detrimental effects.

The simplest acylating agents include [^{18}F]fluorocarboxylic acids, esters and acid halides. However, aliphatic fluorines can be stripped of fluorine *in vivo* by way of α-hydroxylation and subsequent elimination of hydrofluoric acid. Thus, they are typically more susceptible to metabolism than fluoroaromatic prosthetics groups, such as SFB (Vaidyanathan and Zalutsky, 1992), which contain a stable C-F aromatic bond (Park et al., 2001). Compared to the previous AT_1R tracers labeled via O-methylation, including [^{11}C]methyl losartan, [^{11}C]methyl candesartan, [^{11}C]L-159,884 and [^{11}C]KR31173 (Figure 1-11), we hoped that direct substitution on an aromatic ring would produce a tracer with greater resistance to metabolism (Vaidyanathan, 2009). In the literature, SFB is used to label primary amines or thiol groups found in proteins and peptides (Li and Conti, 2010). We figured conjugation with a primary alcohol would be analogous. SFB was synthesized in high yield and purity from the fluorobenzoic acid (Vaidyanathan and Zalutsky, 2006) (Appendix II). However, the same issues that hindered the process of the alkylation reactions, that is formation of the alkoxide and deprotection of the tetrazole, again proved to be an issue. As an ester is relatively easily hydrolysed, this was altogether not too surprising. After an extensive literature search, there was no evidence describing a reaction between SFB and an alcohol. So, in the possibility that SFB reacts only with the amino group, we tried converting the hydroxyl group to an amine. Further, as an amine is more acidic than an alcohol, a weaker base should result in deprotonation. A method was chosen whereby a hydroxyl group is converted to an amine through the azide (Thompson et al., 1993). However, unlike the azide, the amine was

difficult to produce and even more difficult to purify in reasonable yield. Reductions were carried out with $SnCl_2$/PhSH (Bartra et al., 1990; Coleman et al., 2004), Staudinger-type reaction with TPP (Ghosh et al., 2007; Pal et al., 2004; Raju et al., 2003), and LAH (Boyer, 1951). MS did seem to show product formation. The most promising method was from reduction with PhSH and $SnCl_2$ where, by ^{1}H-NMR, the amine seemed to have been produced: the α-hydrogens produced a doublet of doublets at 4.20 ppm (J = 5.64, 0.9 Hz), whereas with TPP a singlet was produced at 4.13 ppm, and with LAH a broad singlet was produced at 3.97 ppm. It is possible that the electronic and steric environment provided by the amine and azide are too similar to cause a noticeable change in the shift of the α-hydrogens. In order to decide whether or not to continue with the amine, we thought we would attempt synthesis of [^{18}F]SFB. We had just received the new TRACERlab FX N Pro module and were learning how to use it. The literature showed various methods for producing SFB, most either starting from the aldehyde or ester. We decided to start with the ester as the transformation steps seemed most amendable to the automated module. However, regardless of what seemed to be a simple reaction (Wüst et al., 2003), the identity of the triflate precursor could not be confirmed by MS or ^{1}H-NMR (and neither could the fluorinated product after attempted substitution with KF/$K_{2.2.2}$. It should be noted that the synthesis of [^{18}F]SFB is complex, oftentimes requiring upwards of 3 steps, 2 reaction vessels, multiple SPE cartridges and/or HPLC purification. Although a 3-step, 1-pot synthesis with Sep-Pak purification has been recently described in the literature (Tang et al., 2010). Thus, most single-reactor modules would not be able to synthesize [^{18}F]SFB, label the target compound, and purify the product, without modification to the module or manual manipulation of the radioactivity.

5.1.2 Click Chemistry

Knowing that click chemistry via the CuAAC reaction was possible with azides, and that by definition these reactions could be performed under mild conditions, it was proposed we use the azide intermediate as a precursor. At the same time, post-doctorate fellow Ana C. Valdivia was working on the synthesis of [^{18}F]FPyKYNE for labeling an azide-modified RGD peptide (Valdivia et al., 2011) and thus we collaborated. Throughout the literature, various catalytic systems have been tested to optimize the CuAAC reaction conditions (Binder and Sachsenhofer, 2007). The Cu(I) catalyst can either be introduced directly as a Cu(I) salt, such as copper(I) iodide (CuI), or prepared *in situ* by oxidation of copper metal or reduction of a Cu(II) salt, such as the reduction of copper(II) sulphate ($CuSO_4$) by sodium ascorbate (Bock et al., 2006). Cu(I) sources tended to result in by-products, lower yield and proceeded more slowly than reactions employing the *in situ* reduction of a Cu(II) salt (Mamat et al., 2009; Rostovtsev et al., 2002; Siegfried, 2000; Sirion et al., 2007; Tornoe et al., 2002). The issues with CuI may be circumvented with a base (Binder and Sachsenhofer, 2007) or stabilizing ligands to prevent re-oxidation to Cu(II), thus inhibiting Cu(II)-catalyzed alkyne homocoupling (Binder and Sachsenhofer, 2007), and to prevent disproportionation to Cu(0) and Cu(II). An aqueous system comprising $CuSO_4$ and NaAsc is the most common reaction condition (Meldal and Tornoe, 2008). Organic co-solvents include DMF, MeCN, DMSO, THF and t-BuOH. Varying amounts of Cu(I) catalyst have been applied successfully and, for the most part, sodium ascorbate is present in excess with respect to Cu(I) (Himo et al., 2005; Meldal and Tornoe, 2008). Ideally the solvent should dissolve all components; however heterogeneous solutions such as DCM/water or toluene/water (Binder and Sachsenhofer, 2007) have proven successful likely due to the high pseudoconcentrations achieved at the solvent interface (Meldal and Tornoe, 2008). A solvent system of tert-

butanol/water or DMSO/water seemed to be a common choice for its reliability and higher yields (Mamat et al., 2009; Sirion et al., 2007).

Using these previous experiments as a starting point, we began testing various reaction conditions. Importantly, azide-modified losartan is insoluble in mostly every solvent at room temperature, except DCM, unless heated to promote dissolution (45°C-80°C). It was found that reaction in DCM/water with $CuSO_4$/NaAsc at 30-40°C was too slow for hot chemistry. A system of DMSO/water at 80°C with $CuSO_4$/NaAsc provided the most reliability and highest yield in a less than 30 min reaction time. Deprotection of the tetrazole was insured by treatment with acid (HCl or TFA) at 70-80°C for 1-2 min and product evolution was verified by analytical HPLC with coinjection of detritylated azide losartan (Figure 5-2).

The CuAAC is not without limitations (Tornoe et al., 2002) of which the greatest issue is alkyne homocoupling, mentioned previously. Further, reactants must contain terminal alkyne or azide functionalities. In terms of biology, the toxicity of the copper catalyst can pose an issue (Wang et al., 2003). Copper has shown to mediate the generation of reactive oxygen species (ROS) (Liu et al., 2006) as well as the oxidation of sodium ascorbate by molecular oxygen, producing hydrogen peroxide (H_2O_2). In addition, copper ions can act as a sacrificial reductant, intercepting ROS and accelerating H_2O_2 decomposition (Hong et al., 2009).

5.2 Radiochemistry

Optimization of the hot click reaction required time and effort. Various solvent systems and Cu(I) sources were tested. It was found that DCM/water reaction was performed with $CuSO_4$/NaAsc at 30-40°C, but was too slow and inconsistent. A system of DMSO/water at 80°C

with $CuSO_4$/NaAsc provided the most reliability and highest yield. A system of MeCN/ H_2O at 80^oC proved successful multiple times (hot and cold reactions), however after noting inconsistency we returned to the literature and realized this may be due to the ability of MeCN to solvate Cu(I). Problems with the reaction were often a result of issues particular to the module, including air leaks (as the module uses positive and negative pressure to move the solvents), clogged lines, and/or contaminated parts (eg. vessels, reagents or lines). Further, hot reactions are prone to failure if there is insufficient drying of the $^{18}F/K_{222}/K_2CO_3$ complex. It should also be noted that in hot reactions the amount of alkyne is minimal compared the amount of azide, whereas in cold reactions, we oftentimes used excess alkyne. The change in stoichiometries could affect the rate of the reaction.

The second major obstacle was the apparent loss of significant amounts of activity following evaporation of the eluent used to wash [^{18}F]FPyKYNE from the silica cartridges. As the eluent was a mixture of hexane (bp 69^oC) and EtOAc (bp 77^oC), evaporation was effected at temperatures in excess of 50^oC and under vacuum. However, Inkster et al (Inkster et al., 2008) had previously noted product loss of [^{18}F]FPy5yne (bp 70^oC) during evaporation, even stating that concentration from a low boiling point solvent was essential. As FPyKYNE has a shorter alkyne chain length (5-C vs 6-C) one could presume it would be more volatile. The protocol was thus modified to include an eluent consisting of equal parts pentanes (bp 36^oC) and diethyl ether (bp 35^oC) followed by concentration at 25-30^oC without vacuum. In theory, distillation could provide a feasible means of purification; however distillation is difficult in automated machines (Inkster et al., 2008). We also modified the protocol to in include a series of 3 silica cartridges. Without fine control over the air pressure in the module, the fluorinated product and its nitro

precursor were simply pushed too quickly through a column of 1 or 2 cartridges to allow for optimal product separation.

Thirdly, finding the appropriate solvent for the semi-prep HPLC proved difficult. Initially the HPLC was run at 5 ml/min (6 MPa) with 35:65 MeCN/H_2O (0.1M AF). Product elution typically occurred around 20 min, closely following the losartan azide precursor at 19 min, with [^{18}F]FPyKYNE arriving at approximately 25 min. However, as there was minimal separation between the azide precursor and the product, contamination occurred frequently. Theoretically, the azide losartan analog would also bind to the AT_1 receptor and thus should be incorporated into the specific activity calculation. During optimization, a solvent system of 33:67 MeCN/H_2O (0.1M AF) at 8 ml/min and 30:70 MeCN/H_2O (0.1M AF) at 10 ml/min were tested. The latter system provided superior peak resolution. The cold standards for detrityl losartan azide and FPyKYNE were injected onto the module's semi-prep HPLC in triplicate to determine the expected elution times and to validate the consistency of the HPLC system. A cold click reaction between FPyKYNE and trityl losartan azide was then performed in the module and the reaction mixture injected in triplicate; elution times remained consistent with the standards injected previously. Detritylated losartan azide precursor eluted first around 20 min, followed by [^{18}F]FPyrLos at 22 min, and lastly, [^{18}F]FPyKYNE at 26 min (Figure 4-2). The peaks were identified by co-injecting the various cold standards with the collected peaks (Figure 5-2).

Specific activities for F-18 compounds are typically only a fraction of the theoretical maximum of 1710 Ci/µmol (63 TBq/µmol) (Welch and Redvanly, 2003). However, one study claimed that removing the Teflon (PTFE) components, leaving only non-fluorinated materials such as PEEK tubing, glass and polypropylene (PP), increased the SA 17- to 30-fold, thereby consistently providing an SA greater than 51 Ci/µmol (1.8 TBq/µmol) from a 60 min beam

(Berridge et al., 2009). Another group found that replacing the Teflon lines with PP increased their SA by a factor of 2 (Fuchtner et al., 2008). Teflon is the most widely used tubing and valve material due to its superior chemical inertness; however, it has the lowest resistance to ionizing radiation of the fluoropolymer family resulting in degradation. Thus, supposing that the radiolysis of Teflon components was the major source of F-19 carrier (Berridge et al., 2009), we replaced the delivery line from the cyclotron to the module with Tefzel, a fluoropolymer that is supposed to be more resilient to radiolysis. We also tried washing the target and delivery lines with O-18 water prior to beaming. These modifications only slightly improved the SA of the [^{18}F]fluoropyridine losartan tracer to just over 4,000 mCi/µmol. However, specific activities of around 22,000 mCi/µmol were being attained for [^{18}F]fluoropiridaz (previously BMS-747158-02), a myocardial perfusion agent that we were synthesizing for Lantheus Medical Imaging (LMI) in an adjacent hot cell. Interestingly, both modules shared the same delivery line from the cyclotron. The difference, however, was that [^{18}F]fluoropiridaz was being synthesized according to strict guidelines set forth by LMI in a different automated module by Eckert and Ziegler. Thus, it was suspected that the major contributors of F-19 in the TRACERlab FX N Pro module were the Teflon tubing between reactors and to the HPLC loop. By changing the tubing within the module, we hope to see a significant increase the SA. It should be noted however, that SA typically obtained for BMS-747158-02 was 1500 to 5500 mCi/µmol ((Yu et al., 2007). Multiple standards of the cold product were made and equal volumes injected in triplicate onto HPLC to assure reliability of the HPLC. We obtained consistent peak areas. It is possible that there are problems with the HPLC injection port, UV detector or peak integration program. For example, the background noise for the UV detector may be so significant that it is hiding the majority of the peak area, and thus the calculated SA is artificially high. Further, identifying other possible

sources of F-19 (eg. targets, reagents, SPE cartridges, glassware, valves, stir bars), and finding alternatives (eg. ceramic valves) should be investigated. With optimization we expect to achieve greater specific activities than those obtained for our C-11 labeled losartan and candesartan analogs, which were upwards of 3600 mCi/μmol and 1000 mCi/μmol, respectively (Antoun, 2010; Kirkpatrick, 2009).

Lastly, there was a significant loss of product during the purification and reformulation steps. The initial method involved rotary evaporation of the HPLC solvent from the collected fraction followed by reformulation. However, with evaporation, we lost approximately one third of the original activity. This loss could have been due to several factors, including solvent bumping, thermal decomposition to volatile bi-products, and transfer of activity between glassware. Further, during reformulation, only about another third of the dry activity could actually be removed from the 75-100 ml glass pear used for evaporation. As the product is insoluble in water reformulation into a saline or sodium bicarbonate solution is difficult. The only organic solvent safe for injection into living animals is EtOH, but its concentration must not exceed 10% of the final volume. In addition, there is an upper limit to the amount of volume that can be injected into rat; for a 400-700 g rat we aimed for less than 1.5 ml. Thus, in order to have sufficient activity for multiple PET scans, with around 0.5 mCi per rat, and taking into account that a scan is roughly 80 min and the half-life of F-18 is 110 min, the desired concentration can limit the volume of EtOH to very minute volumes (ie. 100-400 μl). Even so, the remaining activity was usually fixed to the glassware and could not be removed with larger volumes of EtOH. It was apparent that the reformulation procedure required optimization. In a brief attempt, we tried reformulation with a solution of 5:75:20 EtOH/propargyl alcohol/saline but this did not improve product dissolution. Another idea was to increase its water solubility by converting the product

into a salt (ie. with potassium carbonate). However, this method would still require rotary evaporation. Currently, routine syntheses are relying less on rotary evaporation and more on sep-pak cartridges for product isolation and reformulation. The TRACERLab FX N pro module is actually equipped for solid-phase extraction and reformulation, but due to time constraints we simply performed the sep-pak purification manually in another hot cell and were able to significantly increase the yield.

It should also be noted that although [^{18}F]FPyrLos was synthesized successfully with the dual reactor module, we did see the possibility for a more efficient synthetic route. By first conjugating the azide-modified losartan analog with NO_2PYKYNE, only the F-18 displacement step would have been required in the module. The cold compound was synthesized, but due to time constraints we were unable to investigate the hot chemistry. It is hypothesized however, that the separation of the NO_2 analog and the F-18 labeled analog could be difficult.

5.3 MicroPET Imaging

5.3.1 [^{18}F]FPyrLos as a novel AT_1R tracer

As expected, the majority of activity was taken up and retained by the liver. Although, the liver does contain some AT_1R it is reasonable to suspect that the vast majority of this uptake is due to metabolism and elimination processes. As with [^{11}C]methyl losartan (Antoun, 2010), there was no cardiac uptake. The images did not show any clear delineation of the heart or chambers and uptake was almost indistinguishable from surrounding tissues (Figure 5-3). Multiple ROI drawn over different regions of heart, including the LV and LA cavities, generated nearly identical TAC all of which dropped to a similar baseline level after the initial influx peak. It is not

altogether surprising that we did not observe any cardiac uptake. There is evidence to suggest that the low density AT_1R in the heart of rats or mice can only be imaged once upregulated and not in normal conditions. Even in larger mammals, [^{11}C]KR31173 was unable to identify cardiac AT_1R despite the increased organ size and higher tracer specific activity (Szabo, 2010). However, in a post-MI mouse model (Verjans et al., 2008) and a post-MI rat model with ischemia-reperfusion injury (Higuchi et al., 2010), cardiac AT_1R upregulation was detected by SPECT and PET imaging. It is possible that we were unable to detect an upregulation by microPET in rats 3 weeks post-MI with [^{11}C]methyl losartan due to our low specific activities (Mackasey, 2012).

Unlike [^{11}C]methyl losartan, an interesting phenomenon occurred in about half the rats receiving [^{18}F]FPyrLos in combination with unlabeled candesartan. Once the activity had cleared the kidneys, a slow re-uptake could be observed (Figure 5-4). Sometimes the activity was concentrated to the calyx of the kidney while other times the reuptake was focused to the cortex. Several explanations are plausible, including i) candesartan could be blocking the AT_1R and/or metabolic enzymes in the liver causing a slow displacement of the tracer into the kidneys; ii) the tracer and/or its metabolites are being slowly filtered from the blood into the urine as evidenced by the accumulation of activity in the bladder; or iii) labeled metabolites are binding to another receptor in the cortex, such as the Mas or AT_2 receptor. It is important to note that as Logan analysis is based on reversible binding, and a wash-out of activity, DV values could not be accurately obtained from these scans with the normal protocol using frames 17-26. If background was sufficiently reached before the re-uptake, then only the frames prior to this point were used for the DV calculation (eg. frames 17-20). The DV was not recorded if a linear slope did not accurately fit the data after Logan transformation. It should also be noted that bias exists in the DV estimates because of noise in the PET TAC that propagate as errors in both the

dependent and independent variables of the Logan graphical analysis (Slifstein and Laruelle, 2000).

Despite the increased lipophilicity of the fluoropyridine losartan analog, it did not seem to cross the blood-brain barrier (BBB) by i.v. tail vein injection. The BBB is effectively a wall of endothelial cells formed from the capillaries that perfuse the brain. Tight junctions between these endothelial cells, in addition to specific enzymes and efflux pumps, make the BBB nearly impermeable. Only small neutral lipophilic compounds can freely diffuse across (Waterhouse, 2003). However, with a sufficient amount of drug, such as at therapeutic doses, these enzymes and pumps can become saturated allowing some of the drug to pass. At the nanomolar doses of most PET imaging tracers, saturation is unlikely. It is also plausible that FPyrLos may have a higher affinity for plasma proteins than the BBB proteins, or may simply not have the ideal chemical characteristics for BBB penetration. According to *Lipinski's Rule of 5*, poor absorption or permeation generally occurs if the clogP is > 5 or the MW is > 500 g/mol (Lipinski, C A et al., 1997); FPyrLos has an estimated logP of approximately 7.08 (ChemDraw Ultra 7.0, CambridgeSoft) and a MW of 627.11 g/mol. Further, it may have too many ionizable groups or may contain too many hydrogen bond donors or acceptors (Waterhouse, 2003). If a compound contains ionizable groups, its bioavailability will be influenced by the pH of the environment and the pK_a of its functional groups. Both losartan and FPyrLos contain an acidic tetrazole ring (pk_a 4.25), and a basic imidazole ring (pk_a 2.95) (Tosco et al., 2008). At physiological pH and in the basic environment of the intestinal tract, the tetrazole is likely negatively charged. Interestingly, anionic tetrazoles are almost 10 times more lipophilic than the corresponding carboxylates while having similar acidity (Hansch and Leo, 1995). Thus, the lipophilicity of FPyrLos may not be dramatically affected. Further, the size and chemical composition of the prosthetic group may be

sufficient to increase the lipophilicity regardless of a charged tetrazole ring. Increased lipophilicity has been correlated with higher lung, liver and spleen uptake, and higher affinity to many metabolic enzymes such as the P450 complex (Tosco et al., 2008). This may explain the high GI and spleen uptake of [^{18}F]FPyrLos compared to [^{11}C]methyl losartan (Antoun, 2010).

These preliminary *in vivo* microPET studies demonstrated that tracer uptake (% ID/ml) and DV values decrease dose-dependently in the kidney with blocking, indicating specific binding for the AT_1R. However, even at a 10 mg/kg candesartan blocking dose some activity remains in the kidney; suggesting a greater blocking dose is required for complete displacement, or that the retention may be due to non-specific binding. At this blocking dose, the DV values dropped from 2.76 ± 0.68 ml/cm^3 to 0.96 ± 0.058 ml/cm^3. In Logan analysis, the blood input function is designated a DV value of 1 ml/cm^3. Thus, a DV of 1 ml/cm^3 in the kidney would indicate a lack of tracer binding or retention. This was observed with [^{11}C]methyl losartan (Antoun, 2010), yet the images for [^{18}F]FPyrLos clearly show there is still some activity remaining in the cortex. It appears that the binding characteristics, including specificity and selectivity, will have to be further assessed. Binding studies with various receptor antagonists, *in vitro* autoradiography, *ex vivo* biodistribution and/or metabolite analysis around 45 min, including the urine, should help clarify what we are observing *in vivo*.

5.3.2 Limitations

There are several variables that can affect the consistency of microPET results. First, the time of administration of the candesartan blocking doses. The blocking doses were administered more accurately as a chasing dose and not a co-injection. The time between injection of the tracer and injection of the blocking dose varied between 10-40 seconds. Perhaps not significant,

it should also be mentioned that the concentration of the blocking dose formulation was not consistent throughout the course of the study.

Further, the source of candesartan also varied. A doubly oxidized potassium salt and singly oxidized potassium salt were simply dissolved in a saline solution, whereas the non-ionized candesartan was first dissolved into a small amount of sodium bicarbonate solution with heating and then diluted with saline. Similarly, in the early stages of the study, the composition of the tracer formulation was temporarily changed from a 10% EtOH/saline solution to a 10% EtOH/$NaHCO_3$ solution which may affect its ionization state and *in vivo* distribution.

The specific activity of the injected tracer was also highly variable. The amount of cold mass would not likely affect the results of the blocking scans as the candesartan dose was significantly greater, but may affect the normal baseline scans. At lower specific activity (greater injected mass), the tracer would compete with its cold counterpart for the AT_1R. The exact effect of the cold dose on the DV values would have to be explored further.

A major factor that would affect the imaging results would be the success of the injection – tracer or blocking dose. Oftentimes, finding the tail vein and ensuring a complete and smooth injection proved difficult. Even with a catheter, the line could clog, the rat could move, or catheter location could be incorrect resulting in an interstitial injection.

The analysis itself can also produce variability as all the ROIs are drawn manually. This is particularly important when identifying the LA, which can be difficult for someone inexperienced with cardiac anatomy. Although the time-activity curves between the LA, RA and LV were very similar, the choice of blood pool for DV calculation can change the values considerably. It is also important to recognize that we did not use a true measure of blood activity for the input function, such as from arterial blood sampling, and neither have we corrected for labeled

metabolites in the blood (Laforest et al., 2005). Although accuracy of our results may suffer, the observed trends should remain consistent.

Regarding the kidney ROIs, it is important to check through the other slices in the later frames to ensure that no other organs, such as the liver, spleen or GI, enter the ROI. In general, the right kidney tends to be located higher and closer to the liver than the left kidney. As a result, much of the right kidney, including the cortex, was covered by the liver leaving a rather small, unrepresentative area for an ROI. Thus, only the left kidney was analyzed. However, one should account for spill-over from the high-intensity liver which can result in an over-estimate of the activity in the nearby kidney. For this reason, the ROIs for the left kidney typically comprised only the bottom two-thirds of the kidney. Further, the shape of the ROI had to be manipulated manually in order to avoid possible interference from the GI tract.

5.4 Metabolite Studies

5.4.1 [^{18}F]FPyrLos as a novel AT_1R tracer

The proportion of metabolite (peak 2) in the kidneys at 10 min post-injection was roughly 7%, much less than the 23% found in the kidneys of rats injected with [^{11}C]methyl losartan (Antoun, 2010). Further, only 35% of [^{11}C]methyl losartan remained intact after 10 min, compared to the 65% for [^{18}F]FPyrLos. [^{11}C]Methyl candesartan (Kirkpatrick, 2009), on the other hand, was still 71% intact after 15 min.

Upon blocking the renal AT_1R with unlabeled candesartan, a decrease in the proportion of unchanged tracer (peak 3) and metabolite (peak 2) was observed; however, only the tracer showed a dose-dependent reduction. Conversely, the increasing proportion of peak 1 indicates

that these unretained metabolites do not bind to the AT_1R. When [^{11}C]methyl losartan and [^{11}C]methyl candesartan were co-injected with either losartan or candesartan, there was no significant change in the proportion of the peaks, suggesting their metabolites may be specific for the AT_1R.

This dose-dependent reduction in unchanged tracer agrees with the decreasing DV values noted in the kidney with increasing blocking dose. The plasma shows a similar trend but to a lesser degree (Figure 4-9). In theory, one would expect to find more tracer in the blood when the AT_1R are blocked. It is plausible that with displacement from the kidney, tracer is re-entering the blood and being metabolized, thus increasing the proportion of peak 1. However, it should also be emphasized that there were only two samples run at the 10 mg/kg blocking dose. Increasing the number of runs to at least 3 or 4 should reduce the SD and increase statistical confidence.

5.4.2 Limitations

The same sources of error that would affect distribution of the tracer in the microPET images would also affect the metabolism results. Specific to metabolism studies, however, are issues associated with the column-switch HPLC system, and in particular, the capture cartridge. Ideally, for the control tissues, the capture cartridge should retain close to 100% of the activity injected and be easily removed by the analytical column solvent. As noted previously, the proportion of tracer unretained by the capture cartridge during control studies was used to correct the areas of peak 1 and unchanged tracer in the sample runs. Thus, if the amount of unretained activity was falsely high in the control tissues then the amount of unretained activity in a sample would be falsely reduced and the amount of tracer would be falsely inflated. There

are many factors which can influence the reproducibility of these results, including the type of sorbent, flow rate, method of re-equilibration, amount of tissues run per cartridge, volume injected or possibly even the amount of activity injected. The proportion of unretained activity for [^{18}F]FPyrLos was similar to that for [^{11}C]methyl losartan and much greater than that for [^{11}C]methyl candesartan, which was consistently less than 5% for plasma samples and less than 2% for kidney samples. Although it is possible that the losartan analogs were metabolized to a much greater extent, we decided to try and optimize the protocol for the losartan analogs. A C18 sorbent was tested, but showed no improvement over HLB. Anionic and cationic sorbents, such as MCX (Mixed-mode Cation eXchanger) or MAX (Mixed-mode Cation eXchanger), should be tested in solvents of various pH as well. Subsequently, we looked at re-equilibrating the cartridge between runs with MeOH and water. This modification to the protocol appeared to improve the retention of [^{18}F]FPyrLos.

Another factor which would affect the results would be the time of sacrifice post-injection. Having more or less time to metabolize the drug could significantly alter the proportion of metabolites to unchanged tracer.

Further, it should be explored whether a difference in flow rate affects the radiation peak area on the chromatogram. In theory, a slower flow rate should translate to a wider but shorter peak and a faster flow will provide the opposite effect, but both areas should be consistent. However, depending on the sensitivity of the detector, it is plausible that at a slower flow rate the detector will more accurately detect the number of decay events compared to a faster flow rate where some may be missed, resulting in a shorter peak with a smaller area. This theory can be tested by injecting the same amount of activity at two different flow rates and comparing the areas to the counts determined in a gamma counter.

1. Alkylation with FEtTos and FPrTos

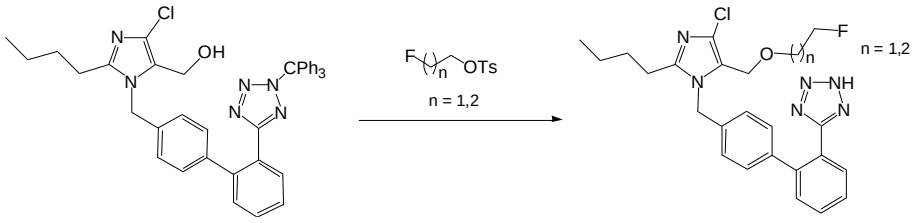

2. Nucleophilic Displacement

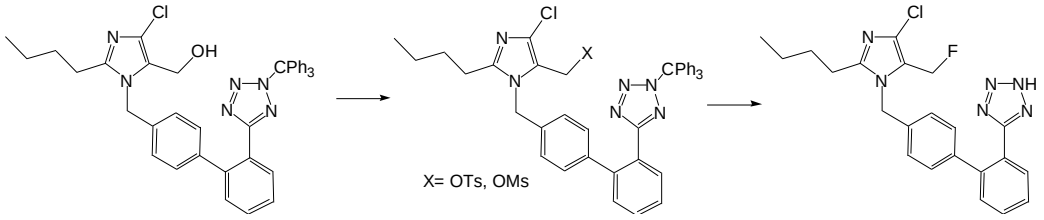

3. Amidation with SFB

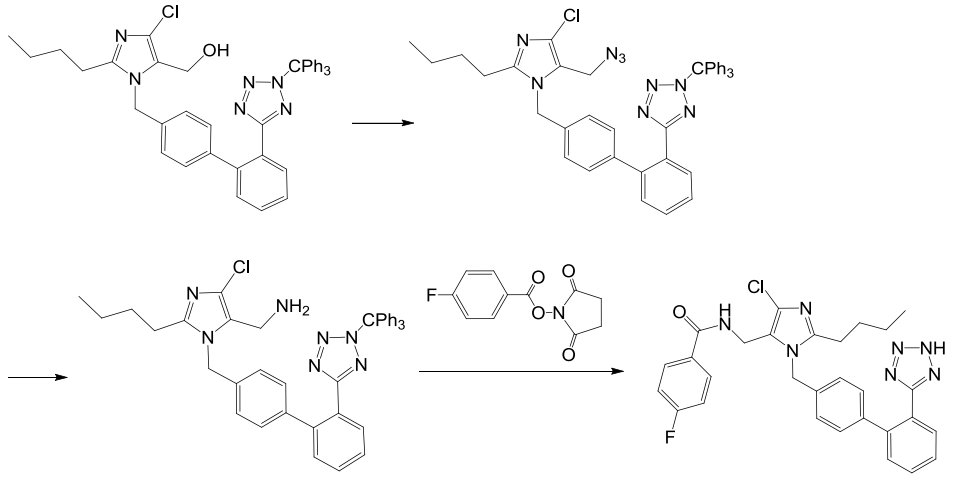

Figure 5-1 Initially proposed strategies for labeling losartan with F-18. OTs: tosylate; OMs: mesylate; FEtTos: fluoroethyl tosylate; FPrTos: fluoropropyl tosylate; SFB: N-succinimidyl 4-fluorobenzoate.

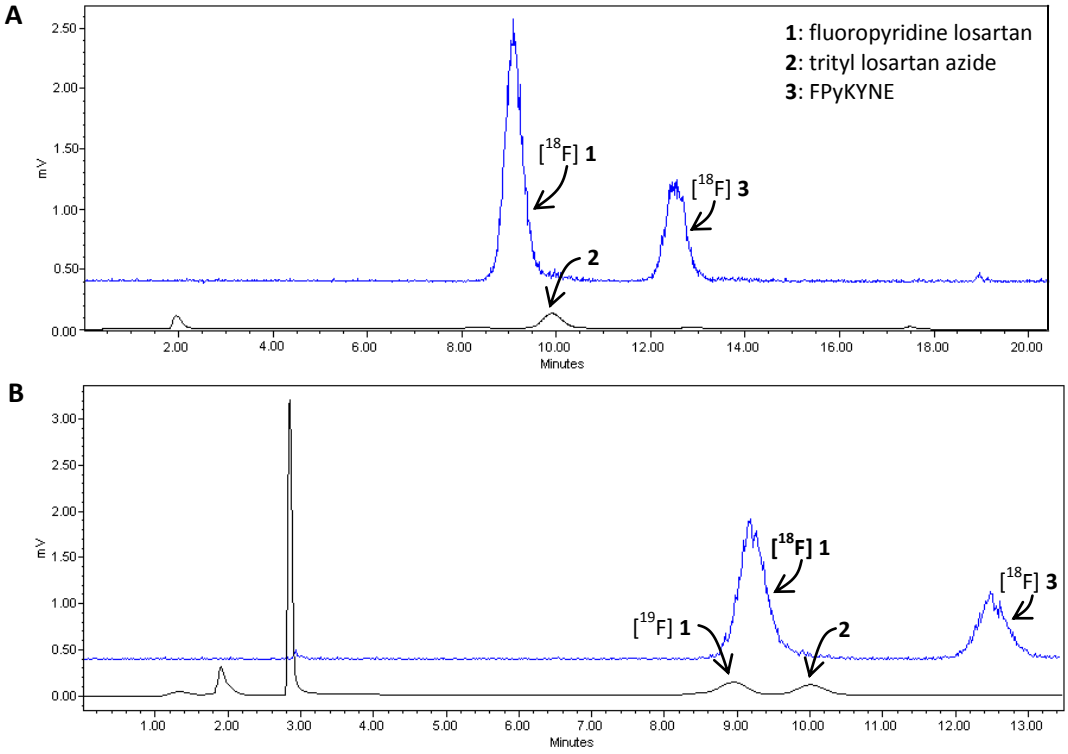

Figure 5-2 Analytical HPLC chromatogram of radioactive products from the [^{18}F]fluoropyridine losartan reaction *(A)* and confirmation of [^{18}F]fluoropyridine losartan identity by appearance of corresponding UV peak (254 nm) at 9 min following co-injection with cold standard (*B*). Radiation spectrum (blue) is overlaid over UV spectrum (black). Column: Phenomenex Luna C18(2), 10 µm, 250 x 4.6 mm; Solvent: 35/65 MeCN/water (0.1 M ammonium formate) at 2 ml/min.

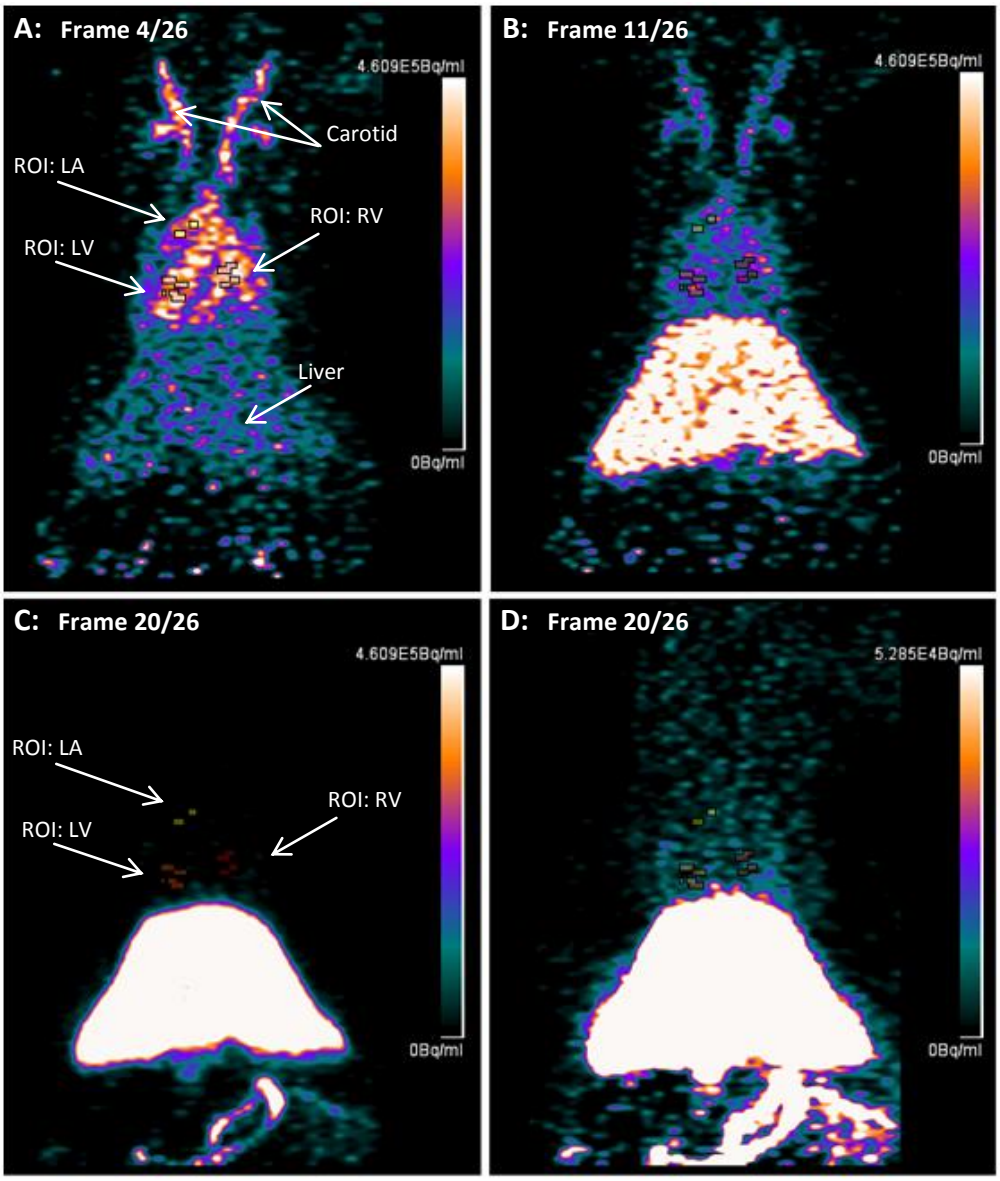

Figure 5-3 MicroPET images of a Sprague Dawley rat injected with [^{18}F]fluoropyridine losartan (2,700 mCi/µmol) showing no myocardial uptake. All images are of the coronal view from slice 53/128: (A) Frame 4/26: 30-40 sec; (B) Frame 11/26: 100-110 sec; (C & D) Frame 20/26: 25-30. Voxel intensity of image D was increased to emphasize lack of cardiac uptake. Rat was injected with 18.4 MBq (0.50 mCi) of tracer. Images were analysed with the Siemens' Inveon Research Workplace analysis software.

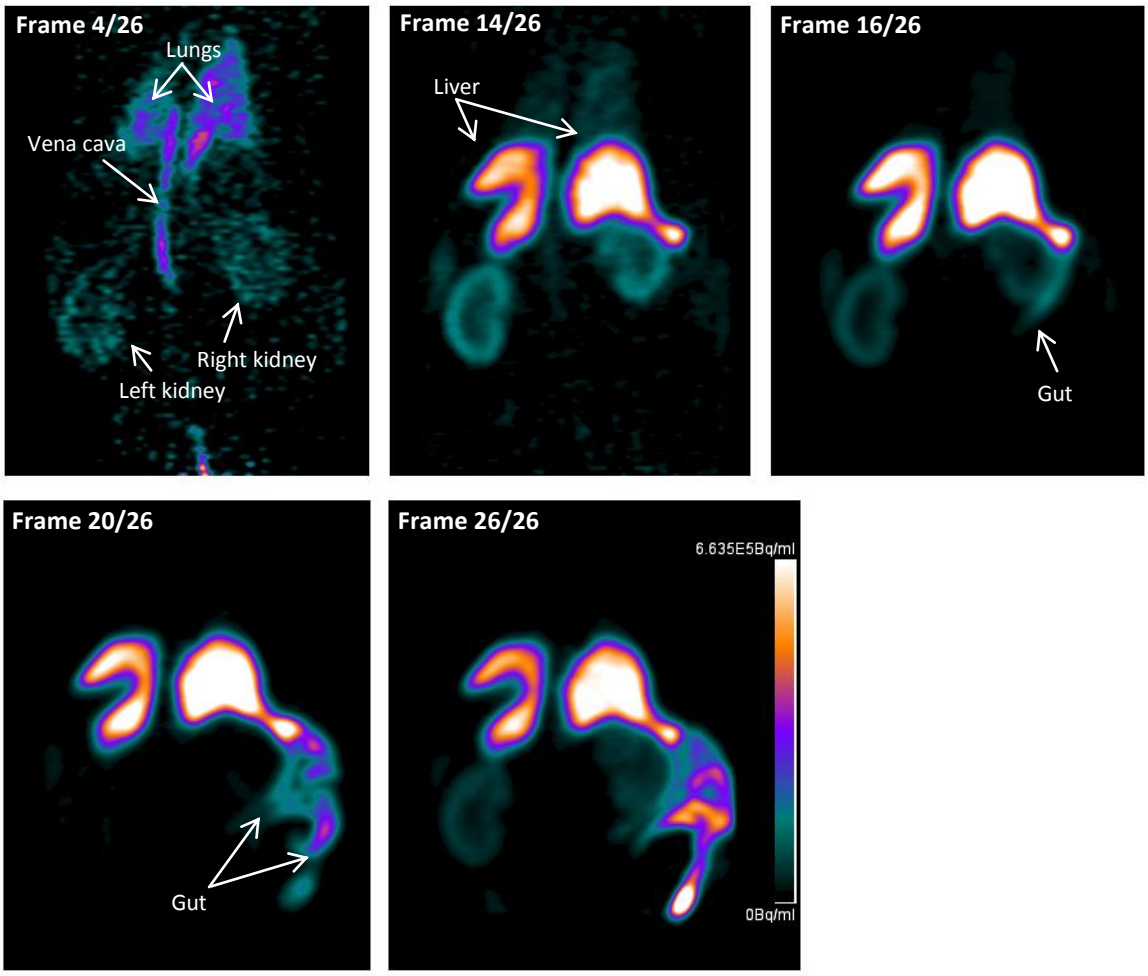

Figure 5-4 MicroPET images of [^{18}F]fluoropyridine losartan in a Sprague Dawley rat co-injected with Candesartan (5 mg/kg) showing activity reuptake in the kindeys. All images are of the coronal view from slice 32/128. Frame 4/26: 30-40 sec, Frame 14/26: 3-4 min, Frame 16/26: 5-10 min, Frame 20/26: 25-30, Frame 26/26: 55-60 min. Rat was injected with 19.4 MBq (0.52 mCi) of tracer. Images were analysed with the Siemens' Inveon Research Workplace analysis software.

6 CONCLUSION

The F-18 labeled prosthetic group, [^{18}F]FPyKYNE, was synthesized and conjugated to losartan to produce [^{18}F]FPyrLos in the desired radiochemical yield (5-10%) and purity (> 97%). Although specific activities (200-4200 mCi/μmol) were not significantly greater than those achieved for our previous C-11 labeled AT_1R tracers (Antoun, 2010; Kirkpatrick, 2009), the potential to achieve higher SA combined with the longer half-life of F-18 make pursuing an F-18 labeled AT_1R tracer worthwhile. Via microPET imaging of rats, we began to characterize the binding profile of [^{18}F]FPyrLos, demonstrating that the fluoropyridine losartan analog retains specificity for the AT_1R. However, further studies are required to quantitatively assess its AT_1R binding affinity, specificity and selectivity. The [^{18}F]fluoroaromatic analog appears to be more resilient to metabolism than our previous AT_1R tracer, [^{11}C]methyl losartan. Column-switch HPLC indicated the presence of only 1 major hydrophilic metabolite in the plasma at 10 min post-injection, which accounted for roughly 7% of the total activity. The proportion of unchanged tracer was roughly 71% in the plasma and 64% in the kidney. Unfortunately, the increase in lipophilicity did not seem to enable penetration of the BBB. However, at the current stage, the tracer does display promise for imaging the kidney. Once injected into larger mammals or animal models with AT_1R upregulation, we will be able to better identify its therapeutic imaging potential.

REFERENCES

Adachi, Y., Saito, Y., Kishimoto, I., Harada, M., Kuwahara, K., Takahashi, N., Kawakami, R., Nakanishi, M., Nakagawa, Y., Tanimoto, K., Saitoh, Y., Yasuno, S., Usami, S., Iwai, M., Horiuchi, M., Nakao, K., 2003. Angiotensin II type 2 receptor deficiency exacerbates heart failure and reduces survival after acute myocardial infarction in mice. Circulation 107, 2406-2408.

Albiston, A., McDowall, S., Matsacos, D., Sim, P., Clune, E., Mustafa, T., Lee, J., Mendelsohn, F., Simpson, R., Connolly, L., Chai, S., 2001. Evidence that the angiotensin IV (AT(4)) receptor is the enzyme insulin-regulated aminopeptidase. J Biol Chem 276, 48623-48626.

Allegretti, P., Seok-ki, C., Roland Gendron, Paul R. Fatheree, Keith Jendza, Robert Murray Mckinnell, Darren Mcmurtrie, Olson, B., 2010. DUAL-ACTING ANTIHYPERTENSIVE AGENTS. Theravance, Inc. (US).

Allen, A.M., Yamada, H., Mendelsohn, F.A., 1990. In vitro autoradiographic localization of binding to angiotensin receptors in the rat heart. Int J Cardiol 28, 25-33.

Allen, A.M., Zhuo, J., Mendelsohn, F.A., 2000. Localization and function of angiotensin AT1 receptors. Am J Hypertens 13, 31S-38S.

Antoun, R., 2010. Characterization of [^{11}C]methyl-losartan as a novel radiotracer for PET imaging of the AT_1 receptor. Cellular and Molecular Medicine. University of Ottawa, Ottawa.

Anversa, P., Leri, A., Li, B., Liu, Y., Di Somma, S., Kajstura, J., 2000. Ischemic cardiomyopathy and the cellular renin-angiotensin system. J Heart Lung Transplant 19, S1-11.

Appukkuttan, P., Dehaen, W., Fokin, V.V., Van der Eycken, E., 2004. A microwave-assisted click chemistry synthesis of 1,4-disubstituted 1,2,3-triazoles via a copper(I)-catalyzed three-component reaction. Org Lett 6, 4223-4225.

Asakura, M., Kitakaze, M., Takashima, S., Liao, Y., Ishikura, F., Yoshinaka, T., Ohmoto, H., Node, K., Yoshino, K., Ishiguro, H., Asanuma, H., Sanada, S., Matsumura, Y., Takeda, H., Beppu, S., Tada, M., Hori, M., Higashiyama, S., 2002. Cardiac hypertrophy is inhibited by antagonism of ADAM12 processing of HB-EGF: metalloproteinase inhibitors as a new therapy. Nat. Med. 8, 35–40.

Asano, K., Dutcher, D.L., Port, J.D., Minobe, W.A., Tremmel, K.D., Roden, R.L., Bohlmeyer, T.J., Bush, E.W., Jenkin, M.J., Abraham, W.T., Raynolds, M.V., Zisman, L.S., Perryman, M.B., Bristow, M.R., 1997. Selective downregulation of the angiotensin II AT1-receptor subtype in failing human ventricular myocardium. Circulation 95, 1193-1200.

Audoly, L.P., Oliverio, M.I., Coffman, T.M., 2000. Insights into the functions of type 1 (AT1) angiotensin II receptors provided by gene targeting. Trends Endocrinol Metab 11, 263-269.

Baker, K.M., Aceto, J.F., 1990. Angiotensin II stimulation of protein synthesis and cell growth in chick heart cells. Am J Physiol 259, H610-618.

Baker, K.M., Booz, G.W., Dostal, D.E., 1992. Cardiac actions of angiotensin II: Role of an intracardiac renin-angiotensin system. Annu Rev Physiol 54, 227-241.

Baker, K.M., Campanile, C.P., Trachte, G.J., Peach, M.J., 1984. Identification and characterization of the rabbit angiotensin II myocardial receptor. Circ Res 54, 286-293.

Baker, K.M., Chernin, M.I., Wixson, S.K., Aceto, J.F., 1990. Renin-angiotensin system involvement in pressure-overload cardiac hypertrophy in rats. Am J Physiol 259, H324-332.

Bartra, M., Romea, P., UrpÃ-, F.l., Vilarrasa, J., 1990. A fast procedure for the reduction of azides and nitro compounds based on the reducing ability of Sn(SR)3-species. Tetrahedron 46, 587-594.

Bayorh, M.A., Ganafa, A.A., Emmett, N., Socci, R.R., Eatman, D., Fridie, I.L., 2005. Alterations in aldosterone and angiotensin II levels in salt-induced hypertension. Clin Exp Hypertens 27, 355-367.

Berk, B.C., Fujiwara, K., Lehoux, S., 2007. ECM remodeling in hypertensive heart disease. J Clin Invest 117, 568-575.

Berl, T., 2004. Angiotensin-converting enzyme inhibitors versus AT1 receptor antagonist in cardiovascular and renal protection: the case for AT1 receptor antagonist. J Am Soc Nephrol 15 (Suppl 1), S71-76.

Berndt, U., Stanetty, C., Wanek, T., Kuntner, C., Stanek, J., Berger, M., Bauer, M., Henriksen, G., Wester, H.J., Kvaternik, H., Angelberger, P., Noe, C., 2008 Synthesis of a [18F]fluorobenzothiazole as potential amyloid imaging agent. J. Label Compd. Radiopharm. 51 137-145.

Berridge, M.S., Apana, S.M., Hersh, J.M., 2009. Teflon radiolysis as the major source of carrier in fluorine-18. J. Label Compd. Radiopharm 52 543-548.

Billet, S., Aguilar, F., Baudry, C., Clauser, E., 2008. Role of angiotensin II AT1 receptor activation in cardiovascular diseases. Kidney Int 74, 1379-1384.

Binder, W.H., Sachsenhofer, R., 2007. 'Click' Chemistry in Polymer and Materials Science. Macromol. Rapid. Commun. 28, 15-54.

Bock, V.D., Hiemstra, H., van Maarseveen, J.H., 2006. CuI-Catalyzed Alkyne–Azide "Click" Cycloadditions from a Mechanistic and Synthetic Perspective. European Journal of Organic Chemistry 2006, 51-68.

Boyer, J.H., 1951. Reduction of Organic Azides to Primary Amines with Lithium Aluminum Hydride. J. Am. Chem. Soc. 73, 5865–5866.

Brink, M., Erne, P., de Gasparo, M., Rogg, H., Schmid, A., Stulz, P., Bullock, G., 1996. Localization of the angiotensin II receptor subtypes in the human atrium. J Mol Cell Cardiol 28, 1789-1799.

Budinger, T.F., Derenzo, S.E., Huesman, R.H., 1984. Instrumentation for positron emission tomography. Ann Neurol 15 Suppl, S35-43.

Bui, J.D., Kimura, B., Phillips, M.I., 1992. Losartan potassium, a nonpeptide antagonist of angiotensin II, chronically administered p.o. does not readily cross the blood-brain barrier. Eur J Pharmacol 219, 147-151.

Burson, J.M., Aguilera, G., Gross, K.W., Sigmund, C.D., 1994. Differential expression of angiotensin receptor 1A and 1B in mouse. Am J Physiol 267, E260-267.

Carini DJ, Duncia JV: *Angiotensin II Receptor Blocking Imidazoles*. European patent application 0253310. Issued to E. I. du Pont de Nemours & Co., Inc., Wilmington, DE, 1988.

Carini, D.J., Duncia, J.V., Aldrich, P.E., Chiu, A.T., Johnson, A.L., Pierce, M.E., Price, W.A., Santella, J.B., 3rd, Wells, G.J., Wexler, R.R., et al., 1991. Nonpeptide angiotensin II receptor antagonists: the discovery of a series of N-(biphenylylmethyl)imidazoles as potent, orally active antihypertensives. J Med Chem 34, 2525-2547.

Chang, R., Lotti, V., 1990. Two distinct angiotensin II receptor binding sites in rat adrenal revealed by new selective nonpeptide ligands. Mol Pharmacol 37, 347-351.

Chang, R., Lotti, V., 1991. Angiotensin receptor subtypes in rat, rabbit and monkey tissues: relative distribution and species dependency. Life Sci 49, 1485-1490.

Chen, T.B., Brenner, N.J., Gibson, R.E., Burns, H.D., Chang, R.S., 1995. Characterization of the binding of [125I]L-735,286: a new nonpeptide angiotensin II AT1 receptor radioligand. Life Sci 56, 629-635.

Cherry, S., 2001. Fundamentals of positron emission tomography and applications in preclinical drug development. J Clin Pharmacol 41, 482-491.

Chien, K.R., Grace, A. A. & Hunter, J. J. , 1998. Molecular biology of cardiac hypertrophy and heart failure. Molecular Basis of Cardiovascular Disease W. B. Saunders, Philadelphia, PA, pp. 211-250.

Chiu, A.T., Dunscomb, J., Kosierowski, J., Burton, C.R., Santomenna, L.D., Corjay, M.H., Benfield, P., 1993. The ligand binding signatures of the rat AT1A, AT1B and the human AT1 receptors are essentially identical. Biochem Biophys Res Commun 197, 440-449.

Chiu, A.T., Herblin, W.F., McCall, D.E., Ardecky, R.J., Carini, D.J., Duncia, J.V., Pease, L.J., Wong, P.C., Wexler, R.R., Johnson, A.L., et al., 1989. Identification of angiotensin II receptor subtypes. Biochem Biophys Res Commun 165, 196-203.

Chiu, A.T., McCall, D.E., Price, W.A., Wong, P.C., Carini, D.J., Duncia, J.V., Wexler, R.R., Yoo, S.E., Johnson, A.L., Timmermans, P.B., 1990. Nonpeptide angiotensin II receptor antagonists. VII.

Cellular and biochemical pharmacology of DuP 753, an orally active antihypertensive agent. J Pharmacol Exp Ther 252, 711-718.

Chiu, A.T., McCall, D.E., Roscoe, W.A., 1992. [125I]EXP985: a highly potent and specific nonpeptide radioligand antagonist for the AT1 angiotensin receptor. Biochem Biophys Res Commun 188, 1030-1039.

Christ, D.D., 1995. Human plasma protein binding of the angiotensin II receptor antagonist losartan potassium (DuP 753/MK 954) and its pharmacologically active metabolite EXP3174. J Clin Pharmacol 35, 515-520.

Cigola, E., Kajstura, J., Li, B., Meggs, L.G., Anversa, P., 1997. Angiotensin II activates programmed myocyte cell death in vitro. Exp Cell Res 231, 363-371.

Coenen, H., Colosimo, M., Shuller, M., Stocklin, G., 1986. Preparation of NCA [18F]CH2BrFvia arninopolyether supported nucleophilic substitution J. Label. Cmpds. Radiopharm. 23, 587-595.

Cohn, J.N., Tognoni, G., 2001. A randomized trial of the angiotensin-receptor blocker valsartan in chronic heart failure. N Engl J Med 345, 1667-1675.

Coleman, R.S., Felpin, F.-X., Chen, W., 2004. Mitomycin Synthetic Studies: Stereocontrolled and Convergent Synthesis of a Fully Elaborated Aziridinomitosane. The Journal of Organic Chemistry 69, 7309-7316.

Crabos, M., Roth, M., Hahn, A.W., Erne, P., 1994. Characterization of angiotensin II receptors in cultured adult rat cardiac fibroblasts. Coupling to signaling systems and gene expression. J Clin Invest 93, 2372-2378.

Crowley, S.D., Gurley, S.B., Herrera, M.J., Ruiz, P., Griffiths, R., Kumar, A.P., Kim, H.S., Smithies, O., Le, T.H., Coffman, T.M., 2006. Angiotensin II causes hypertension and cardiac hypertrophy through its receptors in the kidney. Proc Natl Acad Sci U S A 103, 17985-17990.

Crowley, S.D., Gurley, S.B., Oliverio, M.I., Pazmino, A.K., Griffiths, R., Flannery, P.J., Spurney, R.F., Kim, H.S., Smithies, O., Le, T.H., Coffman, T.M., 2005. Distinct roles for the kidney and systemic tissues in blood pressure regulation by the renin-angiotensin system. J Clin Invest 115, 1092-1099.

Cunningham, V.J.C.A.P., Eugenii A. Rabiner, Antony D. Gee and Roger N. Gunn, 2005. PET studies in drug development: Methodological considerations. Drug Discovery Today: Technologies 4, 311-315.

Danser, A.H., 2010. Cardiac angiotensin II: does it have a function? Am J Physiol Heart Circ Physiol 299, H1304-1306.

De Gasparo, M.K.J.C., T. INAGAMI, J. W. WRIGHT, AND TH. UNGER, 2000. International Union of Pharmacology. XXIII. The Angiotensin II Receptors. Pharmacol Rev 52, 415-472.

Defrise, M., 2001. A short reader's guide to 3D tomographic reconstruction. Comput Med Imaging Graph 25, 113-116.

Della Bruna, R., Ries, S., Himmelstoss, C., Kurtz, A., 1995. Expression of cardiac angiotensin II AT1 receptor genes in rat hearts is regulated by steroids but not by angiotensin II. Journal of hypertension 13, 763-769.

Devereux, R.B., Pickering, T.G., Cody, R.J., Laragh, J.H., 1987. Relation of renin-angiotensin system activity to left ventricular hypertrophy and function in experimental and human hypertension. J Clin Hypertens 3, 87-103.

Diep, Q.N., El Mabrouk, M., Yue, P., Schiffrin, E.L., 2002. Effect of AT(1) receptor blockade on cardiac apoptosis in angiotensin II-induced hypertension. Am J Physiol Heart Circ Physiol 282, H1635-1641.

Diez, J., Fortuno, M.A., Ravassa, S., 1998. Apoptosis in hypertensive heart disease. Curr Opin Cardiol 13, 317-325.

Dimitrijevic, I., Edvinsson, M.-L., Chen, Q., Malmsjö, M., Kimblad, P.-O., Edvinsson, L., 2009. Increased expression of vascular endothelin type B and angiotensin type 1 receptors in patients with ischemic heart disease. BMC Cardiovascular Disorders 9.

Dinh, D.T., Frauman, A.G., Johnston, C.I., Fabiani, M.E., 2001. Angiotensin receptors: distribution, signalling and function. Clin Sci (Lond) 100, 481-492.

Dollé, F., Hinnen, F., Damont, A., Kuhnast, B., Fookes, C., Pham, T., Tavitian, B., Katsifis, A., 2008. Radiosynthesis of [18F]PBR111, a selective radioligand for imaging the translocator protein (18 kDa) with PET. Journal of Labelled Compounds and Radiopharmaceuticals 51, 435-439.

Dostal, D.E., Baker, K.M., 1993. Evidence for a role of an intracardiac renin-angiotensin system in normal and failing hearts. Trends Cardiovasc Med 3, 67-74.

Dubey RK, Jackson EK, Rupprecht HD, RB., S., 1997. Factors controlling growth and matrix production in vascular smooth muscle and glomerular mesangial cells. Curr Opin Nephrol Hypertens 6, 88-105.

Duncia, J.V., Carini, D.J., Chiu, A.T., Johnson, A.L., Price, W.A., Wong, P.C., Wexler, R.R., Timmermans, P.B., 1992. The discovery of DuP 753, a potent, orally active nonpeptide angiotensin II receptor antagonist. Med Res Rev 12, 149-191.

Dzau, V.J., 1988. Circulating versus local renin-angiotensin system in cardiovascular homeostasis. Circulation 77, I4-13.

Dzau, V.J., Ellison, K.E., Brody, T., Ingelfinger, J., Pratt, R.E., 1987. A comparative study of the distributions of renin and angiotensinogen messenger ribonucleic acids in rat and mouse tissues. Endocrinology 120, 2334-2338.

Dzau, V.J., Gibbons, G.H., Cooke, J.P., Omoigui, N., 1993. Vascular biology and medicine in the 1990s: scope, concepts, potentials, and perspectives. Circulation 87, 705-719.

Dzau, V.J., Re, R., 1994. Tissue angiotensin system in cardiovascular medicine. A paradigm shift? Circulation 89, 493-498.

Elton, T.S., Stephan, C.C., Taylor, G.R., Kimball, M.G., Martin, M.M., Durand, J.N., Oparil, S., 1992. Isolation of two distinct type I angiotensin II receptor genes. Biochem Biophys Res Commun 184, 1067-1073.

Erlandsson, M., Karimi, F., Lindhe, O., Langstrom, B., 2009. (18)F-labelled metomidate analogues as adrenocortical imaging agents. Nucl Med Biol 36, 435-445.

Ferreira-Machado, S.C., Rocha Nde, N., Mencalha, A.L., De Melo, L.D., Salata, C., Ribeiro, A.F., Torres Tda, S., Mandarim-De-Lacerda, C.A., Canary, P.C., Peregrino, A.A., Magalhaes, L.A., Cabral-Neto, J.B., Dealmeida, C.E., Up-regulation of angiotensin-converting enzyme and angiotensin II type 1 receptor in irradiated rats. Int J Radiat Biol 86, 880-887.

Ferrieri, R., 2003. Handbook of Radiopharmaceuticals. Wiley, NY.

Fierens, F.L.P., Vanderheyden, P.M.L., de Backer, J.P., and Vauquelin, G. 1999. Insurmountable angiotensin AT1 receptor antagonists: the role of tight antagonistbinding. Eur J Pharmacol 372:199-206.

Fuchtner, F., Preusche, S., Mading, P., Zessin, J., Steinbach, J., 2008. Factors affecting the specific activity of [18F]fluoride from a [18O]water target. Nuklearmedizin 47, 116-119.

Gad, S.C. (Ed.), 2008. Pharmaceutical manufacturing handbook: production and processes. Wiley-Interscience, New Jersey.

Gasc, J., Shanmugam, S., Sibony, M., Corvol, P., 1994 Tissue-specific expression of type 1 angiotensin II receptor subtypes. An in situ hybridization study. Hypertension 24, 531-537.

Geisterfer, A.A., Peach, M.J., Owens, G.K., 1988. Angiotensin II induces hypertrophy, not hyperplasia, of cultured rat aortic smooth muscle cells. Circ Res 62, 749-756.

Ghosh, A.K., Kumaragurubaran, N., Hong, L., Kulkarni, S.S., Xu, X., Chang, W., Weerasena, V., Turner, R., Koelsch, G., Bilcer, G., Tang, J., 2007. Design, synthesis, and X-ray structure of potent memapsin 2 (beta-secretase) inhibitors with isophthalamide derivatives as the P2-P3-ligands. J Med Chem 50, 2399-2407.

Gibbons, G.H., Pratt, R.E., Dzau, V.J., 1992. Vascular smooth muscle cell hypertrophy vs. hyperplasia. Autocrine transforming growth factor-beta 1 expression determines growth response to angiotensin II. J Clin Invest 90, 456-461.

Glaser, M., Arstad, E., 2007. "Click labeling" with 2-[18f]fluoroethylazide for positron emission tomography. Bioconjug Chem 18, 989-993.

Goldenberg, I., Grossman, E., Jacobson, K.A., Shneyvays, V., Shainberg, A., 2001. Angiotensin II-induced apoptosis in rat cardiomyocyte culture: a possible role of AT1 and AT2 receptors. J Hypertens 19, 1681-1689.

Gomes, C.M., Abrunhosa, A.J., Ramos, P., Pauwels, E.K., 2011. Molecular imaging with SPECT as a tool for drug development. Adv Drug Deliv Rev 63, 547-554.

Gothelf, K.V., Jorgensen, K.A., 1998. Asymmetric 1,3-Dipolar Cycloaddition Reactions. Chem. Rev. 98, 863-909.

Goussev A, Sharov VG, Shimoyama H, Tanimura M, Lesch M, Goldstein S, HN, S., 1998. Effects of ACE inhibition on cardiomyocyte apoptosis in dogs with heart failure. Am J Physiol Heart Circ Physiol 275, H626-H631.

Green, M.V., Seidel, J., Vaquero, J.J., Jagoda, E., Lee, I., Eckelman, W.C., 2001. High resolution PET, SPECT and projection imaging in small animals. Comput Med Imaging Graph 25, 79-86.

Griendling, K.K., Lassegue, B., Alexander, R.W., 1996. Angiotensin receptors and their therapeutic implications. Annu Rev Pharmacol Toxicol 36, 281-306.

Hadizad, T., Collins, J., Antoun, R., Beanlands, R.S., DaSilva, J.N., 2011. [^{11}C]Methyl-losartan as a potential ligand for PET imaging angiotensin II AT_1 receptors. J. Label Compd. Radiopharm 54, 754–757.

Hadizad, T., Kirkpatrick, S.A., Mason, S., Burns, K., Beanlands, R.S., Dasilva, J.N., 2009. Novel O-[(11)C]methylated derivatives of candesartan as angiotensin II AT(1) receptor imaging ligands: radiosynthesis and ex vivo evaluation in rats. Bioorg Med Chem 17, 7971-7977.

Hamacher, K., Coenen, H.H., 2002. Efficient routine production of the 18F-labelled amino acid O-2-18F fluoroethyl-L-tyrosine. Appl Radiat Isot 57, 853-856.

Hamill, T.G., Burns, H.D., Dannals, R.F., Mathews, W.B., Musachio, J.L., Ravert, H.T., Naylor, E.M., 1996. Development of [11C]L-159,884: a radiolabelled, nonpeptide angiotensin II antagonist that is useful for angiotensin II, AT1 receptor imaging. Appl Radiat Isot 47, 211-218.

Hansch, C., Leo, A., 1995. Exploring QSAR. Fundamentals and Applications in Chemistry and Biology. In: Society, A.C. (Ed.), Washington, DC.

Hara, T., Kosaka, N., Kishi, H., 2002. Development of (18)F-fluoroethylcholine for cancer imaging with PET: synthesis, biochemistry, and prostate cancer imaging. J Nucl Med 43, 187-199.

Harada, K., Friedman, M., Lopez, J.J., Wang, S.Y., Li, J., Prasad, P.V., Pearlman, J.D., Edelman, E.R., Sellke, F.W., Simons, M., 1996. Vascular endothelial growth factor administration in chronic myocardial ischemia. Am J Physiol 270, H1791-1802.

Harada, K., Komuro, I., Shiojima, I., Hayashi, D., Kudoh, S., Mizuno, T., Kijima, K., Matsubara, H., Sugaya, T., Murakami, K., Yazaki, Y., 1998a. Pressure overload induces cardiac hypertrophy in angiotensin II type 1A receptor knockout mice. Circulation 97, 1952-1959.

Harada, K., Komuro, I., Zou, Y., Kudoh, S., Kijima, K., Matsubara, H., Sugaya, T., Murakami, K., Yazaki, Y., 1998b. Acute pressure overload could induce hypertrophic responses in the heart of angiotensin II type 1a knockout mice. Circ Res 82, 779-785.

Harada, K., Sugaya, T., Murakami, K., Yazaki, Y., Komuro, I., 1999. Angiotensin II type 1A receptor knockout mice display less left ventricular remodeling and improved survival after myocardial infarction. Circulation 100, 2093-2099.

Haubner, R., Kuhnast, B., Mang, C., Weber, W.A., Kessler, H., Wester, H.-J., Schwaiger, M., 2003. [18F]Galacto-RGD: Synthesis, Radiolabeling, Metabolic Stability, and Radiation Dose Estimates. Bioconjugate Chemistry 15, 61-69.

Haywood, G.A., Gullestad, L., Katsuya, T., Hutchinson, H.G., Pratt, R.E., Horiuchi, M., Fowler, M.B., 1997. AT1 and AT2 angiotensin receptor gene expression in human heart failure. Circulation 95, 1201-1206.

Hein, L., Barsh, G.S., Pratt, R.E., Dzau, V.J., Kobilka, B.K., 1995. Behavioural and cardiovascular effects of disrupting the angiotensin II type-2 receptor in mice. Nature 377, 744-747.

Hein, L., Stevens, M.E., Barsh, G.S., Pratt, R.E., Kobilka, B.K., Dzau, V.J., 1997. Overexpression of angiotensin AT1 receptor transgene in the mouse myocardium produces a lethal phenotype associated with myocyte hyperplasia and heart block. Proc Natl Acad Sci U S A 94, 6391-6396.

Hendee, W.R., Ibbott, G.S., Hendee, E.G., 2005 Atomic Structure and Radioactive Decay. Radiation Therapy Physics. John Wiley & Sons, Inc., Hoboken, New Jersey.

Higuchi, S., Ohtsu, H., Suzuki, H., Shira, H., Frank, G.D., Eguchi, S., 2007. Angiotensin II signal transduction through the AT_1 receptor: novel insights into mechanisms and pathophysiology. Clinical Science 112, 417–428.

Higuchi, T., Fukushima, K., Xia, J., Mathews, W.B., Lautamaki, R., Bravo, P.E., Javadi, M.S., Dannals, R.F., Szabo, Z., Bengel, F.M., 2010. Radionuclide imaging of angiotensin II type 1 receptor upregulation after myocardial ischemia-reperfusion injury. J Nucl Med 51, 1956-1961.

Hilton, J., Yokoi, F., Dannals, R.F., Ravert, H.T., Szabo, Z., Wong, D.F., 2000. Column-switching HPLC for the analysis of plasma in PET imaging studies. Nucl Med Biol 27, 627-630.

Himo, F., Lovell, T., Hilgraf, R., Rostovtsev, V.V., Noodleman, L., Sharpless, K.B., Fokin, V.V., 2005. Copper(I)-catalyzed synthesis of azoles. DFT study predicts unprecedented reactivity and intermediates. J Am Chem Soc 127, 210-216.

Hoffman, E.J., Huang, S.-C., Phelps, M.E., 1979. Quantitation in Positron Emission Computed Tomography: 1. Effect of Object Size. Journal of Computer Assisted Tomography 3, 299-308.

Hong, V., Presolski, S.I., Ma, C., Finn, M.G., 2009. Analysis and optimization of copper-catalyzed azide-alkyne cycloaddition for bioconjugation. Angew Chem Int Ed Engl 48, 9879-9883.

Horne, W.S., Yadav, M.K., Stout, C.D., Ghadiri, M.R., 2004. Heterocyclic peptide backbone modifications in an alpha-helical coiled coil. J Am Chem Soc 126, 15366-15367.

Huang, B.S., Ahmad, M., Tan, J., Leenen, F.H., 2009. Chronic central versus systemic blockade of AT(1) receptors and cardiac dysfunction in rats post-myocardial infarction. Am J Physiol Heart Circ Physiol 297, H968-975.

Huisgen, R., 1961. 1,3-Dipolar Cycloadditions. Proceedings of the Chemical Society. October 1961. The Royal Society of Chemistry, pp. 357-369.

Hume, S.P., Myers, R., 2002. Dedicated small animal scanners: a new tool for drug development? Curr Pharm Des 8, 1497-1511.

Hunyady, L., Balla, T., Catt, K.J., 1996. The ligand binding site of the angiotensin AT1 receptor. Trends Pharmacol Sci 17, 135-140.

Hunyady, L., Catt, K.J., 2006. Pleiotropic AT1 receptor signaling pathways mediating physiological and pathogenic actions of angiotensin II. Mol Endocrinol 20, 953-970.

Hutchins, G., Miller, M., Soon, V., Receveur, T., 2008. Small animal PET imaging. ILAR J. 49, 54-65.

Ibrahim, M.M., 2006. RAS inhibition in hypertension. J Hum Hypertens 20, 101-108.

Ichihara, S., Senbonmatsu, T., Price, E., Jr., Ichiki, T., Gaffney, F.A., Inagami, T., 2002. Targeted deletion of angiotensin II type 2 receptor caused cardiac rupture after acute myocardial infarction. Circulation 106, 2244-2249.

Ichiki, T., Labosky, P.A., Shiota, C., Okuyama, S., Imagawa, Y., Fogo, A., Niimura, F., Ichikawa, I., Hogan, B.L., Inagami, T., 1995. Effects on blood pressure and exploratory behaviour of mice lacking angiotensin II type-2 receptor. Nature 377, 748-750.

Inkster, J., Guerin, B., Ruth, T., Adam, M., 2008. Radiosynthesis and bioconjugation of [18F]FPy5yne, a prosthetic group for the 18F labeling of bioactive peptides. J Label Compd Radiopharm 51, 444–452.

Ito, M., Oliverio, M.I., Mannon, P.J., Best, C.F., Maeda, N., Smithies, O., Coffman, T.M., 1995. Regulation of blood pressure by the type 1A angiotensin II receptor gene. Proc Natl Acad Sci U S A 92, 3521-3525.

Itoh, H., Mukoyama, M., Pratt, R.E., Gibbons, G.H., Dzau, V.J., 1993. Multiple autocrine growth factors modulate vascular smooth muscle cell growth response to angiotensin II. J Clin Invest 91, 2268-2274.

Iwai, N., Inagami, T., 1992. Identification of two subtypes in the rat type I angiotensin II receptor. FEBS Lett 298, 257-260.

Jin, M., Wilhelm, M.J., Lang, R.E., Unger, T., Lindpaintner, K., Ganten, D., 1988. Endogenous tissue renin-angiotensin systems. From molecular biology to therapy. Am J Med 84, 28-36.

Johren, O., Dendorfer, A., Dominiak, P., 2004. Cardiovascular and renal function of angiotensin II type-2 receptors. Cardiovasc Res 62, 460-467.

Jones, E., Black, M., Widdop, R., 2004. Angiotensin AT2 receptor contributes to cardiovascular remodelling of aged rats during chronic AT1 receptor blockade. J Mol Cell Cardiol 37, 1023-1030.

Jones, E.S., Vinh, A., McCarthy, C.A., Gaspari, T.A., Widdop, R.E., 2008. AT2 receptors: functional relevance in cardiovascular disease. Pharmacol Ther 120, 292-316.

Kajstura, J., Cigola, E., Malhotra, A., Li, P., Cheng, W., Meggs, L.G., Anversa, P., 1997. Angiotensin II induces apoptosis of adult ventricular myocytes in vitro. J Mol Cell Cardiol 29, 859-870.

Kakinuma, Y., Fogo, A., Inagami, T., Ichikawa, I., 1993. Intrarenal localization of angiotensin II type 1 receptor mRNA in the rat. Kidney Int 43, 1229-1235.

Kaschina, E., Unger, T., 2003. Angiotensin AT1/AT2 receptors: regulation, signalling and function. Blood Press 12, 70-88.

Katoh Y, Komuro I, Shibasaki Y, Yamaguchi H, Y., Y., 1989. Angiotensin II induces hypertrophy and oncogene expression in cultured rat heart myocytes. Circulation 80 (Suppl II):, 11-450 (Abstr.).

Katz, A.M., 1988. Molecular biology in cardiology, a paradigmatic shift. J Mol Cell Cardiol 20, 355-366.

Kawano H, Do YS, Kawano Y, Starnes V, Barr M, Law RE, WA, H., 2000. Angiotensin II has multiple profibrotic effects in human cardiac fibroblasts. . C*irculation* 101, 1130-1137.

Kawano, H., Do, Y., Kawano, Y., Starnes, V., Barr, M., Law, R., Hsueh, W., 2000. Angiotensin II has multiple profibrotic effects in human cardiac fibroblasts. . Circulation 101, 1130-1137.

Kenk, M., Greene, M., Lortie, M., Dekemp, R.A., Beanlands, R.S., Dasilva, J.N., 2008. Use of a column-switching high-performance liquid chromatography method to assess the presence of specific binding of (R)- and (S)-[(11)C]rolipram and their labeled metabolites to the phosphodiesterase-4 enzyme in rat plasma and tissues. Nucl Med Biol 35, 515-521.

Kijima, K., Matsubara, H., Murasawa, S., Maruyama, K., Mori, Y., Ohkubo, N., Komuro, I., Yazaki, Y., Iwasaka, T., Inada, M., 1996. Mechanical stretch induces enhanced expression of angiotensin II receptor subtypes in neonatal rat cardiac myocytes. Circ Res 79, 887-897.

Kilbourn, M.R., Shao, X., 2009. Fluorine-18 Radiopharmaceuticals. In: Ojima, I. (Ed.), Fluorine in Medicinal Chemistry and Chemical Biology. Wiley-Blackwell.

Kim, S., Iwao, H., 2000. Molecular and cellular mechanisms of angiotensin II-mediated cardiovascular and renal diseases. Pharmacol Rev 52, 11-34.

Kirkpatrick, S., 2009. Characterization of the binding properties of ^{11}C-labeled candesartan derivatives as potential angiotensinII AT_1 receptor radioligands for PET imaging Cellular and Molecular Medicine. University of Ottawa, Ottawa.

Kiya, Y., Miura, S., Fujino, M., Imaizumi, S., Karnik, S., Saku, K., 2010. Clinical and pharmacotherapeutic relevance of the double-chain domain of the angiotensin II type 1 receptor blocker olmesartan. Clin Exp Hypertens. 32, 129-136.

Kjeldsen, S.E., Strand, A., Julius, S., Okin, P.M., 2006. Mechanism of angiotensin II type 1 receptor blocker action in the regression of left ventricular hypertrophy. J Clin Hypertens (Greenwich) 8, 487-492.

Koivula, T., Perhola, O., Kämäräinen, E.-L., Lipponen, T., Vepsäläinen, J., Solin, O., 2005. Simplified synthesis of N-(3-[18F]fluoropropyl)-2β-carbomethoxy-3β-(4-fluorophenyl)nortropane ([18F]β-CFT-FP) using [18F]fluoropropyl tosylate as the labelling reagent. J Label Compd Radiopharm 48.

Kojima, M., Shiojima, I., Yamazaki, T., Komuro, I., Zou, Z., Wang, Y., Mizuno, T., Ueki, K., Tobe, K., Kadowaki, T., et al., 1994. Angiotensin II receptor antagonist TCV-116 induces regression of hypertensive left ventricular hypertrophy in vivo and inhibits the intracellular signaling pathway of stretch-mediated cardiomyocyte hypertrophy in vitro. Circulation 89, 2204-2211.

Kolb, H.C., Chen, K., Walsh, J.C. Liang, Q., Padgett, H.C., Karimi, F., 2008. Click chemistry-derived cyclopeptide derivatives as imaging agents for integrins. . WO Patent 2008033561.

Kolb, H.C., Finn, M.G., Sharpless, K.B., 2001. Click Chemistry: Diverse Chemical Function from a Few Good Reactions. Angew Chem Int Ed Engl 40, 2004-2021.

Kolb, H.C., Sharpless, K.B., 2003. The growing impact of click chemistry on drug discovery. Drug Discovery Today 8, 1128-1137.

Komuro, I., Yazaki, Y., 1993. Control of cardiac gene expression by mechanical stress. Annu Rev Physiol 55, 55-75.

Krasikova, R.N., Kuznetsova, O.F., Fedorova, O.S., Maleev, V.I., Saveleva, T.F., Belokon, Y.N., 2008. No carrier added synthesis of O-(2'-[18F]fluoroethyl)-L-tyrosine via a novel type of chiral enantiomerically pure precursor, NiII complex of a (S)-tyrosine Schiff base. Bioorg Med Chem 16, 4994-5003.

Kromer, E.P., Riegger, G.A., 1988. Effects of long-term angiotensin converting enzyme inhibition on myocardial hypertrophy in experimental aortic stenosis in the rat. Am J Cardiol 62, 161-163.

Kuhnast, B., Hinnen, F., Tavitian, B., Dolle, F., 2008. [^{18}F]FPyKYNE, a fluoropyridine-based alkyne reagent designed for the fluorine-18 labelling of macromolecules using click chemistry. J. Label Compd. Radiopharm 51, 336–342.

Kumar, A., Singh, K., Panda, N., Upare, A., Nimbalkar, M., Soudagar, S., 2005. Losartan potassium synthesis. Ipca Laboratories, Mumbai (IN).

Kunapuli, S.P., Kumar, A., 1987. Molecular cloning of human angiotensinogen cDNA and evidence for the presence of its mRNA in rat heart. Circ Res 60, 786-790.

Laforest, R., Sharp, T.L., Engelbach, J.A., Fettig, N.M., Herrero, P., Kim, J., Lewis, J.S., Rowland, D.J., Tai, Y.C., Welch, M.J., 2005. Measurement of input functions in rodents: challenges and solutions. Nuclear Medicine and Biology 32, 679-685.

Le, T.H., Kim, H.S., Allen, A.M., Spurney, R.F., Smithies, O., Coffman, T.M., 2003. Physiological impact of increased expression of the AT1 angiotensin receptor. Hypertension 42, 507-514.

Lee, M.A., Bohm, M., Paul, M., Ganten, D., 1993. Tissue renin-angiotensin systems. Their role in cardiovascular disease. Circulation 87, IV7-13.

Lee, S., Jung, Y., Lee, B., Yun, S., Yoo, S., Shin, H., 1999. Characterization of Angiotensin II Antagonism Displayed by SK-1080, a Novel Nonpeptide AT1-Receptor Antagonist. Journal of Cardiovascular Pharmacology 33, 367-374.

Lee, S.J., Oh, S.J., Chi, D.Y., Kang, S.H., Kil, H.S., Kim, J.S., Moon, D.H., 2007. One-step high-radiochemical-yield synthesis of [18F]FP-CIT using a protic solvent system. Nucl Med Biol 34, 345-351.

Lee, Y.A., Liang, C.S., Lee, M.A., Lindpaintner, K., 1996. Local stress, not systemic factors, regulate gene expression of the cardiac renin-angiotensin system in vivo: a comprehensive study of all its components in the dog. Proc Natl Acad Sci U S A 93, 11035-11040.

Leri, A., Claudio, P.P., Li, Q., Wang, X., Reiss, K., Wang, S., Malhotra, A., Kajstura, J., Anversa, P., 1998. Stretch-mediated release of angiotensin II induces myocyte apoptosis by activating p53 that enhances the local renin-angiotensin system and decreases the Bcl-2-to-Bax protein ratio in the cell. J Clin Invest 101, 1326-1342.

Li, Z.-B., Wu, Z., Chen, K., Chin, F.T., Chen, X., 2007. Click chemistry for (18)F-labeling of RGD peptides and microPET imaging of tumor integrin alphavbeta3 expression. Bioconjug. Chem. 18, 1987-1994.

Li, Z., Conti, P.S., 2010. Radiopharmaceutical chemistry for positron emission tomography. Adv Drug Deliv Rev *In press*.

Liang, B., Leenen, F.H.H., 2008. Prevention of Salt-induced Hypertension and Fibrosis by AT1 -receptor Blockers in Dahl S Rats. J Cardiovasc Pharmacol 51, 457–466.

Lindpaintner, K., Ganten, D., 1991. The cardiac renin-angiotensin system. An appraisal of present experimental and clinical evidence. Circulation Research 68, 905-921.

Linz W, Scholkens BA, D., G., 1989. Converting enzyme inhibition specifically prevents the development and induces regression of cardiac hypertrophy in rats. Clin Exp Hypertens 11, 1325-1350.

Lipinski, C. A., Lombardo, F., Dominy, B. W., Feeney, P. J. 1997. Experimental and computational approaches to estimate solubility and permeability in drug discovery and development settings. Adv. Drug Delivery Rev. 23, 3-25.

Liu, P.Y., Jiang, N., Zhang, J., Wei, X., Lin, H.H., Yu, X.Q., 2006. The oxidative damage of plasmid DNA by ascorbic acid derivatives in vitro: the first research on the relationship between the structure of ascorbic acid and the oxidative damage of plasmid DNA. Chem Biodivers 3, 958-966.

Lo, M.W., Goldberg, M.R., McCrea, J.B., Lu, H., Furtek, C.I., Bjornsson, T.D., 1995. Pharmacokinetics of losartan, an angiotensin II receptor antagonist, and its active metabolite EXP3174 in humans. Clin Pharmacol Ther 58, 641-649.

Lodge, M.A., Braess, H., Mahmoud, F., Suh, J., Englar, N., Geyser-Stoops, S., Jenkins, J., Bacharach, S.L., Dilsizian, V., 2005. Developments in nuclear cardiology: transition from single photon emission computed tomography to positron emission tomography-computed tomography. J Invasive Cardiol 17, 491-496.

Logan, J., Fowler, J.S., Volkow, N.D., Wolf, A.P., Dewey, S.L., Schlyer, D.J., MacGregor, R.R., Hitzemann, R., Bendriem, B., Gatley, S.J., et al., 1990. Graphical analysis of reversible radioligand binding from time-activity measurements applied to [N-11C-methyl]-(-)-cocaine PET studies in human subjects. J Cereb Blood Flow Metab 10, 740-747.

Lopez, J.J., Lorell, B.H., Ingelfinger, J.R., Weinberg, E.O., Schunkert, H., Diamant, D., Tang, S.S., 1994. Distribution and function of cardiac angiotensin AT1- and AT2-receptor subtypes in hypertrophied rat hearts. Am J Physiol 267, H844-852.

Lu, J., Shi, M., Shoichet, M.S., 2009. Click chemistry functionalized polymeric nanoparticles target corneal epithelial cells through RGD-cell surface receptors. Bioconjug Chem 20, 87-94.

Mach, R.H., Schwarz, S.W., 2010. Challenges for Developing PET Tracers: Isotopes, Chemistry, and Regulatory Aspects. PET Clinics 5, 131-153.

Mackasey, K., 2012. Evaluating Angiotensin II Type 1 Receptor (AT1R) Changes in Renal Insufficiency and in Post Coronary Artery Occlusion Animal Models Using [^{11}C]Methyl-Candesartan. Cellular and Molecular Medicine. University of Ottawa, Ottawa.

Mamat, C., Ramenda, T., Wuest, F.R., 2009. Recent Applications of Click Chemistry for the Synthesis of Radiotracers for Molecular Imaging Mini-Reviews in Organic Chemistry 6, 21-34.

Marik, J., Sutcliffe, J.L., 2006. Click for PET: rapid preparation of [18F]fluoropeptides using CuI catalyzed 1,3-dipolar cycloaddition. Tetrahedron Letters 47, 6681-6684.

Mathews, W., Szabo, Z., 2010. Radioligands for the angiotensin II subtype 1 (AT1) receptor. Current topics in medicinal chemistry 10, 1585-1599.

Mathews, W.B., Yoo, S.E., Lee, S.H., Scheffel, U., Rauseo, P.A., Zober, T.G., Gocco, G., Sandberg, K., Ravert, H.T., Dannals, R.F., Szabo, Z., 2004. A novel radioligand for imaging the AT1 angiotensin receptor with PET. Nucl Med Biol 31, 571-574.

Matsubara, H., 2001. Renin-angiotensin system in human failing hearts: message from nonmyocyte cells to myocytes. Circ Res 88, 861-863.

Matsubara, H., Kanasaki, M., Murasawa, S., Tsukaguchi, Y., Nio, Y., Inada, M., 1994. Differential gene expression and regulation of angiotensin II receptor subtypes in rat cardiac fibroblasts and cardiomyocytes in culture. J Clin Invest 93, 1592-1601.

Meggs, L.G., Coupet, J., Huang, H., Cheng, W., Li, P., Capasso, J.M., Homcy, C.J., Anversa, P., 1993. Regulation of angiotensin II receptors on ventricular myocytes after myocardial infarction in rats. Circ Res 72, 1149-1162.

Mehta, P., Griendling, K., 2007 Angiotensin II cell signaling: physiological and pathological effects in the cardiovascular system. Am J Physiol Cell Physiol 292, C82-97.

Meldal, M., Tornoe, C.W., 2008. Cu-catalyzed azide-alkyne cycloaddition. Chem Rev 108, 2952-3015.

Miyata S, Haneda T, Y, N., 1993. The role of cardiac renin-angiotensin system in stretch-induced hypertrophy of cultured neonatal rat heart cells. . Circulation 88(suppl I), 1-614 Abstract.

Moises Canle L., I.D., and Howard Maskill, 2001. Substituent effect upon rates of deamination and base strengths of substituted N-tritylamines. J. Chem. Soc., Perkin Trans. 2.

Morishita, R., Gibbons, G.H., Ellison, K.E., Lee, W., Zhang, L., Yu, H., Kaneda, Y., Ogihara, T., Dzau, V.J., 1994. Evidence for direct local effect of angiotensin in vascular hypertrophy. In vivo gene transfer of angiotensin converting enzyme. J Clin Invest. 94, 423.

Naik, P., Murumkar, P., Giridhar, R., Yadav, M.R., 2010. Angiotensin II receptor type 1 (AT1) selective nonpeptidic antagonists--a perspective. Bioorg Med Chem 18, 8418-8456.

Nakajima, M., Hutchinson, H.G., Fujinaga, M., Hayashida, W., Morishita, R., Zhang, L., Horiuchi, M., Pratt, R.E., Dzau, V.J., 1995. The angiotensin II type 2 (AT2) receptor antagonizes the growth effects of the AT1 receptor: gain-of-function study using gene transfer. Proc Natl Acad Sci U S A 92, 10663-10667.

Nakashima, Y., Fouad, F.M., Tarazi, R.C., 1984. Regression of left ventricular hypertrophy from systemic hypertension by enalapril. Am J Cardiol 53, 1044-1049.

Nickenig, G., Strehlow, K., Roeling, J., Zolk, O., Knorr, A., Bohm, M., 1998. Salt induces vascular AT1 receptor overexpression in vitro and in vivo. Hypertension 31, 1272-1277.

Nicoletti A, Heudes D, Hinglais N, Appay M-D, Philippe M, Sassy-Prigent C, Bariety J, J-B, M., 1995. Left ventricular fibrosis in renovascular hypertensive rats. Effect of losartan and spironolactone. . Hypertension 26, 101-111.

Nio, Y., Matsubara, H., Murasawa, S., Kanasaki, M., Inada, M., 1995. Regulation of Gene Transcription of AngiotensinII Receptor Subtypes in Myocardial Infarction. J. Clin. Invest. 95, 46-54

Nozawa, Y., Miyake, H., Haruno, A., Yamada, S., Uchida, S., Ohkura, T., Kimura, R., Suzuki, H., Hoshino, T., 1996. Down-regulation of angiotensin II receptors in hypertrophied human myocardium. Clin Exp Pharmacol Physiol 23, 514-518.

Nwe, K., Brechbiel, M.W., 2009. Growing Applications of ‘‘Click Chemistry’’ for Bioconjugation in Contemporary Biomedical Research. CANCER BIOTHERAPY AND RADIOPHARMACEUTICALS 24.

Ohkubo, H., Kawakami, H., Kakehi, Y., Takumi, T., Arai, H., Yokota, Y., Iwai, M., Tanabe, Y., Masu, M., Hata, J., et al., 1990. Generation of transgenic mice with elevated blood pressure by introduction of the rat renin and angiotensinogen genes. Proc Natl Acad Sci U S A 87, 5153-5157.

Ohkubo, N., Matsubara, H., Nozawa, Y., Mori, Y., Murasawa, S., Kijima, K., Maruyama, K., Masaki, H., Tsutumi, Y., Shibazaki, Y., Iwasaka, T., Inada, M., 1997. Angiotensin type 2 receptors are reexpressed by cardiac fibroblasts from failing myopathic hamster hearts and inhibit cell growth and fibrillar collagen metabolism. Circulation 96, 3954-3962.

Oishi, Y., Ozono, R., Yano, Y., Teranishi, Y., Akishita, M., Horiuchi, M., Oshima, T., Kambe, M., 2003. Cardioprotective role of AT2 receptor in postinfarction left ventricular remodeling. Hypertension 41, 814-818.

Ozono, R., Matsumoto, T., Shingu, T., Oshima, T., Teranishi, Y., Kambe, M., Matsuura, H., Kajiyama, G., Wang, Z.-Q., Moore, A.F., Carey, R.M., 2000. Expression and localization of angiotensin subtype receptor proteins in the hypertensive rat heart. Am J Physiol Regulatory Integrative Comp Physiol 278, 781-789.

Pal, B., Jaisankar, P., Giri, V.S., 2004. Versatile Reagent for Reduction of Azides to Amines. Synth Comm 34, 1317-1323.

Palmer, M.H., Findlay, R.H., Gaskell, A.J., 1974. Electronic charge distribution and moments of five- and six-membered heterocycles. Journal of the Chemical Society, Perkin Transactions 2, 420-428.

Paradis, P., Dali-Youcef, N., Paradis, F.W., Thibault, G., Nemer, M., 2000. Overexpression of angiotensin II type I receptor in cardiomyocytes induces cardiac hypertrophy and remodeling. Proc Natl Acad Sci U S A 97, 931-936.

Park, B.K., Kitteringham, N.R., O'Neill, P.M., 2001. Metabolism of fluorine-containing drugs. Annu Rev Pharmacol Toxicol 41, 443-470.

Paul, M., Poyan Mehr, A., Kreutz, R., 2006. Physiology of local renin-angiotensin systems. Physiol Rev 86, 747-803.

Pfeffer, M.A., Lamas, G.A., Vaughan, D.E., Parisi, A.F., Braunwald, E., 1988. Effect of captopril on progressive ventricular dilatation after anterior myocardial infarction. N Engl J Med 319, 80-86.

Pfeffer, M.A., McMurray, J.J., Velazquez, E.J., Rouleau, J.L., Kober, L., Maggioni, A.P., Solomon, S.D., Swedberg, K., Van de Werf, F., White, H., Leimberger, J.D., Henis, M., Edwards, S., Zelenkofske, S., Sellers, M.A., Califf, R.M., 2003. Valsartan, captopril, or both in myocardial

infarction complicated by heart failure, left ventricular dysfunction, or both. N Engl J Med 349, 1893-1906.

Pitt, B., Poole-Wilson, P.A., Segal, R., Martinez, F.A., Dickstein, K., Camm, A.J., Konstam, M.A., Riegger, G., Klinger, G.H., Neaton, J., Sharma, D., Thiyagarajan, B., 2000. Effect of losartan compared with captopril on mortality in patients with symptomatic heart failure: randomised trial--the Losartan Heart Failure Survival Study ELITE II. Lancet 355, 1582-1587.

Poole, T.D., Holder, M.S., Gipson, D., 1994. Cardiac angiotensin II receptor populations during aortocaval fistulae, AII and beta adrenergic receptor blockade. Biochem Biophys Res Commun 203, 1865-1874.

Price, P., 2001. PET as a potential tool for imaging molecular mechanisms of oncology in man. Trends Mol Med 7, 442-446.

Purcell, W.P.a.S., J.A. , 1967. Electronic and molecular structure of selected unsubstituted and dimethyl amides from measurements of electric moments and nuclear magnetic resonance. J. Phys. Chem. 71, 4316-4319.

Rahmim, A., Zaidi, H., 2008. PET versus SPECT: strengths, limitations and challenges. Nucl Med Commun 29, 193-207.

Raju, B., Mortell, K., Anandan, S., O'Dowd, H., Gao, H., Gomez, M., Hackbarth, C., Wu, C., Wang, W., Yuan, Z., White, R., Trias, J., Patel, D.V., 2003. N- and C-terminal modifications of negamycin. Bioorg Med Chem Lett 13, 2413-2418.

Ramchandran, R., Takezako, T., Saad, Y., Stull, L., Fink, B., Yamada, H., Dikalov, S., Harrison, D.G., Moravec, C., Karnik, S.S., 2006. Angiotensinergic stimulation of vascular endothelium in mice causes hypotension, bradycardia, and attenuated angiotensin response. Proc Natl Acad Sci U S A 103, 19087-19092.

Ramenda, T., Bergmann, R., Wuest, F., 2007. Synthesis of 18F-labeled Neurotensin(8-13) via Copper-Mediated 1,3-Dipolar [32]Cycloaddition Reaction. Letters in Drug Design; Discovery 4, 279-285.

Regitz-Zagrosek, V., Friedel, N., Heymann, A., Bauer, P., Neuss, M., Rolfs, A., Steffen, C., Hildebrandt, A., Hetzer, R., Fleck, E., 1995. Regulation, chamber localization, and subtype distribution of angiotensin II receptors in human hearts. Circulation 91, 1461-1471.

Reudelhuber, T.L., Bernstein, K.E., Delafontaine, P., 2007. Is Angiotensin II a Direct Mediator of Left Ventricular Hypertrophy? Hypertension 49, 1196-1201.

Rogg, H., de Gasparo, M., Graedel, E., Stulz, P., Burkart, F., Eberhard, M., Erne, P., 1996. Angiotensin II-receptor subtypes in human atria and evidence for alterations in patients with cardiac dysfunction. Eur Heart J 17, 1112-1120.

Rostovtsev, V.V., Green, L.G., Fokin, V.V., Sharpless, K.B., 2002. A stepwise huisgen cycloaddition process: copper(I)-catalyzed regioselective "ligation" of azides and terminal alkynes. Angew Chem Int Ed Engl 41, 2596-2599.

Saavedra, J.M., Hauser, W., Ciuffo, G., Egidy, G., Hoe, K.L., Johren, O., Sembonmatsu, T., Inagami, T., Armando, I., 2001. Increased AT(1) receptor expression and mRNA in kidney glomeruli of AT(2) receptor gene-disrupted mice. Am J Physiol Renal Physiol 280, F71-78.

Sadoshima, J., Izumo, S., 1993. Molecular characterization of angiotensin II-induced hypertrophy of cardiac myocytes and hyperplasia of cardiac fibroblasts: critical role of the AT1 receptor subtype. Circ Res 73, 413-423.

Sadoshima, J., Xu, Y., Slayter, H.S., Izumo, S., 1993. Autocrine release of angiotensin II mediates stretch-induced hypertrophy of cardiac myocytes in vitro. Cell 75, 977-984.

Saha, G.B., 2008. Basics of PET Imaging: Physics, Chemistry, and Regulations. Springer, Cleveland, OH.

Saijonmaa, F.F.O., 2008. Renin-angiotensin system revisited. J Intern Med 264, 224–236.

Santella, J.B., Duncia, J.V., Ensinger, C.L., VanAtten, M.K., Carini, D.J., Wexler, R.R., Chiu, A.T., Wong, P.C., Timmermans, P.B.M.W.M., 1994. Balanced angiotensin II receptor antagonists. III. The effects of substitution at the imidazole 5-position. Bioorganic & Medicinal Chemistry Letters 4, 2235-2240.

Schindler, S. 2000. Reactivity of copper(I) complexes towards di-oxygen. Eur J Inorg Chem 2000;11:2311-2326.

Schirrmacher, R., Weber, M., Schmitz, A., Shiue, C.-Y., Alavi, A., Feilen, P., Schneider, S., Kann, P., Rosch, F., 2002. Radiosynthesis of 1-(4-(2-[18F]fluoroethoxy)benzenesulfonyl)-3-butyl urea: a potential b-cell imaging agent. J Label Compd Radiopharm 45, 763-774.

Seasholtz, T.M., Brown, J.H., 2004. RHO SIGNALING in vascular diseases. Mol Interv 4, 348-357.

Sechi, L.A., Grady, E.F., Griffin, C.A., Kalinyak, J.E., Schambelan, M., 1992. Distribution of angiotensin II receptor subtypes in rat and human kidney. Am J Physiol 262, F236-240.

Sen, S., 1983. Regression of cardiac hypertrophy. Experimental animal model. Am J Med 75, 87-93.

Serneri, G., Boddi, M., Cecioni, I., Vanni, S., Coppo, M., Papa, M., Bandinelli, B., Bertolozzi, I., Polidori, G., Toscano, T., Maccherini, M., Modesti, P., 2001. Cardiac angiotensin II formation in the clinical course of heart failure and its relationship with left ventricular function. Circ Res. 88, 961-968.

Sharma, A., Sorenby, A., Wernerson, A., Efendic, S., Kumagai-Braesch, M., Tibell, A., 2006. Exendin-4 treatment improves metabolic control after rat islet transplantation to athymic mice with streptozotocin-induced diabetes. Diabetologia 49, 1247-1253.

Shirani, J., Narula, J., Eckelman, W.C., Dilsizian, V., 2006. Novel imaging strategies for predicting remodeling and evolution of heart failure: targeting the Renin-Angiotensin system. Heart Fail Clin 2, 231-247.

Sica, D.A., Gehr, T.W., Ghosh, S., 2005. Clinical pharmacokinetics of losartan. Clin Pharmacokinet 44, 797-814.

Sirion, U., Kim, H.J., Lee, J.H., Seo, J.W., Lee, B.S., Lee, S.J., Oh, S.J., Chi, D.Y., 2007. An efficient F-18 labeling method for PET study: Huisgen 1,3-dipolar cycloaddition of bioactive substances and F-18-labeled compounds. Tetrahedron Letters 48, 3953-3957.

Slifstein, M., Laruelle, M., 2000. Effects of statistical noise on graphic analysis of PET neuroreceptor studies. J Nucl Med 41, 2083-2088.

SOLVD Investigators. 1991. Effect of Enalapril on Survival in Patients with Reduced Left Ventricular Ejection Fractions and Congestive Heart Failure. NEJM. 325, 293-302.

Staufenberger, S., Jacobs, M., Brandstatter, K., Hafner, M., Regitz-Zagrosek, V., Ertl, G., Schorb, W., 2001. Angiotensin II type 1 receptor regulation and differential trophic effects on rat cardiac myofibroblasts after acute myocardial infarction. J Cell Physiol 187, 326-335.

Stearns, R.A., Chakravarty, P.K., Chen, R., Chiu, S.H., 1995. Biotransformation of losartan to its active carboxylic acid metabolite in human liver microsomes. Role of cytochrome P4502C and 3A subfamily members. Drug Metab Dispos 23, 207-215.

Stearns, R.A., Miller, R.R., Doss, G.A., Chakravarty, P.K., Rosegay, A., Gatto, G.J., Chiu, S.H., 1992. The metabolism of DuP 753, a nonpeptide angiotensin II receptor antagonist, by rat, monkey, and human liver slices. Drug Metab Dispos 20, 281-287.

Stoll, M., Steckelings, U.M., Paul, M., Bottari, S.P., Metzger, R., Unger, T., 1995. The angiotensin AT2-receptor mediates inhibition of cell proliferation in coronary endothelial cells. J Clin Invest 95, 651-657.

Sugino H, Ozono R, Kurisu S, Matsuura H, Ishida M, Oshima T, Kambe M, Teranishi Y, Masaki H, H., M., mice., A.i.n.i.i.m.o.t.a.I.r.i.t., 2001. Hypertension. 37, 1394-1398.

Suzuki, J., Matsubara, H., Urakami, M., Inada, M., 1993. Rat angiotensin II (type 1A) receptor mRNA regulation and subtype expression in myocardial growth and hypertrophy. Circ Res 73, 439-447.

Szabo, Z., Alachkar, N., Gulaldi, N., Vranesic, M., Chalian, M., Mathews, W., Xia, J., Rabb, H., 2010. PET imaging of the angiotensin subtype 1 receptor (AT1R) in human kidney transplants. J Nucl Med Meeting Abstracts 51, 427.

Tamura, K., Chiba, E., Yokoyama, N., Sumida, Y., Yabana, M., Tamura, N., Takasaki, I., Takagi, N., Ishii, M., Horiuchi, M., Umemura, S., 1999. Renin-angiotensin system and fibronectin gene expression in Dahl Iwai salt-sensitive and salt-resistant rats. J Hypertens 17, 81-89.

Tan, J., Wang, H., Leenen, F.H., 2004. Increases in brain and cardiac AT1 receptor and ACE densities after myocardial infarct in rats. Am J Physiol Heart Circ Physiol 286, H1665-1671.

Tang, G., Tang, X., Wang, X., 2010. A facile automated synthesis of N-succinimidyl 4-[18F]fluorobenzoate ([18F]SFB) for 18F-labeled cell-penetrating peptide as PET tracer. J. Label Compd. Radiopharm 53, 543-547.

Thackeray, J.T., Beanlands, R.S., Dasilva, J.N., 2007. Presence of specific 11C-meta-Hydroxyephedrine retention in heart, lung, pancreas, and brown adipose tissue. J Nucl Med 48, 1733-1740.

Thomas, W.G., Brandenburger, Y., Autelitano, D.J., Pham, T., Qian, H., Hannan, R.D., 2002. Adenoviral-directed expression of the type 1A angiotensin receptor promotes cardiomyocyte hypertrophy via transactivation of the epidermal growth factor receptor. Circ. Res. 90 135–142.

Thomas, W.G., Mendelsohn, F.A., 2003. Angiotensin receptors: form and function and distribution. Int J Biochem Cell Biol 35, 774-779.

Thompson, A.S., Grabowski, E.J.J., 1995. Converting an alcohol to an azide with SN2 inversion using a phosphoryl azide. Merck & Co., Inc., US.

Thompson, A.S., Humphrey, G.R., DeMarco, A.M., Mathre, D.J., Grabowski, E.J.J., 1993. Direct Conversion of Activated Alcohols to Azides Using Diphenyl Phosphorazidate. A Practical Alternative to Mitsunobu Conditions. J Org Chem 58, 5886-5888

Timmermans, P.B., Wong, P.C., Chiu, A.T., Herblin, W.F., 1991. Nonpeptide angiotensin II receptor antagonists. Trends Pharmacol Sci 12, 55-62.

Timmermans, P.B., Wong, P.C., Chiu, A.T., Herblin, W.F., Benfield, P., Carini, D.J., Lee, R.J., Wexler, R.R., Saye, J.A., Smith, R.D., 1993. Angiotensin II receptors and angiotensin II receptor antagonists. Pharmacol Rev 45, 205-251.

Tornoe, C.W., Christensen, C., Meldal, M., 2002. Peptidotriazoles on solid phase: [1,2,3]-triazoles by regiospecific copper(i)-catalyzed 1,3-dipolar cycloadditions of terminal alkynes to azides. J Org Chem 67, 3057-3064.

Tosco, P., Rolando, B., Fruttero, R., Henchoz, Y., Martel, S., Carrupt, P.-A., Gasco, A., 2008. Physicochemical Profiling of Sartans: A Detailed Study of Ionization Constants and Distribution Coefficients. Helvetica Chimica Acta 91, 468-482.

Tsutsumi, Y., Matsubara, H., Ohkubo, N., Mori, Y., Nozawa, Y., Murasawa, S., Kijima, K., Maruyama, K., Masaki, H., Moriguchi, Y., Shibasaki, Y., Kamihata, H., Inada, M., Iwasaka, T., 1998. Angiotensin II type 2 receptor is upregulated in human heart with interstitial fibrosis, and cardiac fibroblasts are the major cell type for its expression. Circ Res 83, 1035-1046.

Tuccinardi, T., Calderone, V., Rapposelli, S., Martinelli, A., 2006. Proposal of a New Binding Orientation for Non-Peptide AT1 Antagonists: Homology Modeling, Docking and Three-Dimensional Quantitative Structure-Activity Relationship Analysis. J. Med. Chem. 49, 4305-4316.

Unger, T., 2002. The Role of the Renin–Angiotensin System in the Development of Cardiovascular Disease. Am J Cardiol 89(suppl), 3A–10A.

Urata, H., Healy, B., Stewart, R.W., Bumpus, F.M., Husain, A., 1989. Angiotensin II receptors in normal and failing human hearts. J Clin Endocrinol Metab 69, 54-66.

Vaidyanathan, G., Zalutsky, M.R., 1992. Labeling of proteins with fluorine-18 using N-succinimidyl 4-[^{18}F]fluorobenzoate. Nucl Med Biol 19, 275-281.

Vaidyanathan, G., Zalutsky, M.R., 2006. Synthesis of N-succinimidyl 4-[^{18}F]fluorobenzoate, an agent for labeling proteins and peptides with ^{18}F. Nat Protoc 1, 1655-1661.

Vaidyanathan, G.B.J.W.a.M.R.Z., 2009. Propargyl 4-[18F]fluorobenzoate: A Putatively More Stable Prosthetic Group for the Fluorine-18 Labeling of Biomolecules via Click Chemistry Current Radiopharmaceuticals 2, 63-74.

Valdivia, A.C., Estrada, M., Hadizad, T., Stewart, D.J., Beanlands, R.S., DaSilva, J.N., 2011. A fast, simple, and reproducible automated synthesis of [^{18}F]FPyKYNE-c(RGDyK) for αvβ3 receptor positron emission tomography imaging. Journal of Labelled Compounds and Radiopharmaceuticals.

Vallabhajosula, S., 2009. Molecular Imaging: Radiopharmaceuticals for PET and SPECT. Springer New York, NY

van Kats, J.P., Danser, A.H., van Meegen, J.R., Sassen, L.M., Verdouw, P.D., Schalekamp, M.A., 1998. Angiotensin production by the heart: a quantitative study in pigs with the use of radiolabeled angiotensin infusions. Circulation 98, 73-81.

van Kats, J.P., Duncker, D.J., Haitsma, D.B., Schuijt, M.P., Niebuur, R., Stubenitsky, R., Boomsma, F., Schalekamp, M.A., Verdouw, P.D., Danser, A.H., 2000. Angiotensin-converting enzyme inhibition and angiotensin II type 1 receptor blockade prevent cardiac remodeling in pigs after myocardial infarction: role of tissue angiotensin II. Circulation 102, 1556-1563.

van Kats, J.P., Methot, D., Paradis, P., Silversides, D.W., Reudelhuber, T.L., 2001. Use of a Biological Peptide Pump to Study Chronic Peptide Hormone Action in Transgenic Mice. Journal of Biological Chemistry 276, 44012-44017.

Vanderheyden, P.M., Fierens, F.L., De Backer, J.P., Fraeyman, N., Vauquelin, G., 1999. Distinction between surmountable and insurmountable selective AT1 receptor antagonists by use of CHO-K1 cells expressing human angiotensin II AT1 receptors. Br J Pharmacol 126, 1057-1065.

Varagic, J., Susic, D., Frohlich, E., 2001. Coronary hemodynamic and ventricular responses to angiotensin type 1 receptor inhibition in SHR: interaction with angiotensin type 2 receptors. Hypertension 37, 1399-1403.

Veerasingham, S.J., Raizada, M.K., 2003. Brain renin-angiotensin system dysfunction in hypertension: recent advances and perspectives. Br J Pharmacol 139, 191-202.

Verjans, J.W., Lovhaug, D., Narula, N., Petrov, A.D., Indrevoll, B., Bjurgert, E., Krasieva, T.B., Petersen, L.B., Kindberg, G.M., Solbakken, M., Cuthbertson, A., Vannan, M.A., Reutelingsperger, C.P., Tromberg, B.J., Hofstra, L., Narula, J., 2008. Noninvasive imaging of angiotensin receptors after myocardial infarction. JACC Cardiovasc Imaging 1, 354-362.

Villarreal, F.J., Kim, N.N., Ungab, G.D., Printz, M.P., Dillmann, W.H., 1993. Identification of functional angiotensin II receptors on rat cardiac fibroblasts. Circulation 88, 2849-2861.

Voros, S., Yang, Z., Bove, C.M., Gilson, W.D., Epstein, F.H., French, B.A., Berr, S.S., Bishop, S.P., Conaway, M.R., Matsubara, H., Carey, R.M., Kramer, C.M., 2006. Interaction between AT1 and AT2 receptors during postinfarction left ventricular remodeling. Am J Physiol Heart Circ Physiol 290, H1004-1010.

Wang, Q., Chan, T.R., Hilgraf, R., Fokin, V.V., Sharpless, K.B., Finn, M.G., 2003. Bioconjugation by copper(I)-catalyzed azide-alkyne [3 + 2] cycloaddition. J Am Chem Soc 125, 3192-3193.

Wang, Z.Q., Moore, A.F., Ozono, R., Siragy, H.M., Carey, R.M., 1998. Immunolocalization of subtype 2 angiotensin II (AT2) receptor protein in rat heart. Hypertension 32, 78-83.

Waterhouse, R.N., 2003. Determination of lipophilicity and its use as a predictor of blood-brain barrier penetration of molecular imaging agents. Mol Imaging Biol 5, 376-389.

Weisman, H., Bush, D., Mannisi, J., Bulkley, B., 1985 Global cardiac remodeling after acute myocardial infarction: a study in the rat model. J Am Coll Cardiol 5, 1355-1362.

Welch, M.J., Redvanly, C.S. (Eds.), 2003. Handbook of radiopharmaceuticals: radiochemistry and applications. Wiley and Sons, West Sussex, England.

Wester, H.J., Herz, M., Weber, W., Heiss, P., Senekowitsch-Schmidtke, R., Schwaiger, M., Stocklin, G., 1999. Synthesis and radiopharmacology of O-(2-[^{18}F]fluoroethyl)-L-tyrosine for tumor imaging. J Nucl Med 40, 205-212.

Wharton, J., Morgan, K., Rutherford, R.A., Catravas, J.D., Chester, A., Whitehead, B.F., De Leval, M.R., Yacoub, M.H., Polak, J.M., 1998. Differential distribution of angiotensin AT2 receptors in the normal and failing human heart. J Pharmacol Exp Ther 284, 323-336.

Whitebread, S., Mele, M., Kamber, B., de Gasparo, M., 1989. Preliminary biochemical characterization of two angiotensin II receptor subtypes. Biochemical and Biophysical Research Communications 163, 284-291.

Widdop, R.E., Jones, E.S., Hannan, R.E., Gaspari, T.A., 2003. Angiotensin AT2 receptors: cardiovascular hope or hype? Br J Pharmacol 140, 809-824.

Wiemer, G., Scholkens, B.A., Wagner, A., Heitsch, H., Linz, W., 1993. The possible role of angiotensin II subtype AT2 receptors in endothelial cells and isolated ischemic rat hearts. J Hypertens Suppl 11, S234-235.

Wolf, K., Della Bruna, R., Bruckschlegel, G., Schunkert, H., Riegger, G.A., Kurtz, A., 1996. Angiotensin II receptor gene expression in hypertrophied left ventricles of rat hearts. J Hypertens 14, 349-354.

Wong, P.C., Price, W.A., Chiu, A.T., Duncia, J.V., Carini, D.J., Wexler, R.R., Johnson, A.L., Timmermans, P.B., 1990a. Nonpeptide angiotensin II receptor antagonists. IX. Antihypertensive activity in rats of DuP 753, an orally active antihypertensive agent. J Pharmacol Exp Ther 252, 726-732.

Wong, P.C., Price, W.A., Chiu, A.T., Duncia, J.V., Carini, D.J., Wexler, R.R., Johnson, A.L., Timmermans, P.B., 1990b. Nonpeptide angiotensin II receptor antagonists. VIII. Characterization of functional antagonism displayed by DuP 753, an orally active antihypertensive agent. J Pharmacol Exp Ther 252, 719-725.

Wong, P.C., Price, W.A., Jr., Chiu, A.T., Duncia, J.V., Carini, D.J., Wexler, R.R., Johnson, A.L., Timmermans, P.B., 1990c. Nonpeptide angiotensin II receptor antagonists. XI. Pharmacology of EXP3174: an active metabolite of DuP 753, an orally active antihypertensive agent. J Pharmacol Exp Ther 255, 211-217.

Wu, L., Iwai, M., Nakagami, H., Chen, R., Suzuki, J., Akishita, M., de Gasparo, M., Horiuchi, M., 2002. Effect of angiotensin II type 1 receptor blockade on cardiac remodeling in angiotensin II type 2 receptor null mice. Arterioscler Thromb Vasc Biol 22, 49-54.

Wüst, F., Hultsch, C., Bergmann, R., Johannsen, B., Henle, T., 2003. Radiolabelling of isopeptide N^{e}-(*y*-glutamyl)-L-lysine by conjugation with N-succinimidyl-4-[^{18}F]Fluorobenzoate. Appl. Radiat. Isot. 59, 43-48.

Xia, J., Seckin, E., Xiang, Y., Vranesic, M., Mathews, W.B., Hong, K., Bluemke, D.A., Lerman, L.O., Szabo, Z., 2008. Positron-emission tomography imaging of the angiotensin II subtype 1 receptor in swine renal artery stenosis. Hypertension 51, 466-473.

Xu, J., Carretero, O.A., Liao, T.D., Peng, H., Shesely, E.G., Liu, T.S., Yang, J.J., Reudelhuber, T.L., Yang, X.P., 2010. Local angiotensin II aggravates cardiac remodeling in hypertension. Am J Physiol Heart Circ Physiol 299, H1328-1338.

Xu, J., Carretero, O.A., Liu, Y.H., Shesely, E.G., Yang, F., Kapke, A., Yang, X.P., 2002. Role of AT2 receptors in the cardioprotective effect of AT1 antagonists in mice. Hypertension 40, 244-250.

Yamada, T., Horiuchi, M., Dzau, V.J., 1996. Angiotensin II type 2 receptor mediates programmed cell death. Proc Natl Acad Sci U S A 93, 156-160.

Yamamoto, F., Aoki, M., Furusawa, Y., Ando, K., Kuwabara, Y., Masuda, K., Sasaki, S., Maeda, M., 2002. Synthesis and evaluation of 4-bromo-1-(3-[^{18}F]fluoropropyl)-2-nitroimidazole with a low energy LUMO orbital designed as brain hypoxia-targeting imaging agent. Biol Pharm Bull 25, 616-621.

Yamano, Y., Ohyama, K., Chaki, S., Guo, D.F., Inagami, T., 1992. Identification of amino acid residues of rat angiotensin II receptor for ligand binding by site directed mutagenesis. Biochem Biophys Res Commun 187, 1426-1431.

Yamazaki, T., Komuro, I., Kudoh, S., Zou, Y., Shiojima, I., Mizuno, T., Takano, H., Hiroi, Y., Ueki, K., Tobe, K., 1995. Angiotensin II partly mediates mechanical stress-induced cardiac hypertrophy. Circ Res 77, 258-265.

Yasuda, N., Miura, S., Akazawa, H., Tanaka, T., Qin, Y., Kiya, Y., Imaizumi, S., Fujino, M., Ito, K., Zou, Y., Fukuhara, S., Kunimoto, S., Fukuzaki, K., Sato, T., Ge, J., Mochizuki, N., Nakaya, H., Saku, K., Komuro, I., 2008. Conformational switch of angiotensin II type 1 receptor underlying mechanical stress-induced activation. EMBO Rep 9, 179-186.

Yu, M., Guaraldi, M.T., Mistry, M., Kagan, M., McDonald, J.L., Drew, K., Radeke, H., Azure, M., Purohit, A., Casebier, D.S., Robinson, S.P., 2007. BMS-747158-02: a novel PET myocardial perfusion imaging agent. J Nucl Cardiol 14, 789-798.

Zhai, P., Galeotti, J., Liu, J., Holle, E., Yu, X., Wagner, T., Sadoshima, J., 2006. An angiotensin II type 1 receptor mutant lacking epidermal growth factor receptor transactivation does not induce angiotensin II-mediated cardiac hypertrophy. Circ Res 99, 528-536.

Zhu, Y., Zhu, Y., Lu, N., Wang, M., Wang, Y., Yao, T., 2003. Role of angiotensin AT1 and AT2 receptors in cardiac hypertrophy and cardiac remodelling Clinical and Experimental Pharmacology and Physiology 30, 911-918.

Zhu, Y.C., Zhu, Y.Z., Gohlke, P., Stauss, H.M., Unger, T., 1997. Effects of angiotensin-converting enzyme inhibition and angiotensin II AT1 receptor antagonism on cardiac parameters in left ventricular hypertrophy. Am J Cardiol 80, 110A-117A.

Zhuo, J., Alcorn, D., Allen, A.M., Mendelsohn, F.A., 1992. High resolution localization of angiotensin II receptors in rat renal medulla. Kidney Int 42, 1372-1380.

Zober, T., Mathews, W., Seckin, E., Yoo, S., Hilton, J., Xia, J., Sandberg, K., Ravert, H., Dannals, R., Szabo, Z., 2006. PET Imaging of the AT1 receptor with [^{11}C]KR31173. Nucl Med Biol 33, 5-13.

Zou, Y., Akazawa, H., Qin, Y., Sano, M., Takano, H., Minamino, T., Makita, N., Iwanaga, K., Zhu, W., Kudoh, S., Toko, H., Tamura, K., Kihara, M., Nagai, T., Fukamizu, A., Umemura, S., Iiri, T., Fujita, T., Komuro, I., 2004. Mechanical stress activates angiotensin II type 1 receptor without the involvement of angiotensin II. Nat Cell Biol 6, 499-506.

Appendix I - *Product Chracterization*

Fluoroethyl tosylate

Toluene-4-sulfonic acid 2-fluoro-ethyl ester

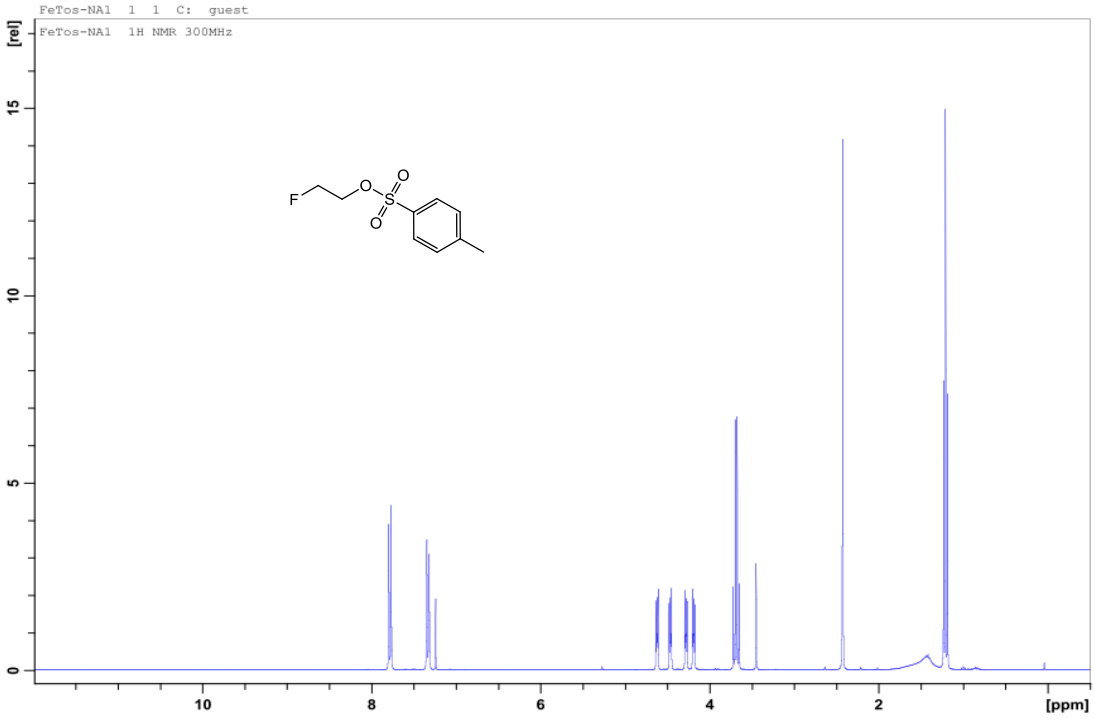

2c2631 Scan 10 RT=1:50 100%=124499 mv 14 Jul 109 20:14
HRP +EI

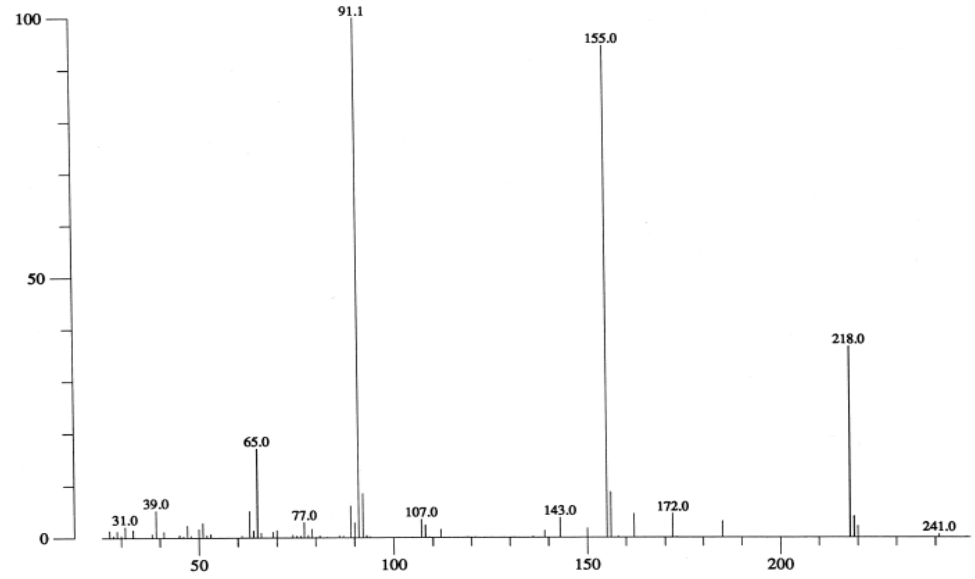

Fluoropropyl tosylate

Toluene-4-sulfonic acid 3-fluoro-propyl ester

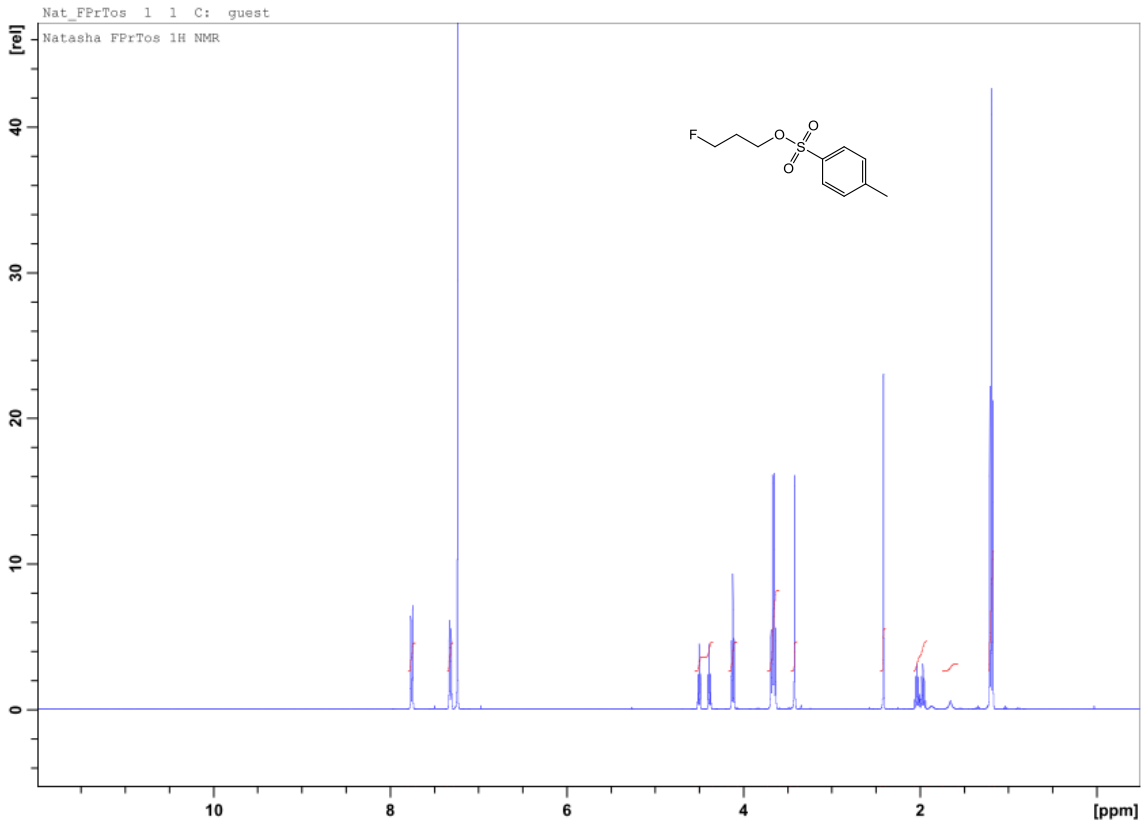

SFB

N-succinimidyl 4-fluorobenzoate

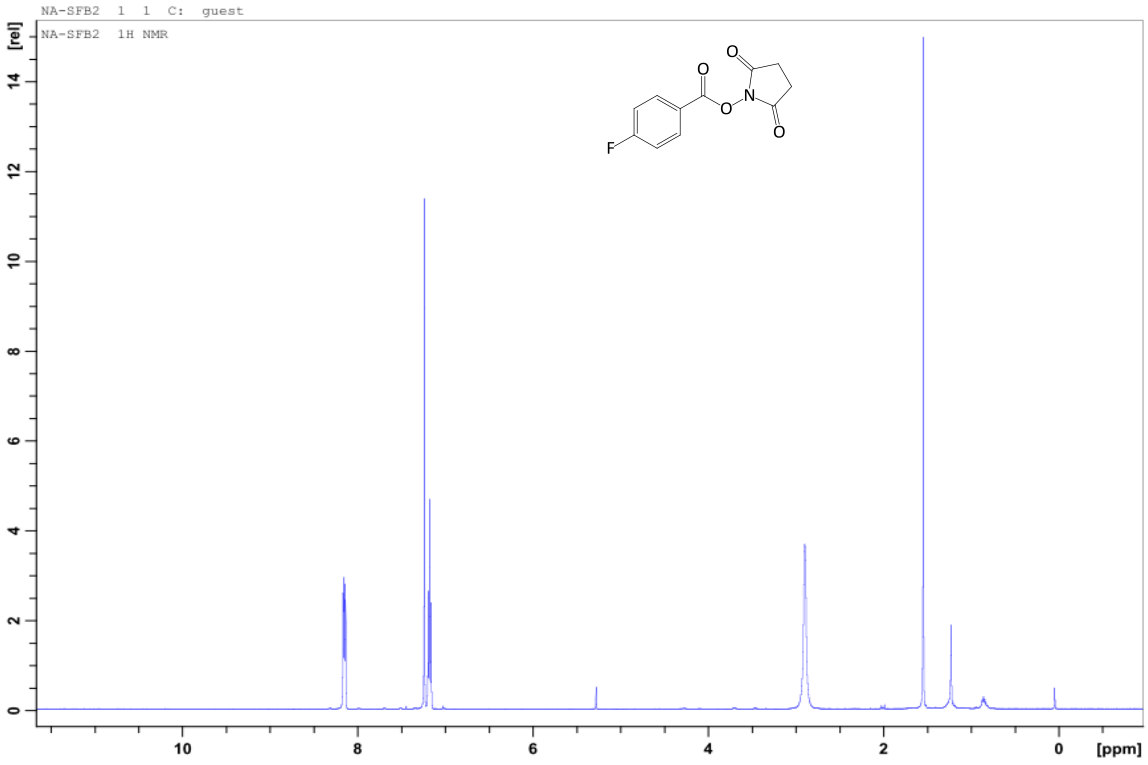

2c3095 Scan 4 RT=0:36 100%=477467 mv 29-Oct-2009 04:02
HRP +EI sfb-2

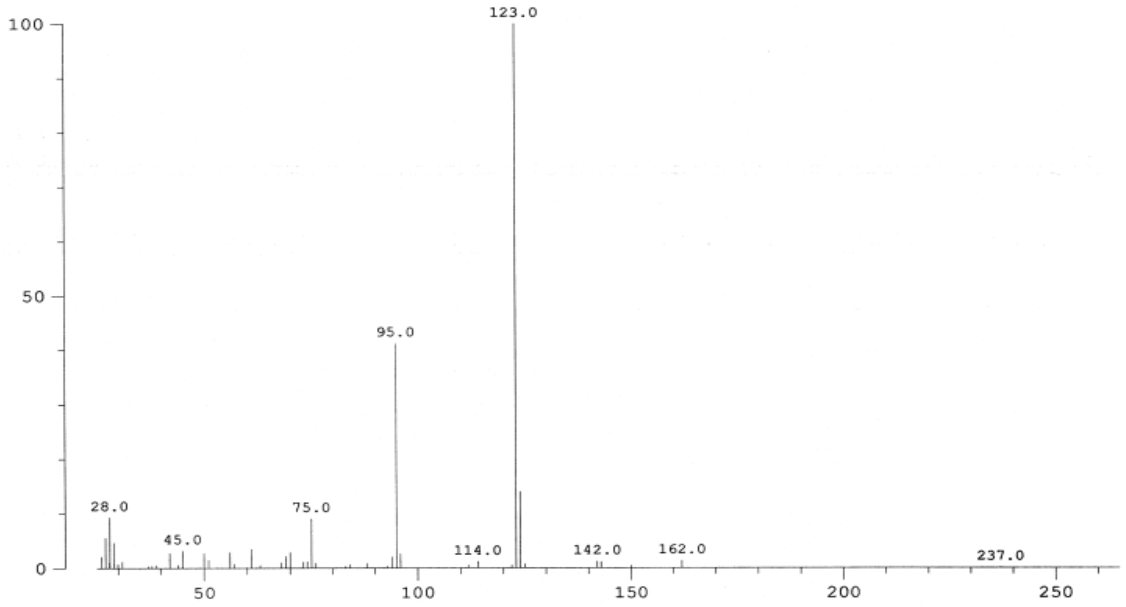

NO_2PyKYNE

2-Nitro-3-pent-4-yn-1-yloxypyridine

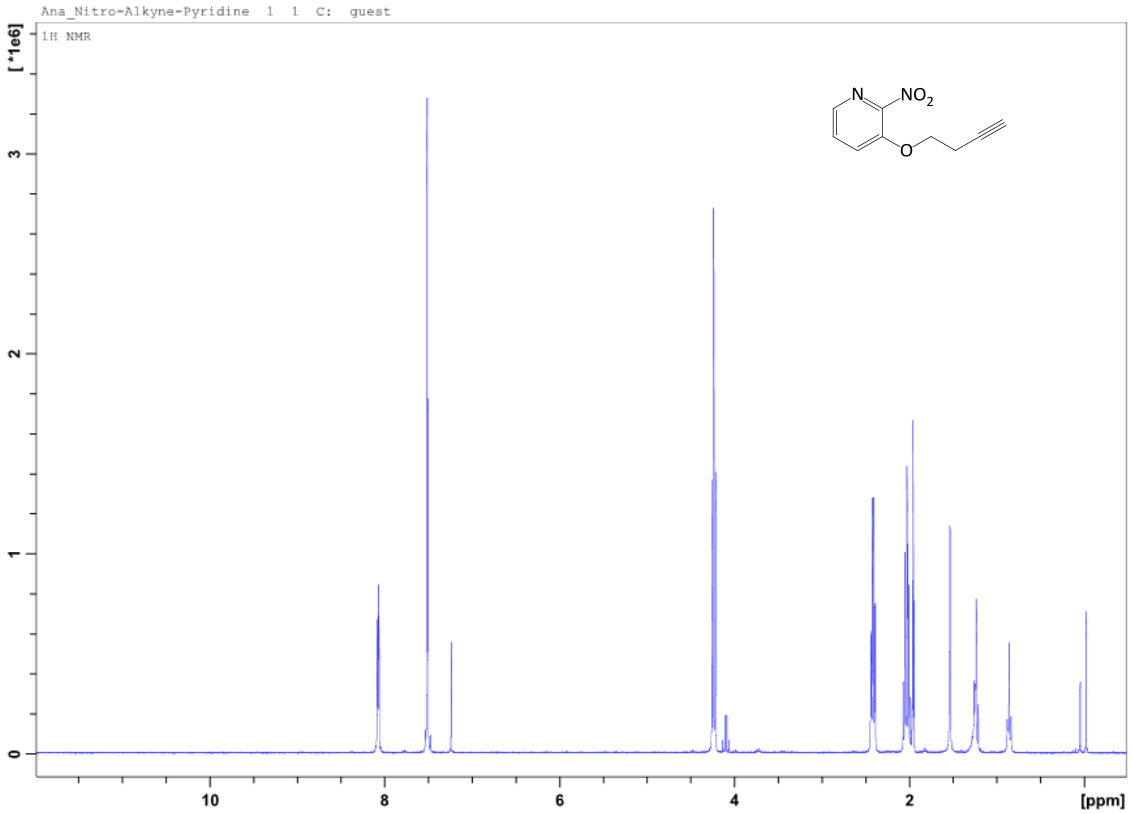

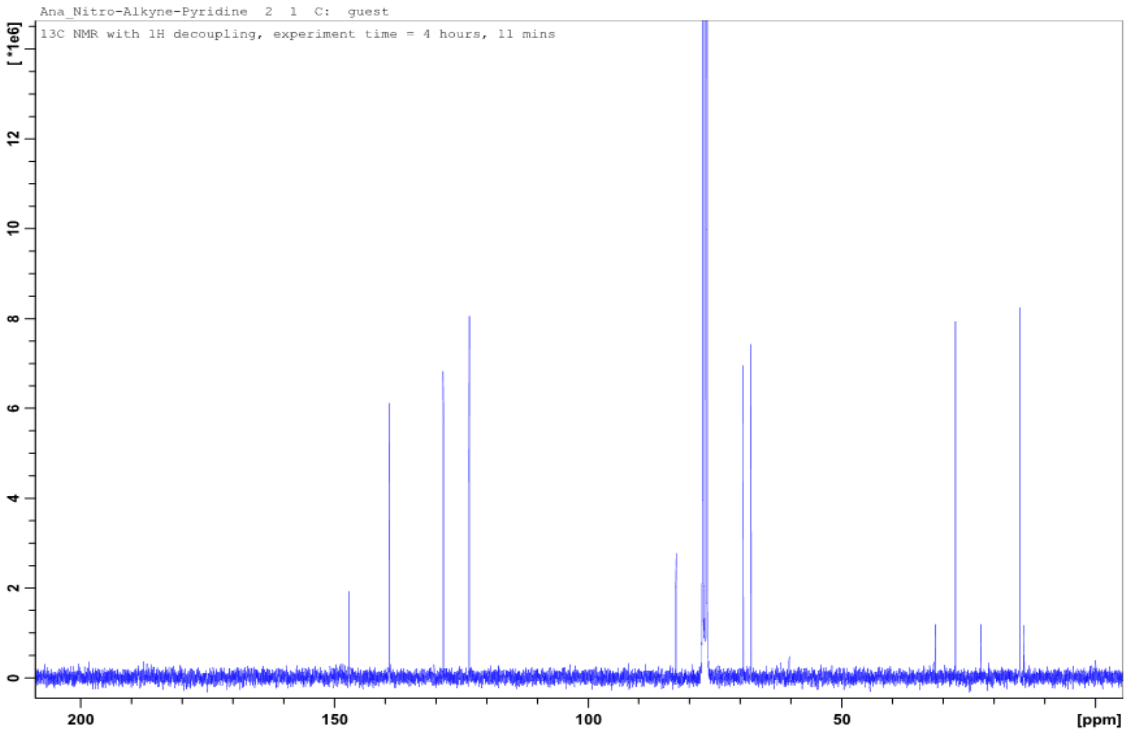

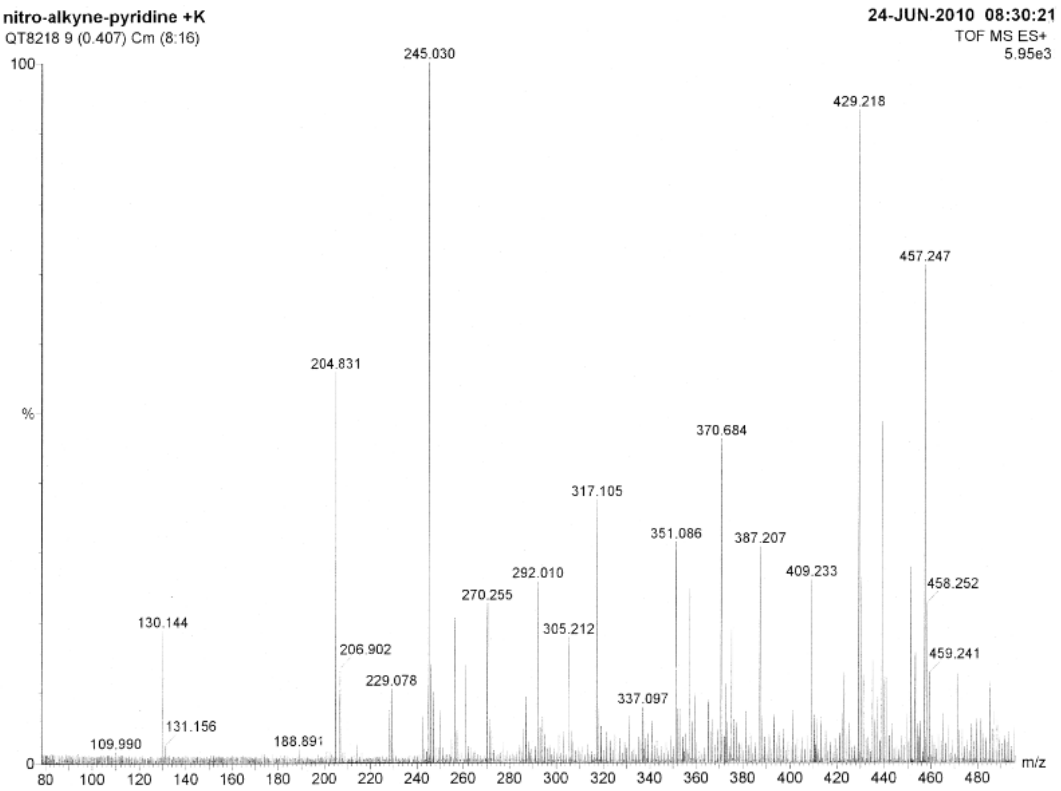
nitro-alkyne-pyridine +K
QT8218 9 (0.407) Cm (8:16)
24-JUN-2010 08:30:21
TOF MS ES+
5.95e3
100
%
0
245.030
429.218
457.247
204.831
370.684
317.105
351.086
387.207
409.233
292.010
270.255
458.252
130.144
305.212
206.902
459.241
229.078
337.097
131.156
109.990
188.891
m/z
80 100 120 140 160 180 200 220 240 260 280 300 320 340 360 380 400 420 440 460 480

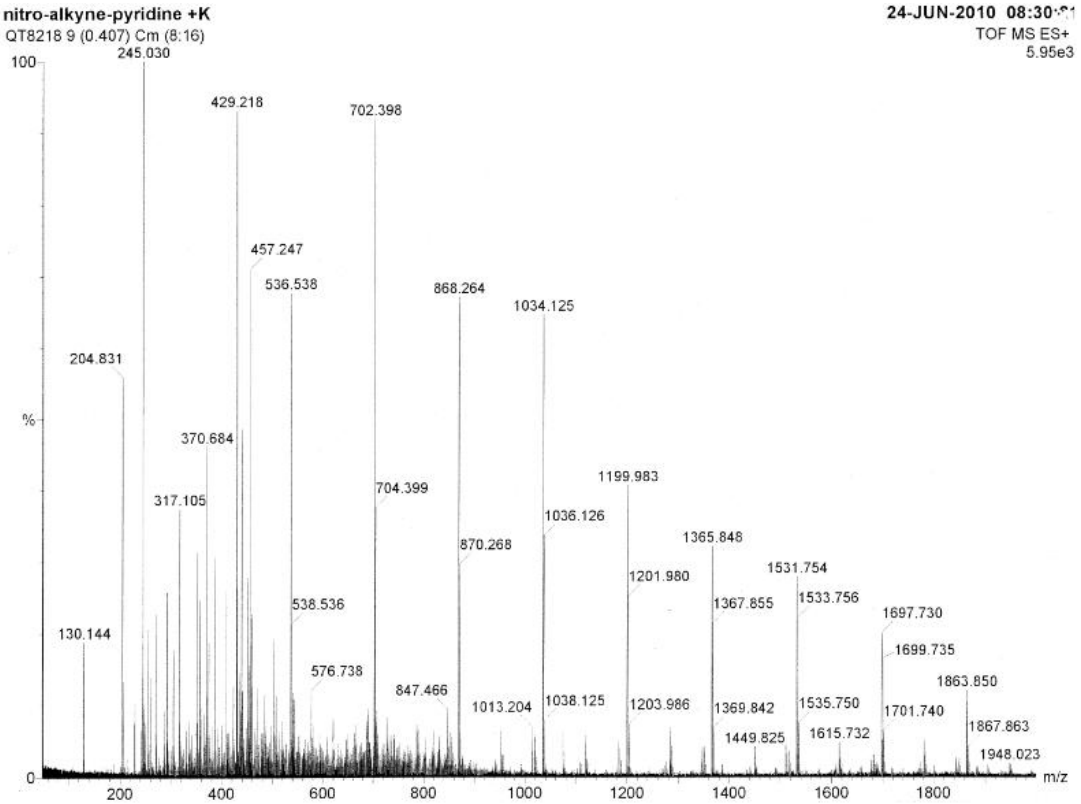
nitro-alkyne-pyridine +K
QT8218 9 (0.407) Cm (8:16)
TOF MS ES+
5.95e3
100
%
0
245.030
429.218
702.398
457.247
536.538
868.264
1034.125
204.831
370.684
704.399
1199.983
317.105
1036.126
870.268
1365.848
1201.980
1531.754
538.536
1367.855
1533.756
1697.730
130.144
1699.735
576.738
1863.850
847.466
1013.204
1038.125
1203.986
1369.842
1535.750
1701.740
1867.863
1449.825
1615.732
1948.023
m/z
200 400 600 800 1000 1200 1400 1600 1800

FPyKYNE

2-fluoro-3-pent-4-yn-1-yloxypyridine

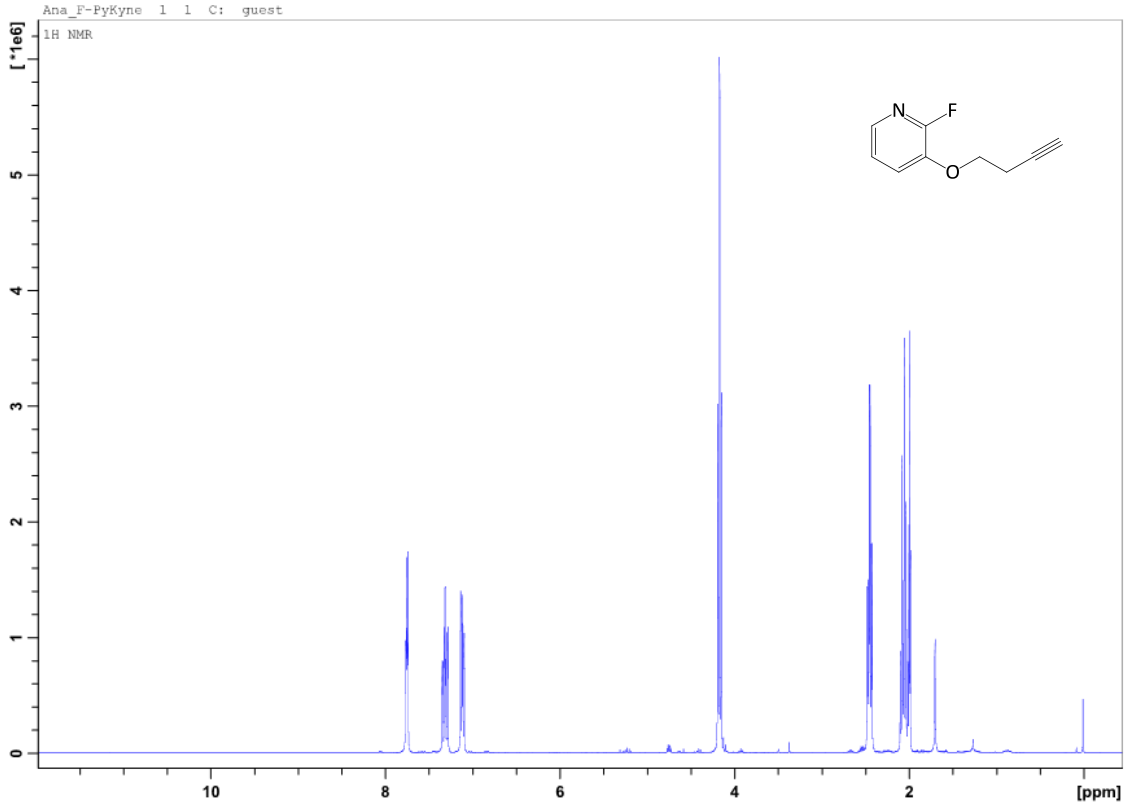

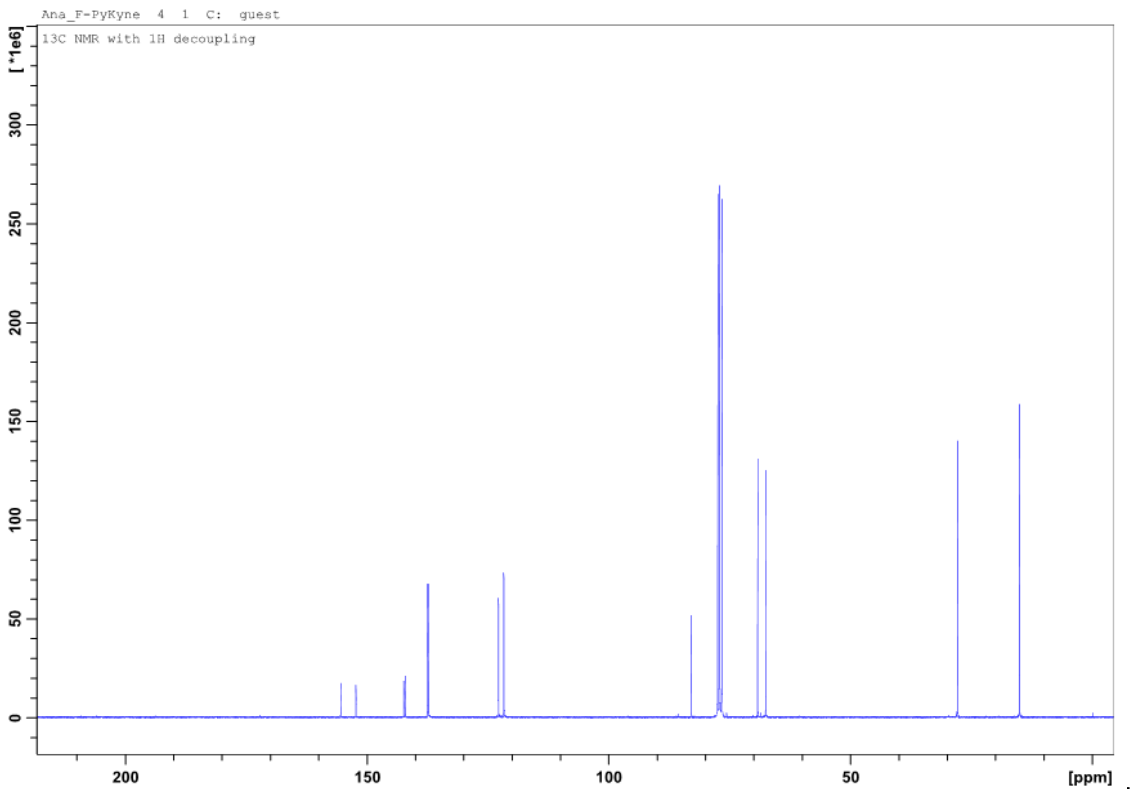

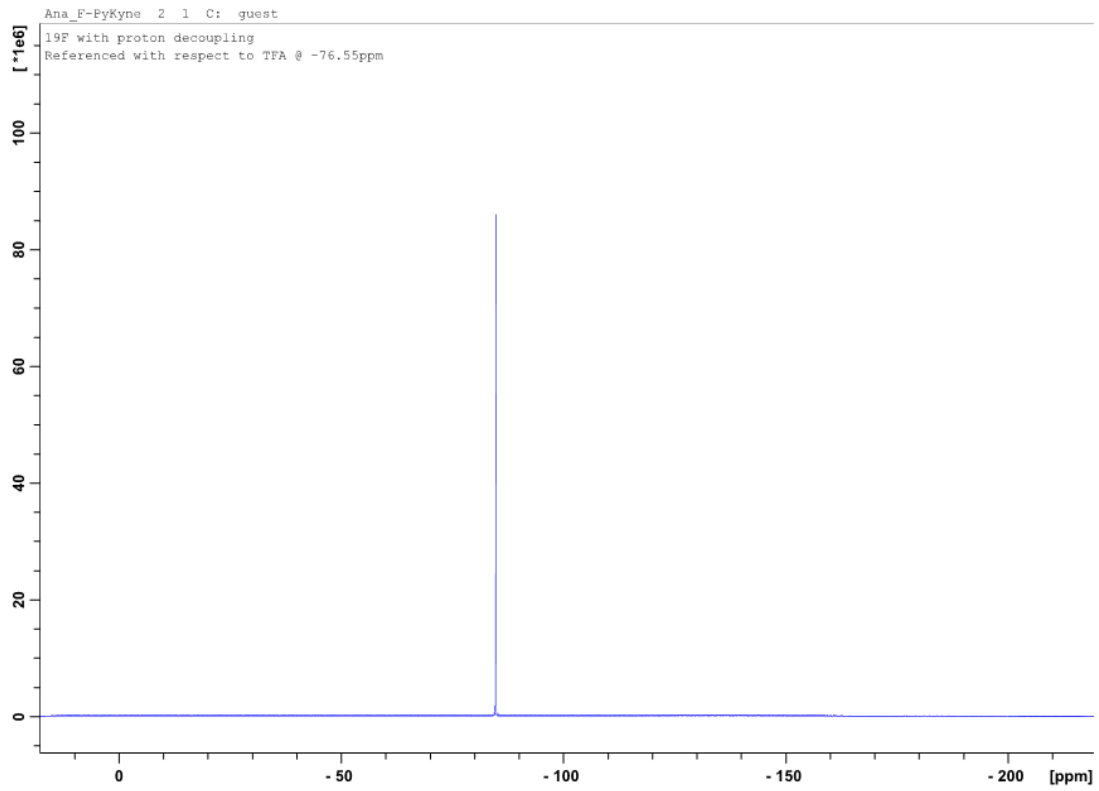

2c3969 Scan 5 RT=0:53 100%=313286 mv 29-Jun-2010 04:54
HRP +EI fpykyne

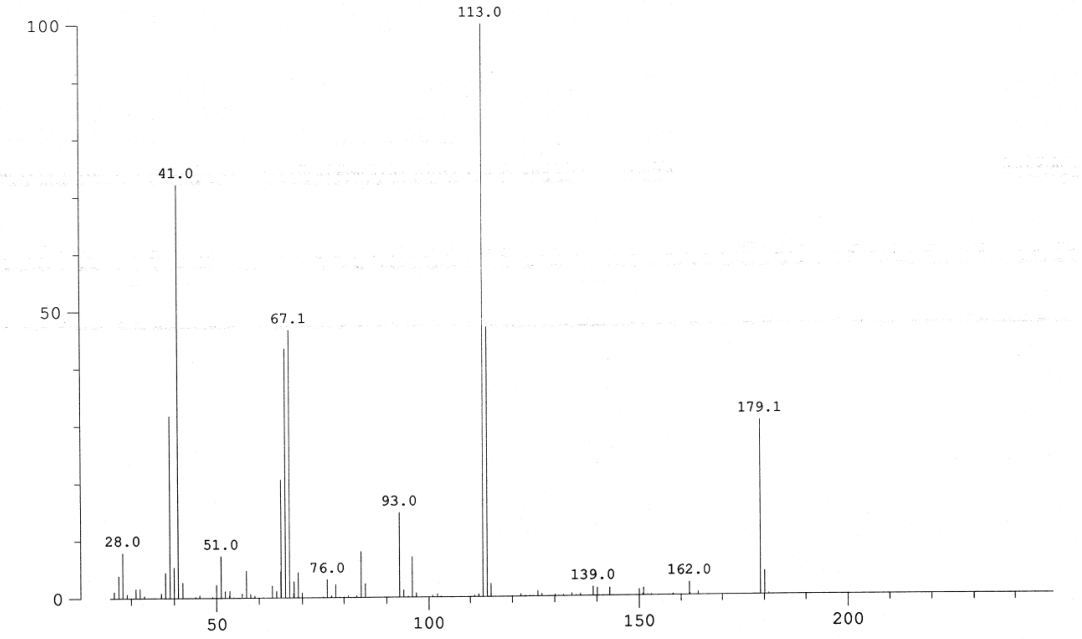

Trityl azide losartan

5-[4'-(5-Azidomethyl-2-butyl-4-chloro-imidazol-1-ylmethyl)-biphenyl-2-yl]-2-trityl-2H-tetrazole

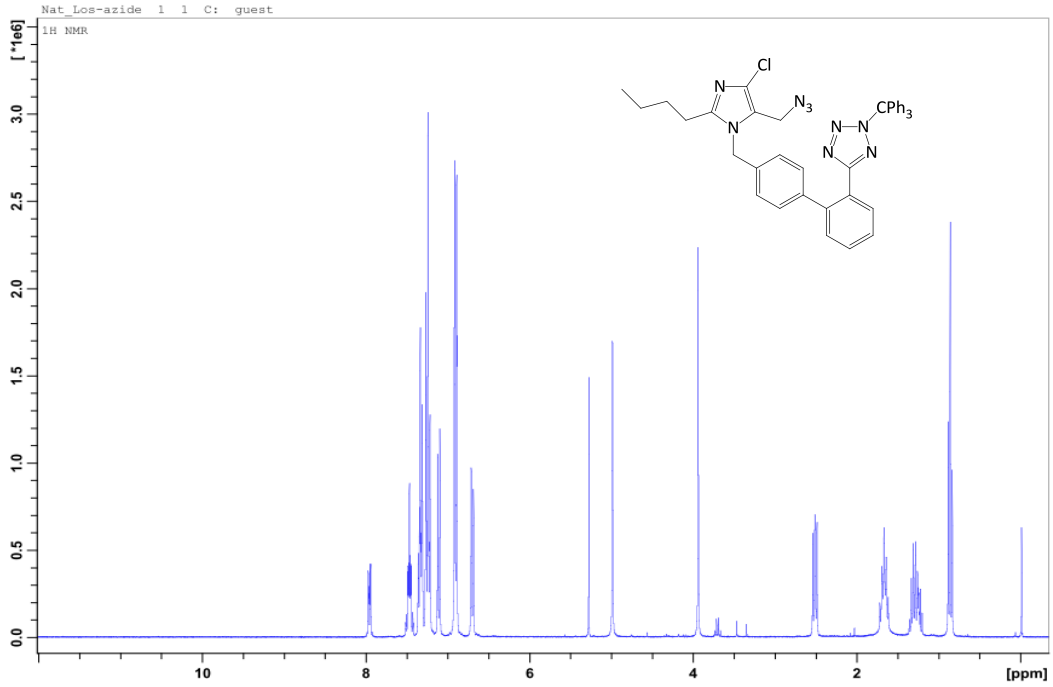

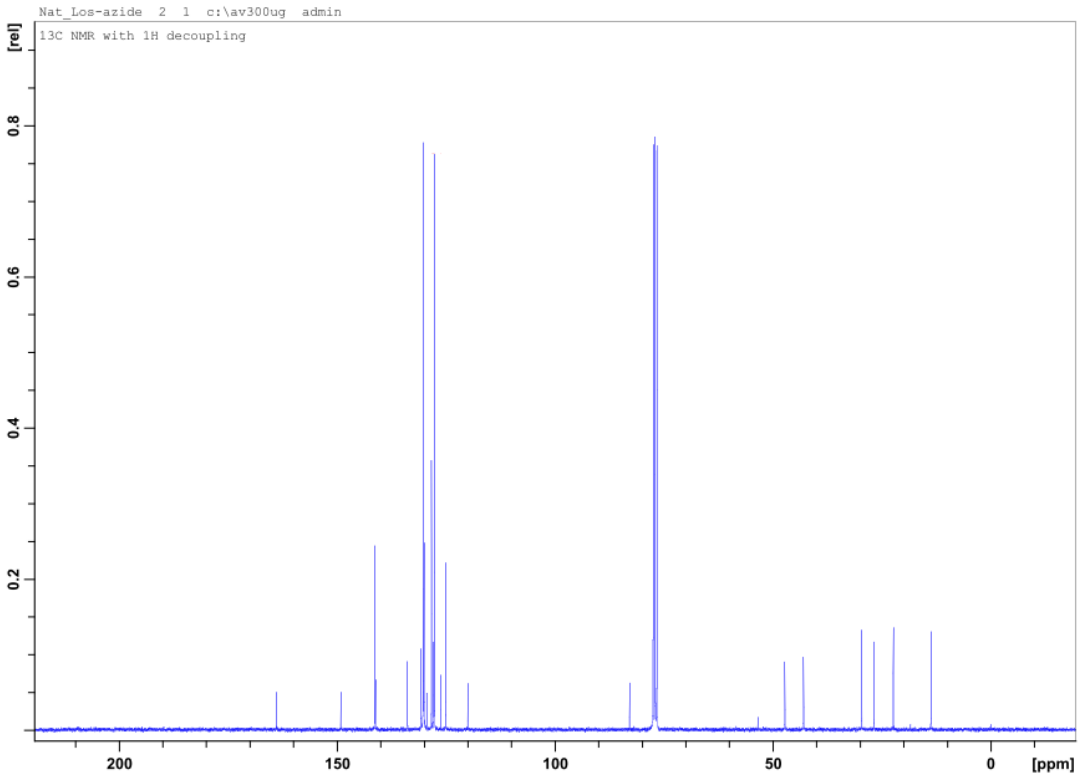

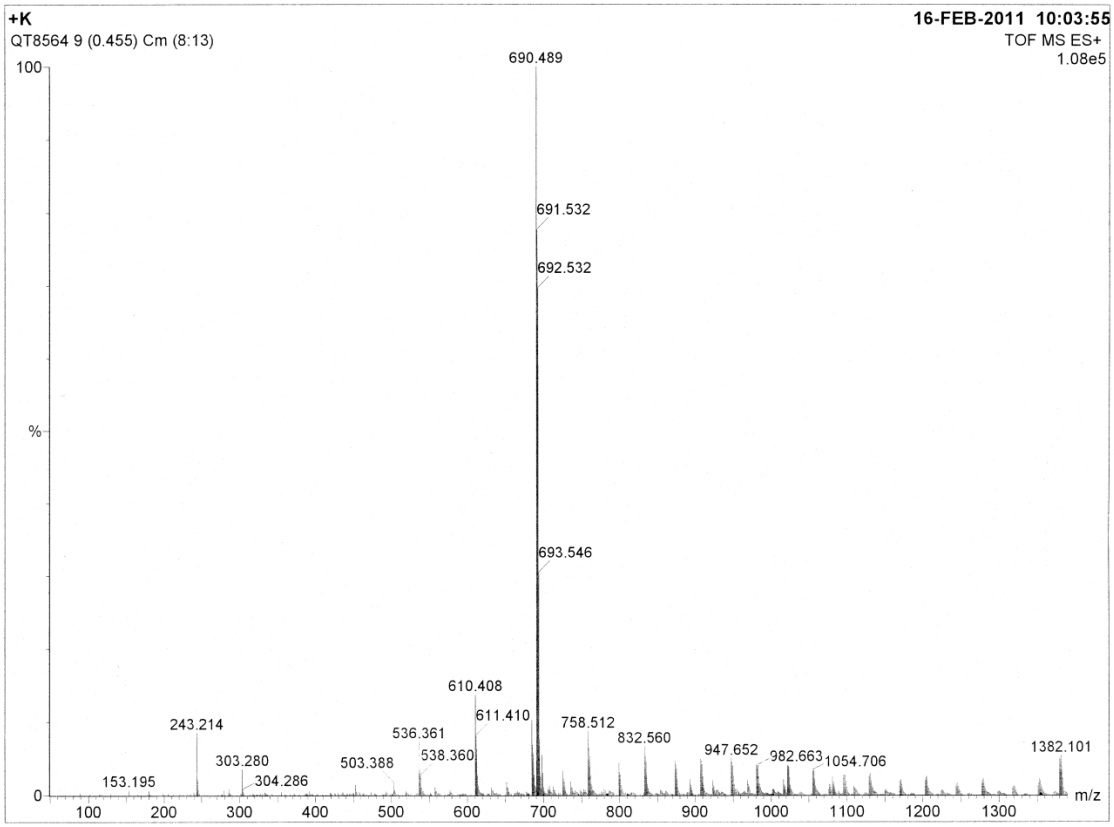
+K
QT8564 9 (0.455) Cm (8:13)
16-FEB-2011 10:03:55
TOF MS ES+
1.08e5
100
%
0
690.489
691.532
692.532
693.546
610.408
611.410
243.214
536.361
538.360
758.512
832.560
947.652
982.663
1054.706
1382.101
303.280
304.286
503.388
153.195
m/z
100 200 300 400 500 600 700 800 900 1000 1100 1200 1300

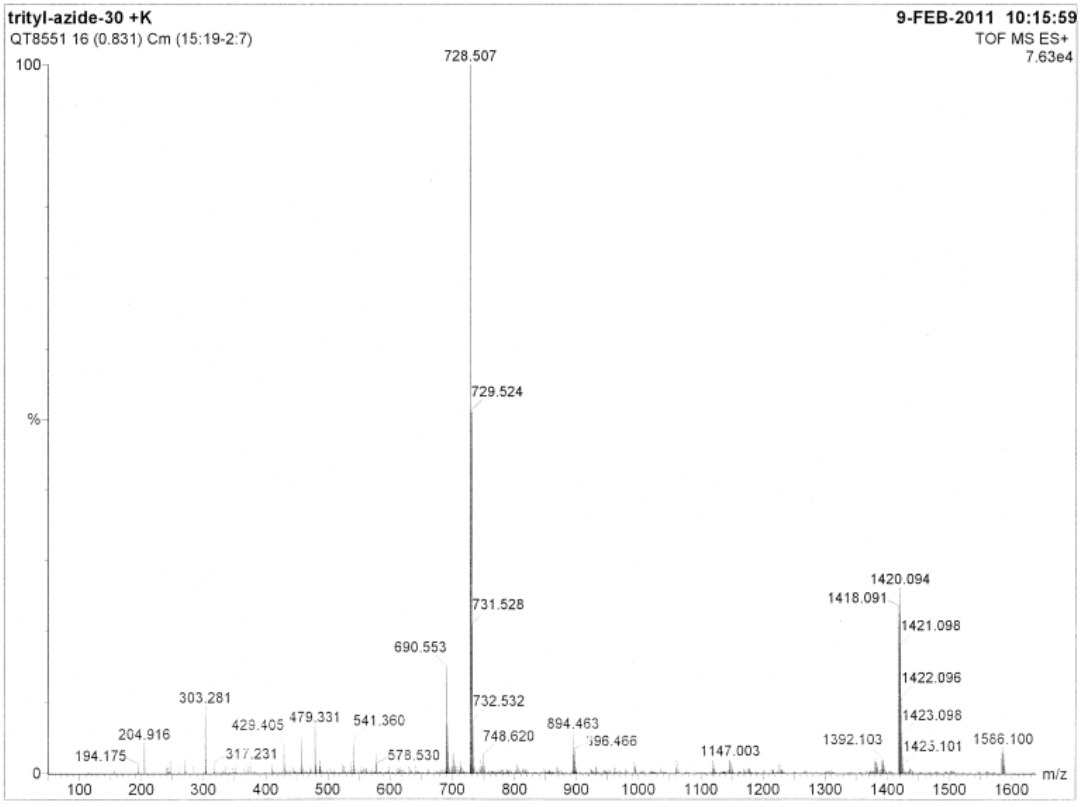
trityl-azide-30 +K
QT8551 16 (0.831) Cm (15:19-2:7)
9-FEB-2011 10:15:59
TOF MS ES+
7.63e4
100
%
0
728.507
729.524
731.528
690.553
732.532
303.281
204.916
429.405
479.331
541.360
748.620
894.463
1147.003
1392.103
1420.094
1418.091
1421.098
1422.096
1423.098
1423.101
1586.100
194.175
317.231
578.530
m/z
100 200 300 400 500 600 700 800 900 1000 1100 1200 1300 1400 1500 1600

Azide losartan

5-[4'-(5-Azidomethyl-2-butyl-4-chloro-imidazol-1-ylmethyl)-biphenyl-2-yl]-2H-tetrazole

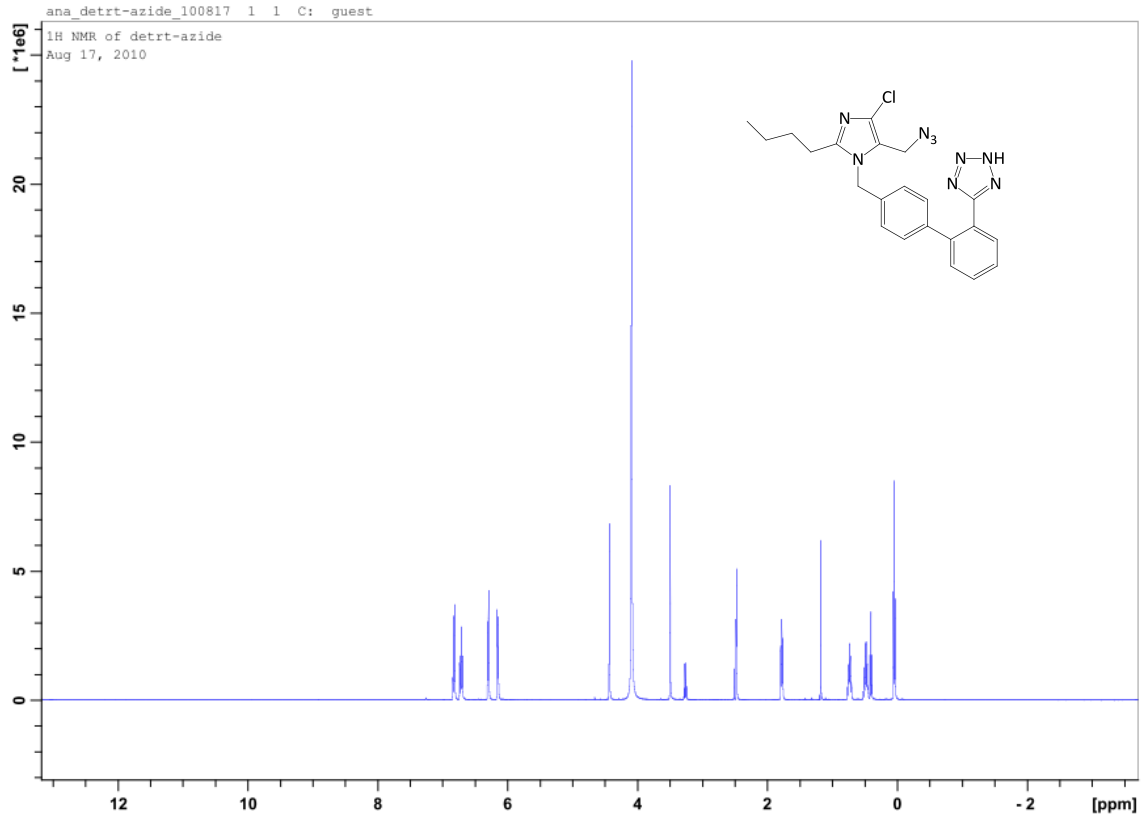

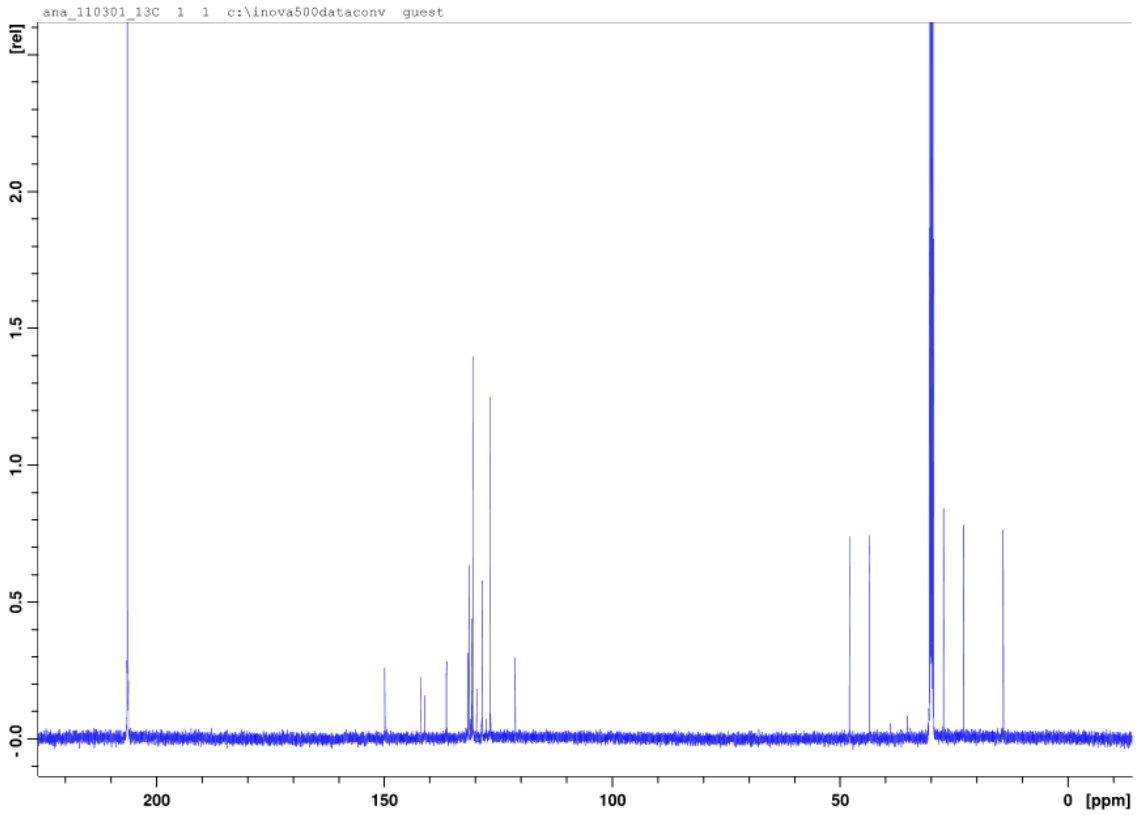

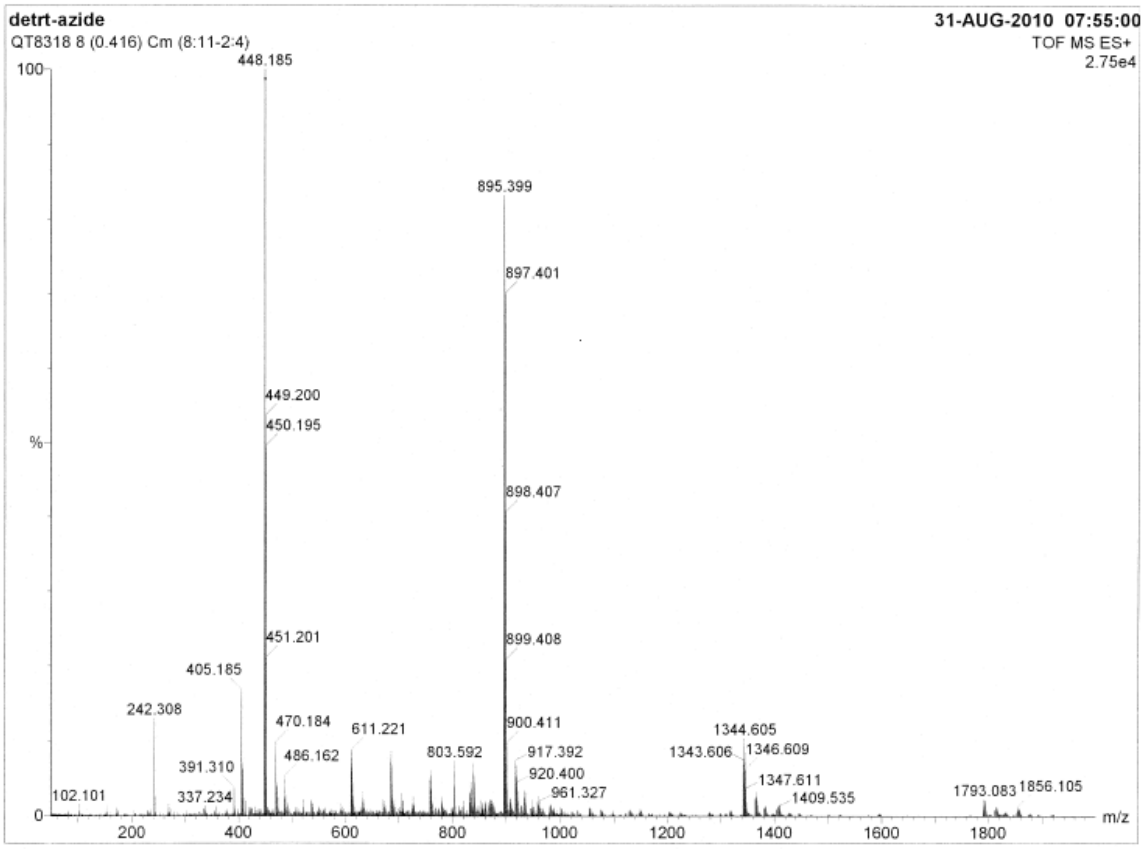
detrt-azide
QT8318 8 (0.416) Cm (8:11-2:4)
31-AUG-2010 07:55:00
TOF MS ES+
2.75e4
100
%
0
448.185
895.399
897.401
449.200
450.195
898.407
451.201
899.408
405.185
242.308
470.184
611.221
900.411
486.162
803.592
917.392
920.400
391.310
961.327
337.234
102.101
1344.605
1343.606
1346.609
1347.611
1409.535
1793.083
1856.105
200
400
600
800
1000
1200
1400
1600
1800
m/z

Fluoropyridine losartan

3-[3-(1-{2-Butyl-5-chloro-3-[2'-(2-trityl-2H-tetrazol-5-yl)-biphenyl-4-ylmethyl]-3H-imidazol-4-ylmethyl}-1H-[1,2,3]triazol-4-yl)-propoxy]-2-fluoro-pyridine

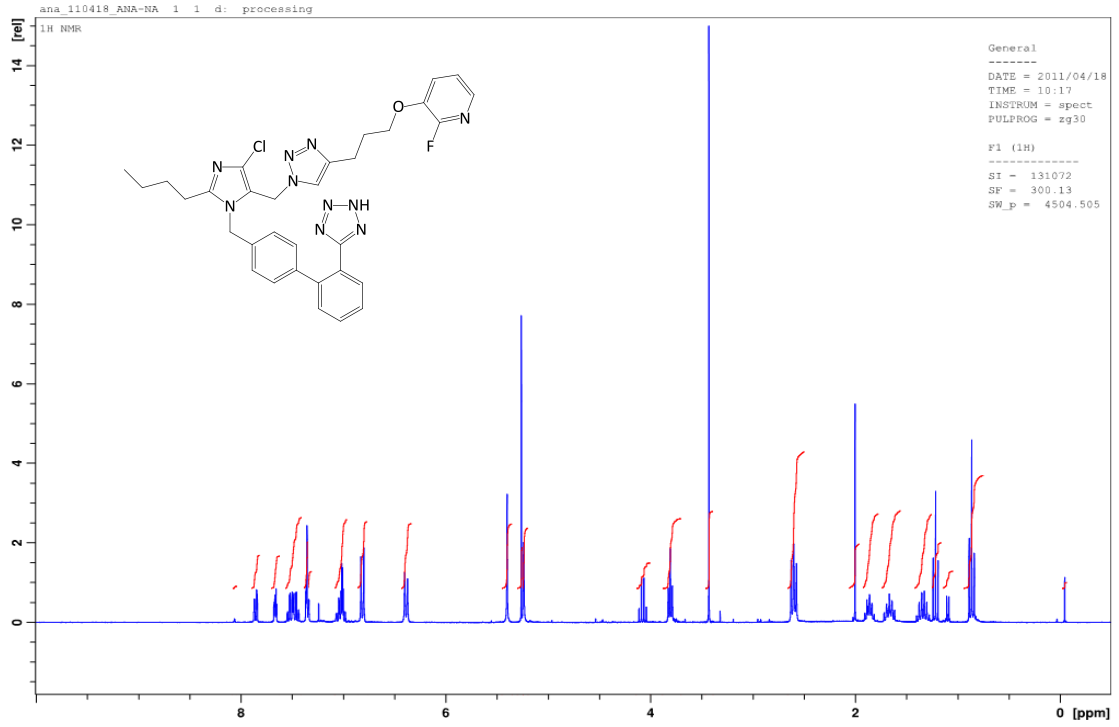

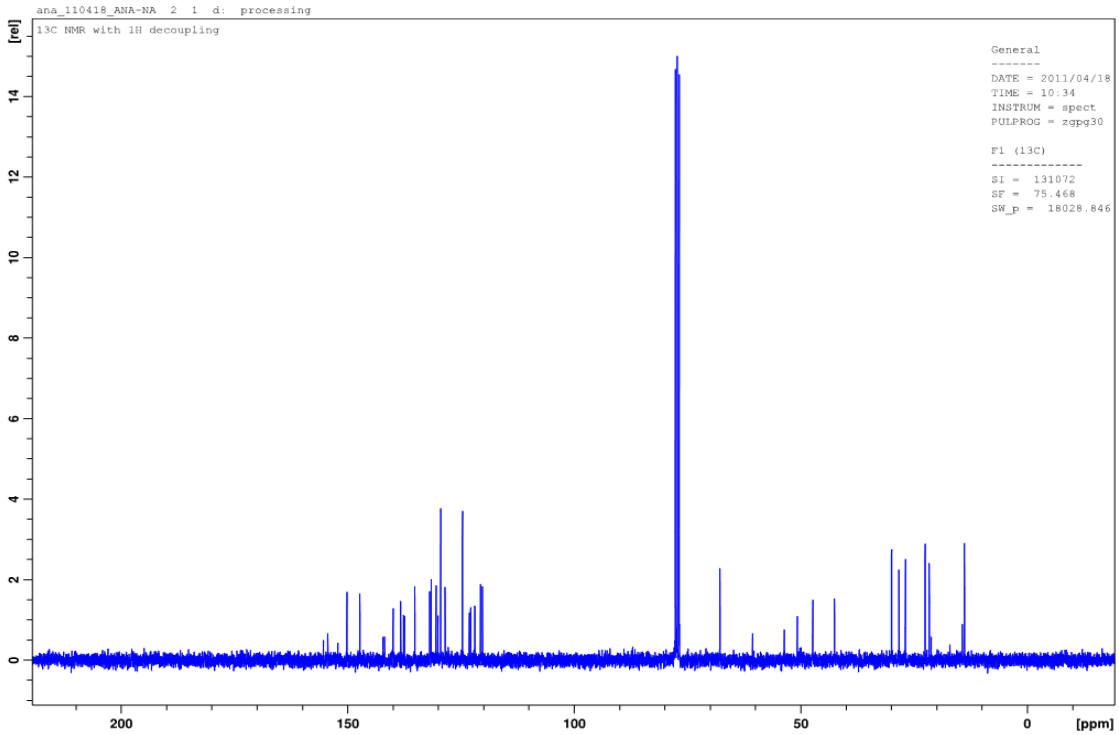

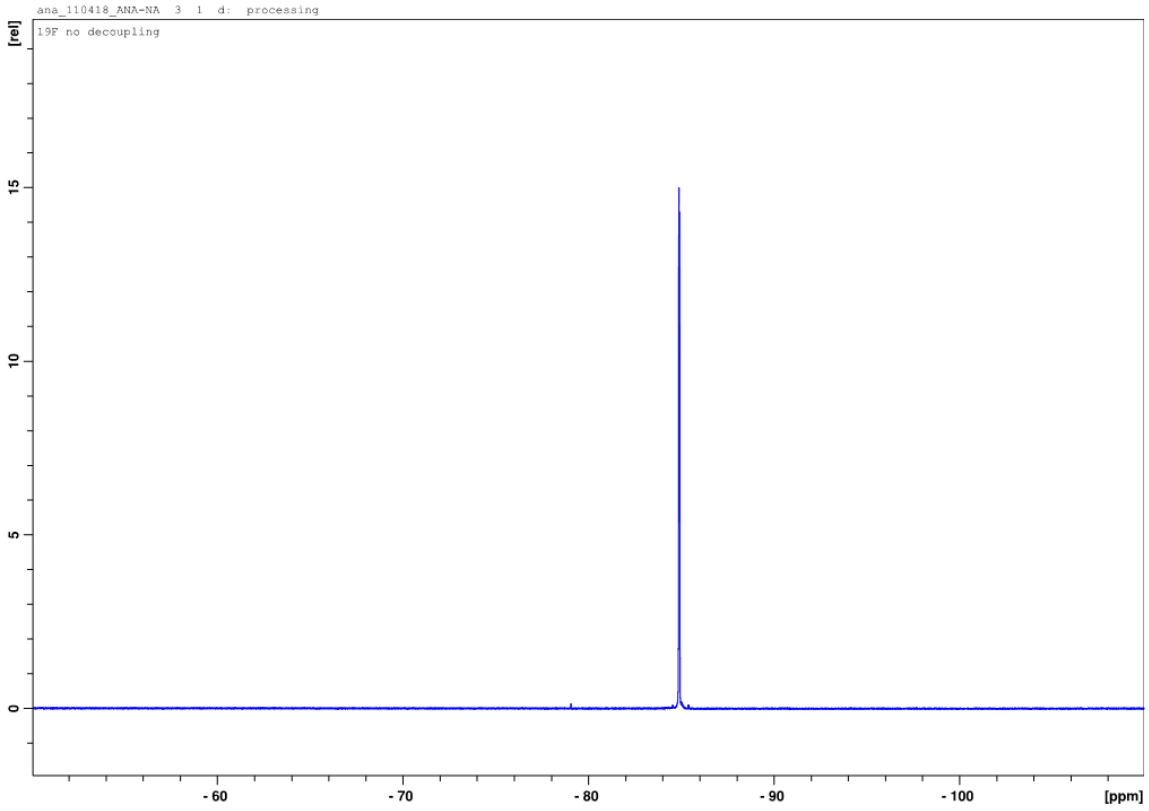
ana_110418_ANA-NA 3 1 d: processing
19F no decoupling
[rel]
15
10
5
0
- 60
- 70
- 80
- 90
- 100
[ppm]

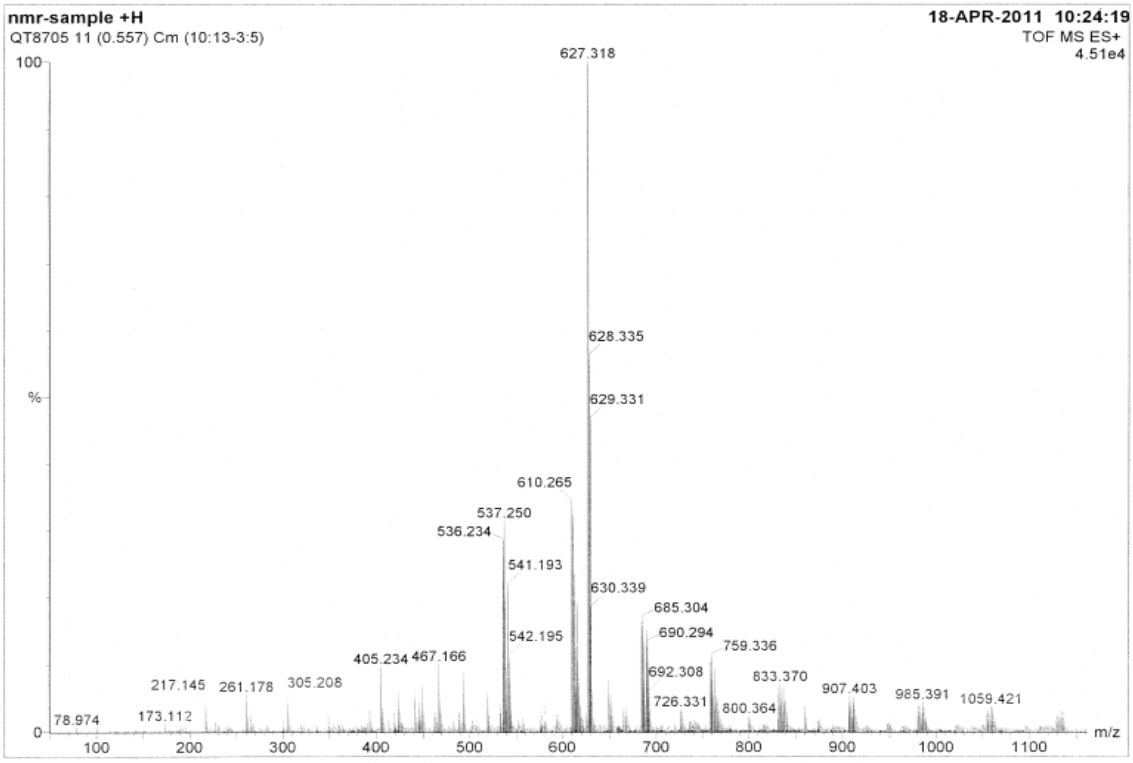
nmr-sample +H
QT8705 11 (0.557) Cm (10:13-3:5)
18-APR-2011 10:24:19
TOF MS ES+
4.51e4
100
%
0
627.318
628.335
629.331
610.265
537.250
536.234
541.193
630.339
685.304
690.294
542.195
759.336
692.308
405.234
467.166
833.370
907.403
985.391
1059.421
217.145
261.178
305.208
726.331
800.364
78.974
173.112
100
200
300
400
500
600
700
800
900
1000
1100
m/z

Nitropyridine trityl losartan

3-[3-(1-{2-Butyl-5-chloro-3-[2'-(2-trityl-2H-tetrazol-5-yl)-biphenyl-4-ylmethyl]-3H-imidazol-4-ylmethyl}-1H-[1,2,3]triazol-4-yl)-propoxy]-2-nitro-pyridine